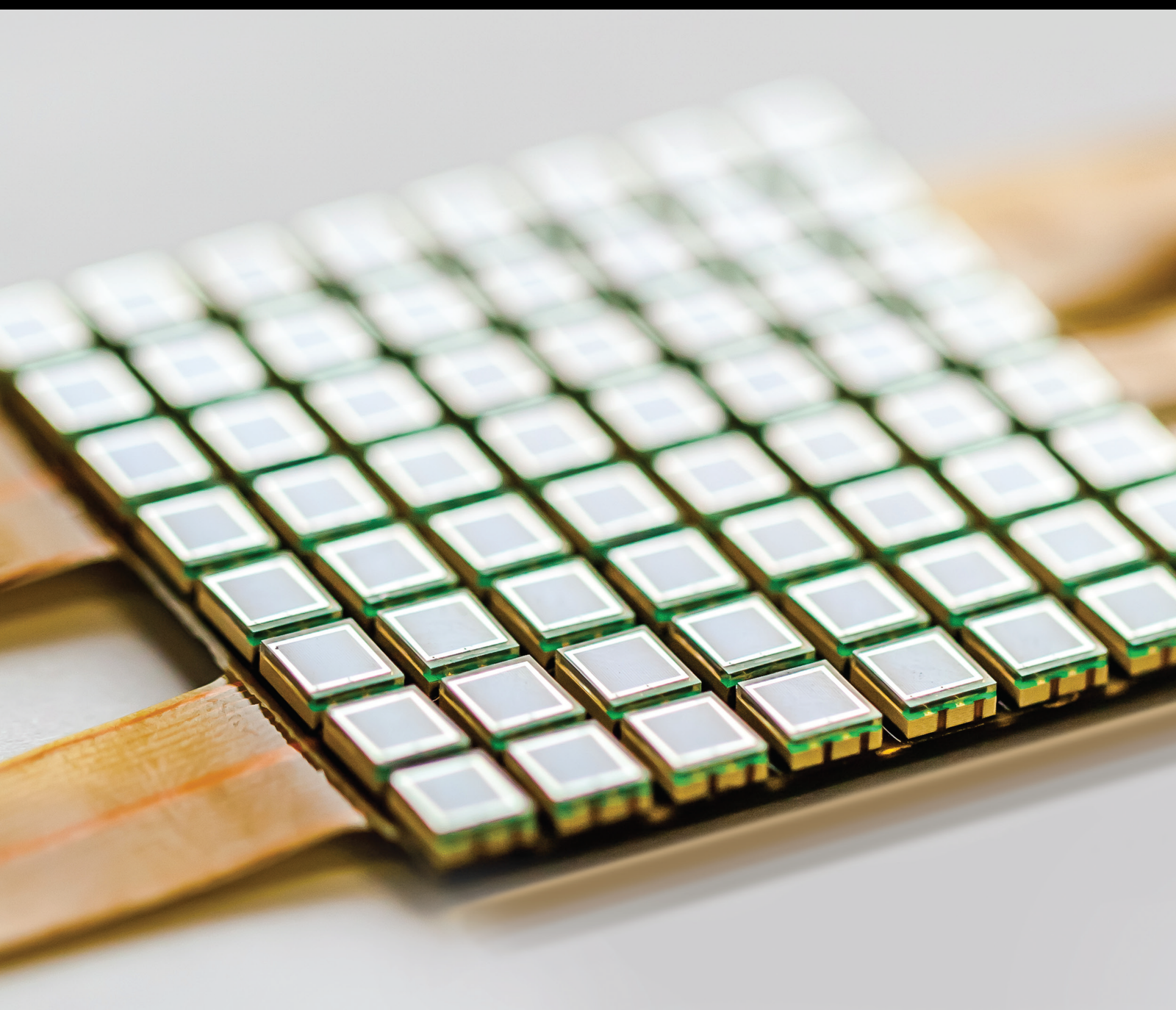


Sensor Systems for Personal Wellbeing and Healthcare

Lead Guest Editor: Janez Trontelj

Guest Editors: Marjan Gusev, Andrej Kosir, and Jurij Tasic





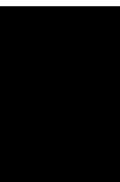
Sensor Systems for Personal Wellbeing and Healthcare

Journal of Sensors

Sensor Systems for Personal Wellbeing and Healthcare

Lead Guest Editor: Janez Trontelj

Guest Editors: Marjan Gusev, Andrej Kosir, and
Jurij Tasic





Copyright © 2020 Hindawi Limited. All rights reserved.

This is a special issue published in "Journal of Sensors." All articles are open access articles distributed under the Creative Commons Attribution License, which permits unrestricted use, distribution, and reproduction in any medium, provided the original work is properly cited.

Chief Editor

Harith Ahmad , Malaysia

Associate Editors

Duo Lin , China
Fanli Meng , China
Pietro Siciliano , Italy
Guiyun Tian, United Kingdom

Academic Editors

Ghufran Ahmed , Pakistan
Constantin Apetrei, Romania
Shonak Bansal , India
Fernando Benito-Lopez , Spain
Romeo Bernini , Italy
Shekhar Bhansali, USA
Matthew Brodie, Australia
Ravikumar CV, India
Belén Calvo, Spain
Stefania Campopiano , Italy
Binghua Cao , China
Domenico Caputo, Italy
Sara Casciati, Italy
Gabriele Cazzulani , Italy
Chi Chiu Chan, Singapore
Sushank Chaudhary , Thailand
Edmon Chehura , United Kingdom
Marvin H Cheng , USA
Lei Chu , USA
Mario Collotta , Italy
Marco Consales , Italy
Jesus Corres , Spain
Andrea Cusano, Italy
Egidio De Benedetto , Italy
Luca De Stefano , Italy
Manel Del Valle , Spain
Franz L. Dickert, Austria
Giovanni Diraco, Italy
Maria de Fátima Domingues , Portugal
Nicola Donato , Italy
Sheng Du , China
Amir Elzawwy, Egypt
Mauro Epifani , Italy
Congbin Fan , China
Lihang Feng, China
Vittorio Ferrari , Italy
Luca Francioso, Italy


Libo Gao , China
Carmine Granata , Italy
Pramod Kumar Gupta , USA
Mohammad Haider , USA
Agustin Herrera-May , Mexico
María del Carmen Horrillo, Spain
Evangelos Hristoforou , Greece
Grazia Iadarola , Italy
Syed K. Islam , USA
Stephen James , United Kingdom
Sana Ullah Jan, United Kingdom
Bruno C. Janegitz , Brazil
Hai-Feng Ji , USA
Shouyong Jiang, United Kingdom
Roshan Prakash Joseph, USA
Niravkumar Joshi, USA
Rajesh Kaluri , India
Sang Sub Kim , Republic of Korea
Dr. Rajkishor Kumar, India
Rahul Kumar , India
Nageswara Lalam , USA
Antonio Lazaro , Spain
Chengkuo Lee , Singapore
Chenzong Li , USA
Zhi Lian , Australia
Rosalba Liguori , Italy
Sangsoon Lim , Republic of Korea
Huan Liu , China
Jin Liu , China
Eduard Llobet , Spain
Jaime Lloret , Spain
Mohamed Louzazni, Morocco
Jesús Lozano , Spain
Oleg Lupan , Moldova
Leandro Maio , Italy
Pawel Malinowski , Poland
Carlos Marques , Portugal
Eugenio Martinelli , Italy
Antonio Martinez-Olmos , Spain
Giuseppe Maruccio , Italy
Yasuko Y. Maruo, Japan
Zahid Mehmood , Pakistan
Carlos Michel , Mexico
Stephen. J. Mihailov , Canada
Bikash Nakarmi, China

Ehsan Namaziandost , Iran
Heinz C. Neitzert , Italy
Sing Kiong Nguang , New Zealand
Calogero M. Oddo , Italy
Tinghui Ouyang, Japan
SANDEEP KUMAR PALANISWAMY ,
India
Alberto J. Palma , Spain
Davide Palumbo , Italy
Abinash Panda , India
Roberto Paolesse , Italy
Akhilesh Pathak , Thailand
Giovanni Pau , Italy
Giorgio Pennazza , Italy
Michele Penza , Italy
Sivakumar Poruran, India
Stelios Potirakis , Greece
Biswajeet Pradhan , Malaysia
Giuseppe Quero , Italy
Linesh Raja , India
Maheswar Rajagopal , India
Valerie Renaudin , France
Armando Ricciardi , Italy
Christos Riziotis , Greece
Ruthber Rodriguez Serrezuela , Colombia
Maria Luz Rodriguez-Mendez , Spain
Jerome Rossignol , France
Maheswaran S, India
Ylias Sabri , Australia
Sourabh Sahu , India
José P. Santos , Spain
Sina Sareh, United Kingdom
Isabel Sayago , Spain
Andreas Schütze , Germany
Praveen K. Sekhar , USA
Sandra Sendra, Spain
Sandeep Sharma, India
Sunil Kumar Singh Singh , India
Yadvendra Singh , USA
Afaque Manzoor Soomro , Pakistan
Vincenzo Spagnolo, Italy
Kathiravan Srinivasan , India
Sachin K. Srivastava , India
Stefano Stassi , Italy

Danfeng Sun, China
Ashok Sundramoorthy, India
Salvatore Surdo , Italy
Roshan Thotagamuge , Sri Lanka
Guiyun Tian , United Kingdom
Sri Ramulu Torati , USA
Abdellah Touhafi , Belgium
Hoang Vinh Tran , Vietnam
Aitor Urrutia , Spain
Hana Vaisocherova - Lislalova , Czech
Republic
Everardo Vargas-Rodriguez , Mexico
Xavier Vilanova , Spain
Stanislav Vitek , Czech Republic
Luca Vollero , Italy
Tomasz Wandowski , Poland
Bohui Wang, China
Qihao Weng, USA
Penghai Wu , China
Qiang Wu, United Kingdom
Yuedong Xie , China
Chen Yang , China
Jiachen Yang , China
Nitesh Yelve , India
Aijun Yin, China
Chouki Zerrouki , France


Contents

Wireless Photoplethysmography Sensor for Continuous Blood Pressure Biosignal Shape Acquisition

C. Bambang Dwi Kuncoro, Win-Jet Luo, and Yean-Der Kuan 



Research Article (9 pages), Article ID 7192015, Volume 2020 (2020)

Bed Position Classification by a Neural Network and Bayesian Network Using Noninvasive Sensors for Fall Prevention

Waranrach Viriyavit  and Virach Sornlertlamvanich 

Research Article (14 pages), Article ID 5689860, Volume 2020 (2020)

Noninvasive Glucose Measurement Using Machine Learning and Neural Network Methods and Correlation with Heart Rate Variability

Marjan Gusev , Lidija Poposka, Gjoko Spasevski, Magdalena Kostoska, Bojana Koteska, Monika Simjanoska , Nevena Ackovska, Aleksandar Stojmenski, Jurij Tasic, and Janez Trontelj

Review Article (13 pages), Article ID 9628281, Volume 2020 (2020)

Piezoresistive Breathing Sensing System with 3D Printed Wearable Casing

Erik Vanegas, Raul Igual , and Inmaculada Plaza 

Research Article (19 pages), Article ID 2431731, Volume 2019 (2019)

Research Article

Wireless Photoplethysmography Sensor for Continuous Blood Pressure Biosignal Shape Acquisition

C. Bambang Dwi Kuncoro,^{1,2} Win-Jet Luo,² and Yean-Der Kuan ³

¹Electrical and Instrumentation Laboratory, Politeknik Negeri Bandung, Jl. Gegerkalong Hilir, Ds. Ciwaruga, Bandung, 40012 Jawa Barat, Indonesia

²Graduate Institute of Precision Manufacturing, National Chin-Yi University of Technology, No. 57, Sec. 2, Zhongshan Rd., Taiping Dist., Taichung City 41170, Taiwan

³Department of Refrigeration, Air Conditioning and Energy Engineering, National Chin-Yi University of Technology, No. 57, Sec. 2, Zhongshan Rd., Taiping Dist., Taichung City 41170, Taiwan

Correspondence should be addressed to Yean-Der Kuan; ydkuan@ncut.edu.tw

Received 8 August 2019; Accepted 8 January 2020; Published 24 February 2020

Guest Editor: Jurij Tasic

Copyright © 2020 C. Bambang Dwi Kuncoro et al. This is an open access article distributed under the Creative Commons Attribution License, which permits unrestricted use, distribution, and reproduction in any medium, provided the original work is properly cited.

Blood pressure assessment plays a vital role in day-to-day clinical diagnosis procedures as well as personal monitoring. Thus, blood pressure monitoring devices must afford convenience and be easy to use with no side effects on the user. This paper presents a compact, economical, power-efficient, and convenient wireless plethysmography sensor for real-time blood pressure biosignal monitoring. The proposed sensor facilitates blood pressure signal shape sensing, signal conditioning, and data conversion as well as its wireless transmission to a monitoring terminal. Received data can, subsequently, be compiled and stored on a computer via a Wi-Fi module. During monitoring, users can observe blood pressure signals being processed and displayed on the graphical user interface (GUI)—developed using a virtual instrumentation (VI) application. The proposed device comprises a finger clip optical pulse sensor, analogue signal preprocessing, microcontroller, and Wi-Fi module. It consumes approximately 500 mW power when operating in the active mode and synthesized using commercial off-the-shelf (COTS) components. Experimental results reveal that the proposed device is reliable and facilitates efficient blood pressure monitoring. The proposed wireless photoplethysmographic (PPG) sensor is a preliminary (or first) version of the intended device manifestation. It provides raw blood pressure data for further classification. Additionally, the collected data concerning the blood pressure wave shape can be easily analysed for use in other biosignal observations, interpretations, and investigations. The design approach also allows the device to be built into a wearable system for further research purposes.

1. Introduction

Several innovations have led to significant advances in health-care systems by enhancing both functionality and capability of different monitoring systems. Acute, precarious diseases can be diagnosed at their early stages using new-age electronic equipment. Modern diagnostic and therapeutic approaches bear high operation costs and require expensive equipment.

Moreover, in recent years, the advent of wearable technology has afforded accurate recording and precise processing of biosignals. Blood pressure is a vital physiological

parameter that indicates the functional well-being of the cardiovascular system [1]. Conventional blood pressure-monitoring devices are either limited in scope with regard to systolic and diastolic blood pressure measurements [2] or unreliable and uncomfortable from the viewpoint of prolonged use. Therefore, there exists the need for a noninvasive, ambulatory care system for long-term blood pressure monitoring while accounting for details concerning blood pressure variability. Availability of such a system would facilitate easy and timely prediction of serious cardiovascular diseases during antihypertensive therapy sessions [3].

During development of psychophysiology-monitoring systems, it is important to consider aspects, such as convenience, comfort, and minimum side effects on the user. Such systems detect and record physiological biosignals of patients through a sensor attached to their body. Although the said signals are stored and processed locally, monitoring systems must comprise a wireless module to allow effective signal transmission as and when required. A wearable biosignal monitoring instrument is preferred owing to its afforded comfort and convenience of use. Moreover, embedded sensors in such devices can be placed directly in contact with the user's (patient's) body, and their pulse can be recorded. Wearable technology has proven to be effective and promising in medical and clinical applications owing to its noninvasive, comfortable, and accurate measurement techniques.

Several researchers have proposed numerous methods to collect and analyse psychophysiological biosignals. An extant study [4] proposed a mechanism to sense blood volume and pulse signals from fingertips using transmission-mode photoplethysmography. The proposed sensor was sensitive, economic, and consumed less power. It employed a light-emitting diode as a transmitter and a phototransistor as detector. A microcontroller processes signals obtained from the sensor. Advantages of this mechanism were cost-effectiveness, compactness, and reduced power consumption.

Ghamari et al. [5] proposed a wireless PPG device enclosed in a wristband-type unit, wherein arterial-pulse data were collected using a sensor, and the same were analysed by the said device. The said device comprised an optical sensor, signal conditioning unit, microcontroller, and Bluetooth module. Collected pulse data were monitored, filtered, amplified, processed, and transferred to another smart device. Additionally, the authors proposed a model using two Gaussian functions to describe photoplethysmographic signals.

Shimazaki and Hara [6] proposed a heart rate- (HR-) sensing device with motion artefact (MA) cancellation along with PPG and MA sensors [6]. The said device was claimed to produce accurate results even in cases of vigorous physical exercise owing to use of two sensors—HR sensor fitted to subjects' waist (back) and a device (Holter monitor) fitted to their chests to monitor ECG waveforms. The authors described the MA cancellation principle in detail, albeit they did not discuss adequate values of relevant design parameters.

Gothwal [7] proposed an economic, wearable PPG system using available components. The device comprised an optical sensor (IR transmitter and receiver), preprocessing unit (buffer amplifier, two-stage band pass filter, amplifier, and comparator), processor (microcontroller), and display unit. Biosignals acquired from subjects' fingers were provided as input to the IR transmitter and receiver. To avoid excessive loading, acquired signals were passed through the buffer amplifier using a coupling mechanism between the IR-receiver output and bandpass-filter input. Subsequently, the output from the buffer amplifier was processed using the microcontroller.

In another study [8], a heart rate monitor (HRM) based on the reflectance photoplethysmography technique was developed to sense pulses from subjects' fingertips. Sensed pulse signals were filtered and amplified using a two-stage

operational amplifier (Op-Amp), and the same were processed using a microcontroller. The recorded heart rate was displayed on a liquid-crystal display (LCD) in beats per minute (BPM). The proposed device was claimed to be convenient, inexpensive, and portable compared with the competition. Athletes could use this device to monitor their heart rate with minimal errors.

Zangróniz et al. [9] introduced a wearable photoplethysmography sensor capable of assessing mental distress. The proposed design employed optical plethysmograms to obtain blood volume information using an appropriate sensor. Additionally, a discriminant tree-based model was developed to determine parameter dependencies. Assessment of the proposed model revealed an overall accuracy of 82.35%.

Similarly, a multipurpose photoplethysmographic sensor was proposed in [10] to detect multiwavelength photoplethysmographs by penetrating skin at various depths. The proposed device was named "SmartPPG," and it could operate under transmission and reflection modes with the transmission mode being confined to thin body parts—fingers and earlobes. A light source was used to illuminate parts of the skin under observation, thereby reflecting photoplethysmographs. Operation in the reflection mode optimized both the light wavelength and distance between its source and photodetector.

Botman et al. [11] developed a device to monitor cardiovascular activity. The device is dedicated working in an automated workstation for data collection and analysis in large-scale medical measurements. The proposed design was based on a PPG sensor attached to body parts, such as the nose-bridge, earlobe, fingers, and wrist, to facilitate evaluation of physiological parameters, such as the heart rate and pulse-wave characteristics.

Leier et al. [12] proposed use of a smart optical sensor to monitor different tissue layers constituting the cardiovascular system. Based on acquired PPG signals, the proposed sensor could extract physiological parameters, such as the heart and breath rates, skin microcirculation dynamics, oxygen saturation, and vasomotion activity. The said sensor could be attached to patient bodies at four different points depending on their distance from the four photodetectors. The system comprised 32 light-emitting sources capable of emission at four different wavelengths. All electronic components, including LEDs and photodiodes, were moulded using medical-grade silicone to facilitate ease and comfort of wearability.

Ishikawa et al. [13] presented a wristband-type PPG heart rate sensor [13] capable of detecting heart rate variability. Additionally, the device was equipped with a motion artefact cancellation framework to handle motion artefacts during daily activities. During assessment of the proposed sensor operation, activities of the arm, finger, and wrist were observed to cause significantly negligible motion artefacts. Additionally, assessment results revealed that the proposed device and coupled motion cancellation framework can be continuously used to monitor heart rate variability. Moreover, the device could be used to recognize and analyse emotions.

Spigulis et al. [14] developed a wireless PPG sensor combining GaAs-radiation emitting and Si-photon diodes placed adjacent to each other to imitate PPG reflection. A

microcontroller processed sampled signals at programmable sampling frequencies (e.g., 100 Hz) using a 10-bit analogue-to-digital converter. Processed signals were subsequently transmitted in real time via a Bluetooth module within 10 m range.

Abovementioned extant researches focus primarily on heart rate analysis using PPG sensors followed by local display of monitoring results on the device-LCD. While some extant studies allow data to be stored on external storage devices, others support data transmission to portable monitoring devices via direct (USB and/or SPI interfaces) or wireless (Bluetooth or GPRS) connections. Any further processing of raw data can be performed post their collection. Additionally, there exist commercial products that can be directly employed in clinical and psychophysiological applications [15–17]; however, these products do not provide users access to raw data.

This paper presents a device capable of recording blood pressure biosignal shapes for psychophysiological and clinical purposes. The proposed device incorporates a Wi-Fi module (ISM-Industry, Scientific, Medical band) for transmitting, displaying, and storing acquired biosignal data at a monitoring terminal (computer). Wave shapes used in this study were acquired from healthy volunteers, and acquired data was continuously monitored in real-time on an interactive GUI while simultaneously being used for blood pressure monitoring. Collected data concerning the blood pressure wave shape can be easily analysed for use in other biosignal observations, interpretations, and investigations. The device is aimed at maximizing comfort, convenience, affordability, and compactness while minimizing side effects (if any), operational costs, and power consumption. The proposed wireless PPG sensor is a preliminary (or first) version of the intended device manifestation. It provides raw blood pressure data for further classification, and the design approach allows the device to be built into a wearable system for further research purposes.

2. Materials and Methods

2.1. Photoplethysmography (PPG). The term “photoplethysmography” is derived from the Greek word “plethysmos,” which means “to increase.” As mentioned in [18], plethysmography means “[...] finding variations in the size of a body part owing to variations in the amount of blood passing through or contained in that body part.” Pulsatile tissue volumes can be measured using conventional plethysmographs, such as strain gauges, capable of measuring changes under extreme conditions. This technique can be applied to all blood vessels to determine their overall change in volume. Arterial pulsations are the most significant, whereas capillaries are quite noncompliant because they exclusively record minor pulsations. Venous oscillations might occur depending on the measurement technique, albeit such oscillations are often cancelled under application of external pressure [19]. Arterial blood pressure can be measured indirectly using a plethysmogram [20].

Photoplethysmography is similar to traditional plethysmography, albeit not identical. When operating in the

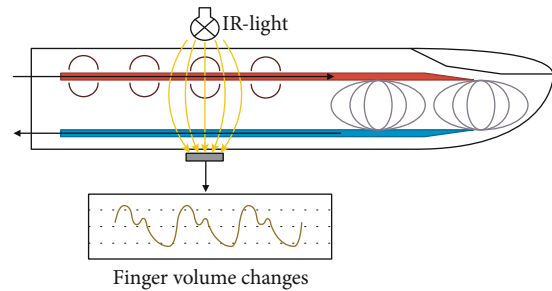


FIGURE 1: Principle of photoplethysmography [21].

transmission mode, PPG devices use an LED operating on one side of the tissue and a photodetector on the other to demonstrate the obstruction and absorption of incident light. If both the LED and photodetector are placed adjacent to each other, all incident lights may reflect off the tissue surface. Plethysmographic devices cannot measure blood pressure; however, they can evaluate changes in the blood volume. The plethysmographic principle is depicted in Figure 1.

Volumetric changes in blood vessels were first reported by Hertzman [22] using the term “photoplethysmography,” and they described two plethysmograph signal components—pulsatile (volume pulse) and baseline (blood volume). Accordingly, plethysmograph signals comprising alternating current (AC) components are indicative of the total absorbance owing to the arterial blood pulsatile component, whereas those comprising direct current (DC) components reveal absorbance caused by other nonpulsatile components as well as the constant flow of arterial and venous blood. Typical plethysmograph signals are depicted in Figure 2.

Absolute changes in blood volume can be accurately measured using the chamber-plethysmography method, wherein volumetric changes (dV/dt) can be transformed into blood flow (F) using the relation $F = dV/dt$. However, some cases only concern relative volumes. Such cases provide information pertaining to time exclusively without any consideration of the amplitude or signal shape. In such cases, electrical impedance plethysmography or photoplethysmography can help provide required information. A literature review regarding plethysmography has been reported in [23], and a more comprehensive review concerning PPG can be found in [24].

Arterial blood pressure is the main cause of PPG signal variations, and as described in Figure 3, the PPG dependence on arterial blood pressure is similar to that of true plethysmograms [19, 25].

2.2. Proposed System. A schematic of the wireless photoplethysmography sensor design proposed in this paper is depicted in Figure 4. Acquired PPG signals are first provided as input to a microcontroller through a signal conditioning (filter and amplifier) circuit. Data obtained is subsequently analysed and organised into packets suitable for transmission over a Wi-Fi network through a universal asynchronous receiver transmitter (UART). Data received by the Wi-Fi

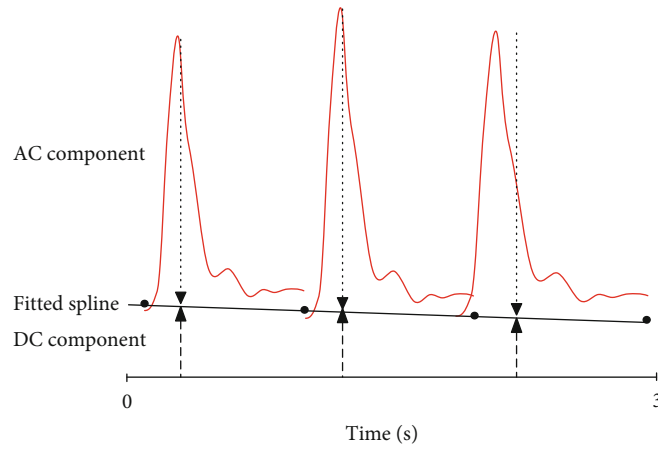


FIGURE 2: AC and DC plethysmograph signals.

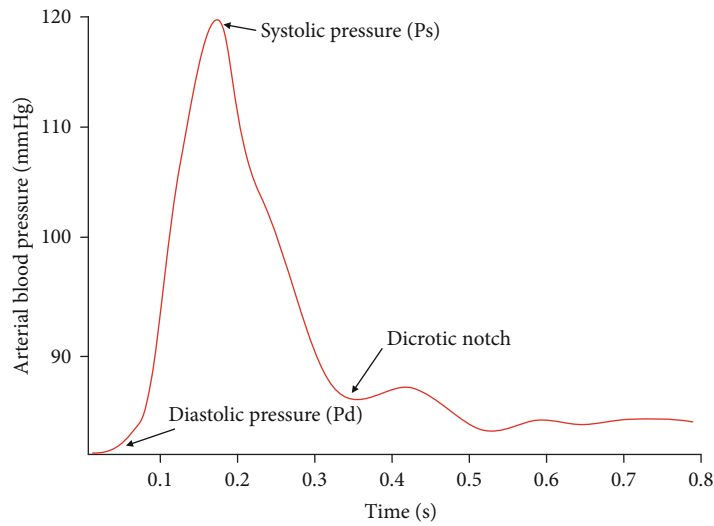


FIGURE 3: Radial arterial blood pressure waveform cycle (AC component).

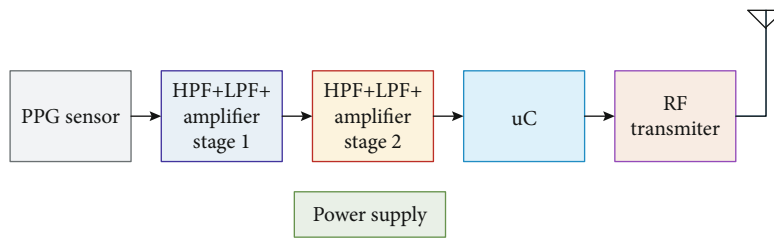


FIGURE 4: Block diagram of wireless PPG sensor.

module is transmitted to a computer where it can be displayed and/or stored.

An LED placed at one end of a finger emits infrared light through the skin. Arterial blood partially absorbs this emitted light which changes according to the pulse. The photodetector placed at the other end of the finger receives any nonabsorbed light and generates an associated continuous pulse signal.

A two-stage analogue preprocessing block filters and amplifies signals received from the sensor. The first stage

comprises a passive high-pass filter (HPF) with cut-off frequency $f_c = 0.7$ Hz intended to eliminate DC signal components. Additionally, an active low-pass filter (LPF) with constant gain and cut-off frequency of 101 and 2.34 Hz, respectively, was incorporated in the first stage. The said HPF-LPF combination eliminates unwanted DC signal components, thereby reducing noise interference above 60 Hz. The configuration of the second stage is identical to that of the first stage. These filter (first) and amplifier (second) stages modify the PPG sensor signal close to the TTL

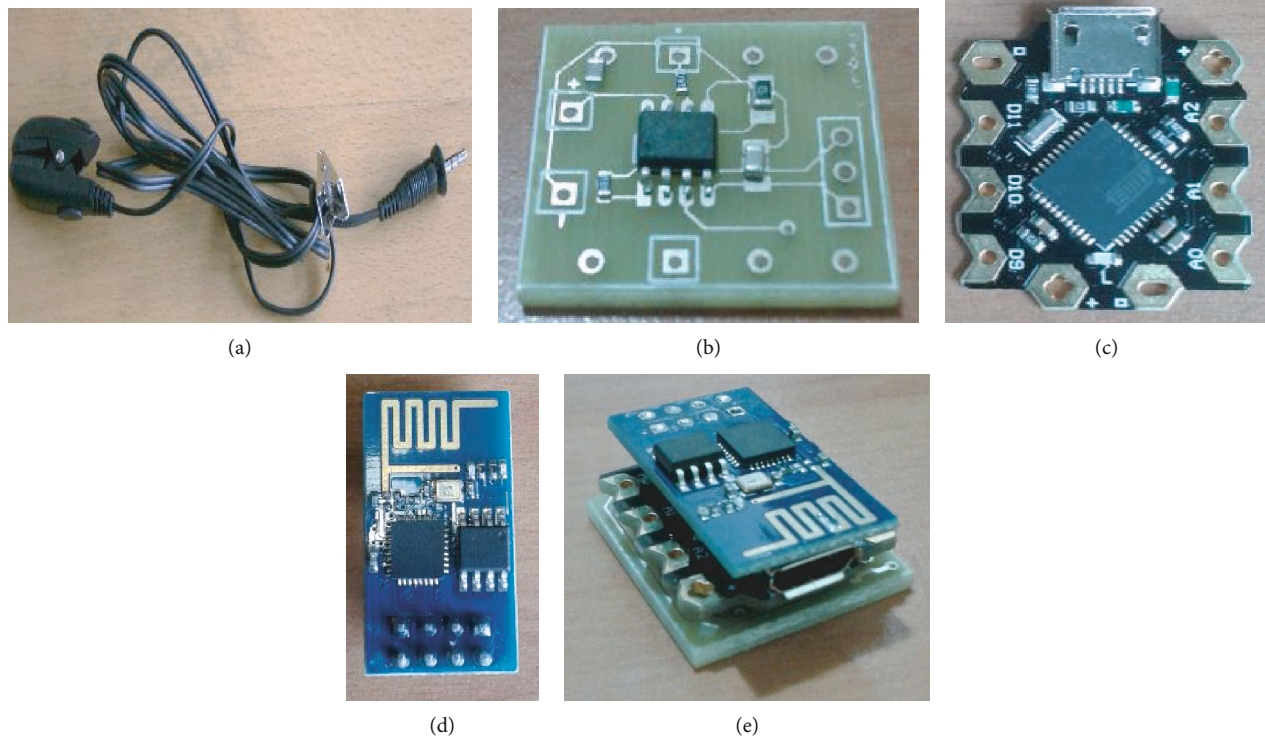


FIGURE 5: Developed devices. (a) Finger clip optical pulse sensor. (b) Analogue preprocessing. (c) Arduino Beetle board. (d) ESP8266 Wi-Fi module. (e) Wireless PPG sensor module implementation.

(transistor-transistor logic) pulse, which is synchronized with the heart rate.

The microcontroller forms the main component of the wireless PPG sensor, since it serves as an integrated data acquisition system incorporating several features, including low power consumption, compact size, and low cost. It converts analogue skin impedance signals to their digital equivalents prior to processing them. Additionally, the microcontroller communicates with the wireless block through the UART serial port.

The wireless block performs RF communication between the PPG sensor and a remote receiver via Wi-Fi connectivity. Collected data is relayed over a UART serial port to a Wi-Fi module, which transmits the same to a laptop or a personal computer (PC). The Wi-Fi module was selected owing to its free bandwidth and wide operating range (typically 50 m). The power-supply block dissipates power to other components at the required supply voltage, which is regulated to achieve optimum device functionality.

3. Results and Discussion

3.1. Device Implementation. The proposed setup uses the “finger clips” sensor manufactured by Kyto Electronics (finger pulse sensor HRM-2511B), as depicted in Figure 5(a). Additionally, the monitoring device comprises optoelectronic components, an infrared LED, and a phototransistor. The LED cathode and phototransistor emitter were electrically connected with each other as well as other devices using a standard 3.5 mm connection jack.

The analogue preprocessing circuit was built using a standard 2-layer FR4 PCB board (1.6 mm thickness), as depicted in Figure 5(b). The PCB schematic and board layout were developed using the Altium Design tool. The PCB board measured $20 \times 22 \text{ mm} \times 1.6 \text{ mm}$. The Microchip operational amplifier—MCP6004—and Maxim Integrated voltage reference—MAX6190—were selected as components of the PPG analogue preprocessing circuit. MCP6004 is a low-power amplifier that exhibits other features favourable for analogue preprocessing, as described in [26]. MAX6190 is a precision, micropower, and low-dropout voltage reference. It has a maximum series-mode bandgap referencng of $35 \mu\text{A}$ quiescent supply current, which makes it ideal for use in combination with battery-powered instruments [27].

An Arduino Beetle board was selected for use in signal processing owing to its ease of use, easy availability, and flexibility with regard to creation of powerful applications while using preexisting libraries. The said Beetle board is depicted in Figure 5(c). Because this is an early stage in the design and development of the intended device, minimum hardware that is both power-efficient and cost-effective was considered herein.

The Arduino Beetle is a minimized version of the powerful Arduino Leonardo board, albeit it offers identical functionalities. Its key feature is its compactness—it measures only $20 \times 22 \text{ mm}$. Additional features of this board are listed in [28].

For wireless data transmission, a 2.4 GHz ESP8266 Wi-Fi module, depicted in Figure 5(d), was employed in this study. The ESP8266 offers a complete, self-contained Wi-Fi networking solution that can either be applied ad hoc or using

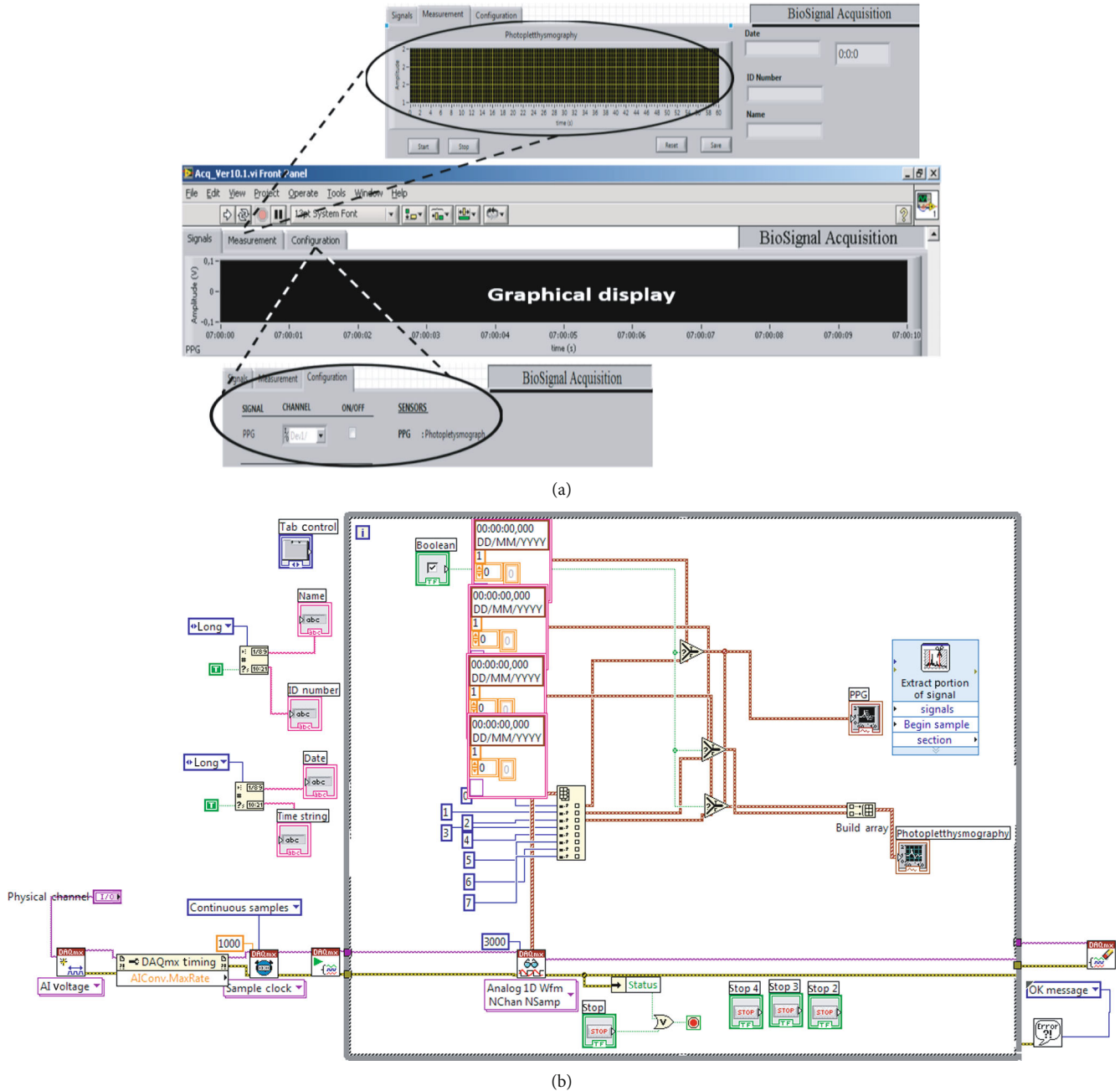


FIGURE 6: LabView virtual instrumentation for PPG acquisition. (a) GUI developed in LabView. (b) Signal acquisition algorithm.

a network infrastructure. Additional features concerning the ESP8266 Wi-Fi platform can be found in [29].

Figure 5(e) depicts the first version of the proposed wireless PPG module hardware. As can be seen, the front-end analogue preprocessing unit is interfaced with the Arduino Beetle board and ESP8266 Wi-Fi module. The front-end analogue preprocessing unit was designed to match the size of the Arduino Beetle board. A stackable system was formed with the front-end analogue preprocessing unit, Arduino Beetle, and ESP8266 Wi-Fi module comprising the bottom, middle, and top layers of the system, respectively. All blocks within the device were regulated to operate at 3 V voltage. The power source employed two 3 V coin batteries and

consumed approximately 500 mW power when operating in the active mode, which was defined in accordance with the power consumed by main components—the sensor, preamplifier (preamp), microcontroller, and Wi-Fi module [26–30].

3.2. GUI Implementation. The LabView software was used to develop a graphical user interface (GUI) to monitor the shape of blood pressure signals, as illustrated in Figure 6.

Signals obtained from the wireless PPG sensor can be scanned, configured, and examined using the GUI, as depicted in Figure 6(a), which shows variations in the blood pressure signal amplitude (V) against acquisition time (s). In this study, blood pressure signals obtained from different

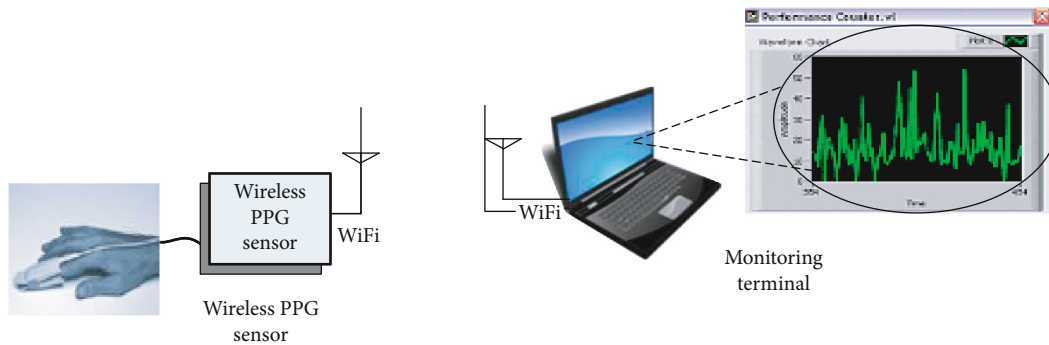


FIGURE 7: Experimental setup used in this study.



FIGURE 8: Finger clip pulse sensor.

participants were preprocessed, collected, and stored on a dedicated database. The proposed algorithm continuously acquires and processes raw blood pressure data, as depicted in Figure 6(b), and several toolboxes were employed in conjunction with the LabView software for rapid blood pressure data acquisition and monitoring [31]. Blood pressure signals acquired from participants were stored in a data logger for future psychophysiology and healthcare research purposes.

3.3. Experimental Procedure. During experiments performed in this study, PPG signals were collected using a finger clip instrument; the operation of which is based on the transmission photoplethysmography phenomenon. An IR-LED installed within the finger clip (with approximately 18 mA current rating) emits infrared waves through the finger, subsequent to which the photodiode performs signal detection, thereafter converting them to corresponding voltage values using a voltage-divider circuit. This generated signal corresponds to the volume of blood flowing within the finger, and therefore, reflects pulse waves generated within blood vessels. Experiments and tests were performed to assess the proposed PPG sensor system. The experimental setup is depicted in Figure 7.

During experiments, the PPG sensor—via the finger clip instrument—was attached to a healthy participant finger to obtain biosignals (Figure 8). Acquired biosignals were transmitted to the processing module for preprocessing, storage,

analysis, and organizing data into packets for transmission over the Wi-Fi module. These data packets received by the monitoring terminal (notebook/PC) along with raw PPG biosignals were stored in the data logger, and the same can be viewed in GUI.

3.4. Experimental Results and Discussions. Figure 9 depicts the graphical representation of blood pressure signals. Processed signals can be stored locally on a notebook or personal computer.

Using the above interface (Figure 9), users can observe the shape of their blood pressure signal and associated variation trends in real time during the monitoring experiment. This facilitates early detection of anomalies in blood pressure detection.

Results obtained via assessment of raw blood pressure signals acquired from healthy participants are depicted in Figure 10. Data stored in the data logger during measurement as well as blood pressure signals include artefacts owing to interference of ambient light.

Hertzman [22] defined two important PPG-AC pulse waveform phases—anacrotic (rising edge of a pulse) and catacrotic (falling edge of a pulse). The shape of a blood pressure signal representing the anacrotic and catacrotic phases is depicted in Figure 11 (using the signal from Figure 10 above).

The anacrotic phase denotes the systolic pressure, whereas the catacrotic phase concerns the diastolic pressure and peripheral wave reflections. As depicted in the figure, a dicrotic notch can be observed in the catacrotic phase for participants demonstrating a compliant healthy arterial system.

The PPG signal depicted in Figure 9 can be directly observed during blood pressure measurements with regard to the systolic and diastolic phases. The context of this research is limited to providing raw blood pressure data. However, its scope can be extended to include an analytic method that facilitates estimation of cuffless blood pressure using the PPG signal generated in this research. The regression tree is a suitable analytic approach that can be used for blood pressure estimation [32]. Raw PPG signals require initial processing (preprocessing) to smoothen (i.e., remove signal artefacts) PPG signals. A filter can be employed to perform the said preprocessing, which can subsequently be followed by two-dimensional normalization (width and

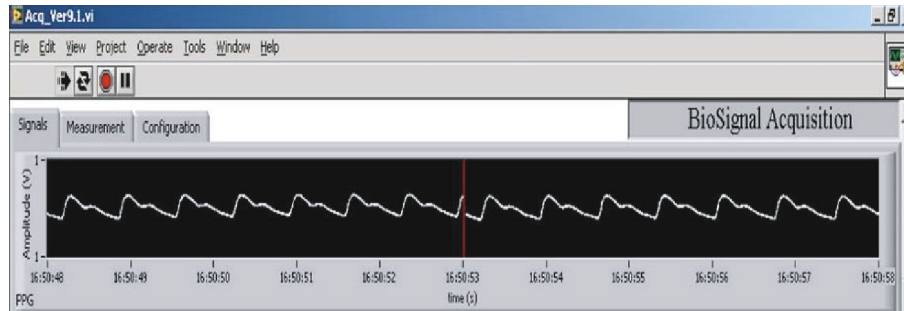


FIGURE 9: Graphical representation of blood pressure signals.

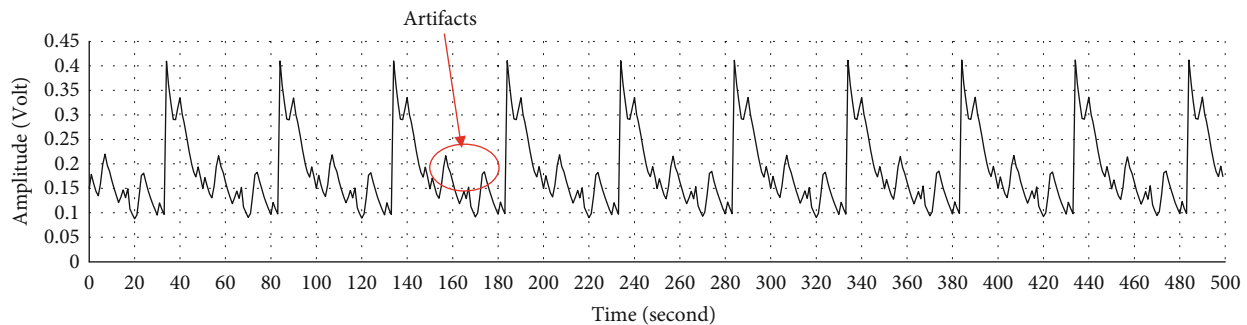


FIGURE 10: Raw blood pressure signal data obtained via photoplethysmography measurement.

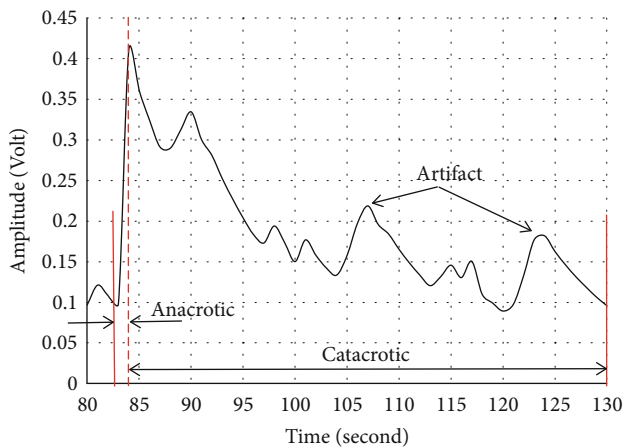


FIGURE 11: Shape of raw blood pressure signal depicting anacrotic and catacrotic phases.

amplitude) of filtered PPG signals. Preprocessed PPG segments comprise pulse area, rising time, and widths of range 25%, 50%, and 75%. Thus, the three most significant PPG waveform features are the pulse area, pulse rising time, and pulse width of 25%, which can be further processed using the regression tree.

4. Conclusions

This paper presents a simple, compact, inexpensive, power-efficient, comfortable, noninvasive, real-time, and durable wireless photoplethysmograph sensor for monitoring the

shape of blood pressure signals. This study implements the first version of the said wireless photoplethysmograph sensor, and initial assessment results (for stationary test scenarios) reveal realisation of reliable blood pressure signal shape monitoring. Additionally, the proposed wireless sensor provides raw blood pressure data that can be utilized for future blood pressure estimations and classifications. In the proposed system, artefacts within PPG signals can be reduced by attaching a Velcro strip around the finger, minimizing ambient light interference, and ensuring accurate placement of the sensor on the participant's finger.

The proposed device in conjunction with a wearable system can be implemented to support further research pertaining to psychophysiology and healthcare applications. As a future endeavour, the authors intend to develop a more convenient and compact wireless PPG wearable sensor capable of acquiring data during physical activities. The said sensor can be combined with an analytic method to accurately estimate and classify blood pressure levels.

Data Availability

Research data is not available owing to concerns related to participant privacy.

Conflicts of Interest

The authors declare no conflict of interest.

Acknowledgments

The authors would like to thank the Ministry of Science and Technology of Taiwan (MOST 107-3113-E-008-003) for funding this research.

References

- [1] Q. Wang, Y. Wang, Z. Mei, and Z. Liu, "An improved algorithm for non-invasive blood pressure measurement," in *International Symposium on Bioelectronics and Bioinformatics 2011*, pp. 41–44, Suzhou, China, November 2011.
- [2] Z. Marcinkevics, M. Greve, J. I. Aivars, R. Erts, and A. H. Zehtabi, "Relationship between arterial pressure and pulse wave velocity using photoplethysmography during the post-exercise recovery period," *Acta Universitatis Latviensis*, vol. 753, pp. 59–68, 2009.
- [3] B. P. McGrath, "Ambulatory blood pressure monitoring," *The Medical Journal of Australia*, vol. 176, no. 12, pp. 588–592, 2002.
- [4] V. K. Jayasree, P. J. Shaija, V. P. N. Nampoori, C. P. Girijavallabhan, and P. Radhakrishnan, "A simple and novel integrated opto-electronic system for blood volume pulse sensing and heart rate monitoring," *International Journal of Optomechatronics*, vol. 1, no. 4, pp. 392–403, 2007.
- [5] M. Ghamari, C. Soltanpur, S. Cabrera, R. Romero, R. Martinek, and H. Nazeran, "Design and prototyping of a wristband-type wireless photoplethysmographic device for heart rate variability signal analysis," in *2016 38th Annual International Conference of the IEEE Engineering in Medicine and Biology Society (EMBC)*, pp. 4967–4970, Orlando, FL, USA, August 2016.
- [6] T. Shimazaki and S. Hara, "Design of PPG-based heart rate sensor enabling motion artefact cancellation," *Heart*, vol. 100, no. 60, p. 20, 2015.
- [7] P. Gothwal, "Designing of PPG based heart-beat monitor," *International Journal for Research in Applied Science & Engineering Technology*, vol. 4, no. VIII, pp. 86–89, 2016.
- [8] K. O. Enalume and A. M. Epemu, "Development of a reflectance photoplethysmogram based heart rate monitoring device," *International Journal of Medical Imaging*, vol. 5, no. 5, pp. 53–57, 2017.
- [9] R. Zangróniz, A. Martínez-Rodrigo, M. López, J. Pastor, and A. Fernández-Caballero, "Estimation of mental distress from photoplethysmography," *Applied Sciences*, vol. 8, no. 1, p. 69, 2018.
- [10] D. U. Uguz, B. Venema, S. Leonhardt, and D. Teichmann, "Multifunctional photoplethysmography sensor design for respiratory and cardiovascular diagnosis," *World Congress on Medical Physics and Biomedical Engineering 2018. IFMBE Proceedings, vol 68/2*, L. Lhotska, L. Sukupova, I. Lacković, and G. Ibbott, Eds., pp. 905–909, Springer, Singapore, 2018.
- [11] S. Botman, D. Borchevkin, V. Petrov, E. Bogdanov, M. Patrushev, and N. Shusharina, "Photoplethysmography-based device designing for cardiovascular system diagnostics," *World Academy of Science, Engineering and Technology International Journal of Medical, Health, Biomedical, Bioengineering and Pharmaceutical Engineering*, vol. 9, no. 9, pp. 689–693, 2015.
- [12] M. Leier, K. Pilt, D. Karai, and G. Jervan, "Smart photoplethysmographic sensor for pulse wave registration at different vascular depths," in *2015 37th Annual International Conference of the IEEE Engineering in Medicine and Biology Society (EMBC)*, pp. 1849–1852, Milan, Italy, August 2015.
- [13] T. Ishikawa, Y. Hyodo, K. Miyashita, K. Yoshifuji, Y. Komoriya, and Y. Imai, "Wearable motion tolerant PPG sensor for instant heart rate in daily activity," in *Proceedings of the 10th International Joint Conference on Biomedical Engineering Systems and Technologies (BIOSTEC 2017)*, pp. 126–133, Porto, Portugal, 2017.
- [14] J. Spigulis, R. Erts, V. Nikiforovs, and E. Kviesis-Kipge, "Wearable wireless photoplethysmography sensors," in *Proceedings Volume 6991, Biophotonics: Photonic Solutions for Better Health Care; 69912O*, pp. 126–133, Strasbourg, France, May 2008.
- [15] *Apple Watch series 4* June 2019, <https://www.apple.com/watch/>.
- [16] *Fitbit Ionic™ Watch* June 2019, <https://www.fitbit.com/ionic>.
- [17] *Garmin* June 2019, <https://www.garmin.com/en-US>.
- [18] A. Peters, *The British Medical Association Illustrated Medical Dictionary*, Dorling Kindersley Ltd, London, United Kingdom, 2nd edition, 2007.
- [19] A. Reisner, P. A. Shaltis, D. McCombie, and H. H. Asada, "Utility of the photoplethysmogram in circulatory monitoring," *Anesthesiology*, vol. 108, no. 5, pp. 950–958, 2008.
- [20] M. Hirai, S. L. Nielsen, and N. A. Lassen, "Blood pressure measurement of all five fingers by strain gauge plethysmography," *Scandinavian Journal of Clinical & Laboratory Investigation*, vol. 36, no. 7, pp. 627–632, 1976.
- [21] *Figures* January 2019, <http://www.cnsystems.at/en/vascular-unloading-technique>.
- [22] A. B. Hertzman, "Observation on the finger volume pulse recorded photoelectrically," *American Journal of Physiology*, vol. 119, pp. 334–335, 1937.
- [23] J. W. Clark, M. R. Neuman, W. H. Olson et al., *Medical instrumentation: application and design*, Wiley, 1998.
- [24] J. Allen, "Photoplethysmography and its application in clinical physiological measurement," *Physiological Measurement*, vol. 28, no. 3, pp. R1–R39, 2007.
- [25] J. Ando, A. Kawarada, M. Shibata, K. Yamakoshi, and A. Kamiya, "Pressure-volume relationships of finger arteries in healthy subjects and patients with coronary atherosclerosis measured non-invasively by photoelectric plethysmography," *Japanese Circulation Journal*, vol. 55, no. 6, pp. 567–575, 1991.
- [26] *Microchip operational amplifier MCP6004* December 2018, <http://ww1.microchip.com/downloads/en/DeviceDoc/21733j.pdf>.
- [27] *Maxim Integrated voltage reference MAX6190* December 2019, <http://datasheets.maximintegrated.com/en/ds/MAX6190-MAX6198.pdf>.
- [28] *Arduino Beetle* March 2019, http://www.dfrobot.com/wiki/index.php/Beetle_SKU:DFR0282.
- [29] *Wi-Fi Module - ESP8266* January 2019, <https://www.sparkfun.com/products/13252>.
- [30] *PPG_kyto_hrm2511* March 2019, http://www.geertlangereis.nl/sensorwiki/doku.php?id=methods:ppg:ppg_kyto_hrm2511.
- [31] J. Olansen and E. Rosow, *Virtual Bio-Instrumentation, Biomedical, Clinical and Healthcare Applications in LabVIEW*, Prentice Hall PTR, 2002.
- [32] S. G. Khalid, J. Zhang, F. Chen, and D. Zheng, "Blood pressure estimation using photoplethysmography only: comparison between different machine learning approaches," *Journal of Healthcare Engineering*, vol. 2018, 13 pages, 2018.

Research Article

Bed Position Classification by a Neural Network and Bayesian Network Using Noninvasive Sensors for Fall Prevention

Waranrach Viriyavit ^{1,2} and Virach Sornlertlamvanich ^{1,3}

¹School of ICT, Sirindhorn International Institute of Technology, Thammasat University, Pathum Thani 12120, Thailand

²Department of Medical Engineering, Chiba University, Chiba 263-8522, Japan

³Department of Data Science, Musashino University, Tokyo 135-8181, Japan

Correspondence should be addressed to Virach Sornlertlamvanich; virach@gmail.com

Received 16 August 2019; Revised 9 December 2019; Accepted 3 January 2020; Published 31 January 2020

Guest Editor: Andrej Kosir

Copyright © 2020 Waranrach Viriyavit and Virach Sornlertlamvanich. This is an open access article distributed under the Creative Commons Attribution License, which permits unrestricted use, distribution, and reproduction in any medium, provided the original work is properly cited.

Falls from a bed often occur when an elderly patient attempts to get out of bed or comes close to the edge of a bed. These mishaps have a high possibility of serious injuries, such as bruises, soreness, and bone fractures. Moreover, a lack of repositioning the body of a bedridden elderly person may cause bedsores. To avoid such a risk, a continuous activity monitoring system is needed for taking care of the elderly. In this study, we propose a bed position classification method based on the sensor signals collected from only four sensors that are embedded in a panel (composed of two piezoelectric sensors and two pressure sensors). It is installed under the mattress on the bed. The bed positions considered are classified into five different classes, i.e., off-bed, sitting, lying center, lying left, and lying right. To collect the training dataset, three elderly patients were asked for consent to participate in the experiment. In our approach, a neural network combined with a Bayesian network is adopted to classify the bed positions and put a constraint on the possible sequences of the bed positions. The results from both the neural network and Bayesian network are combined by the weighted arithmetic mean. The experimental results have a maximum accuracy of position classification of 97.06% when the proportion of coefficients for the neural network and the Bayesian network is 0.3 and 0.7, respectively.

1. Introduction

Due to the significant growth of the elderly population in today's demography, the needs of geriatric care have increased. A survey of the National Statistical Office of Thailand has shown that the single elderly increased to 8.7% in 2014, and 18.76% of the elderly population live with their spouse only [1]. This is one of the results from gradual changes in the Thai social structure. Most young people have to spend their time earning money. Increasingly, elderly people are abandoned to stay alone at home or are left in a nursing home during working hours.

Without being carefully watched over, elderly patients can fall which is a major cause of trouble in nursing care [2]. The accident can cause severe injuries, such as bruises, soreness, and bone fractures. The National Statistical Office

of Thailand reported that 11.6% of elderly people have experienced a fall, and 46.3% of them were treated and 7.8% of them were hospitalized as an inpatient [1]. Moreover, falls are the leading cause of death and disability in elderly people, as high as 40.4% [3]. An injury at a higher age has a higher possibility of death because of health weaknesses [1]. The Department of Disease Control, Ministry of Public Health of Thailand, reported that 1,049 elderly people died from falls in 2015 [4]. In 2014, Tsai et al. conducted a study of the factors of fall injuries in the elderly patients at a medical center in Taiwan [5]. They found that 8.7% of elderly patients who participated in the study had repeatedly fallen in the previous year. Some of them (28.6%) fell at the bedside, in which most of the cases are an unassisted bed exit [5]. However, there is also a risk of rolling out of bed when an elderly patient lies too close to the edge of the bed. In addition, the bedridden

elderly patients are often unable to reposition themselves, which is a cause of bedsores. Desirable bodily movement can alleviate the prolonged pressure over the body. The most widely accepted way of preventing bedsores is to turn the elderly body every two hours. Therefore, continuous monitoring is inevitable for the elderly to prevent falls and bedsores. This requires a large number of caregivers with respect to the growth of the elderly population. Geriatric care can be highly costly and faces a shortage in the number of caregivers, which is only 11.1% of the elderly population as reported in [1]. This is leading to an inefficiency of nursing care services in the near future. The monitoring system for bed fall and bedsores prevention can be a complementary utility to support caregivers and to diminish their workloads. The system must be able to detect the position of an elderly patient on the bed and movement which comes close to falling in an allowable time period for a caregiver to assist the elderly patient.

A wearable device is widely used for an elderly activity monitoring system [6, 7]. However, in most cases, the elderly can feel uncomfortable with their daily living activities, which leads to discontinuous monitoring [8, 9]. Also, a video camera is unacceptable for the elderly because of privacy concerns. As a result, a noncontact sensing device is a proper approach for continuously monitoring elderly activity [10–29]. There are some reports of using an ultrasonic sensor, air pressure sensor, and vibration sensor [10–12]. Though the aforementioned studies can determine whether the patient is in the bed or not, this is not enough to prevent a fall. To prevent falls, the system needs to detect the position of lying with respect to the edge of the bed. To prevent bedsores, the duration of the same position of lying can be observed by monitoring movement. Some previous studies used commercial pressure mat systems to detect the bed position [13–21]. However, their proposed pressure mat systems need a large number of sensors which are not practical and are costly in actual practice. Some studies proposed approaches to reduce the number of sensing array sensors. The minimum number of sensors in the aforementioned studies is 16 sensors, as reported by Hsia et al. [21]. Although the studies have shown promising results in bed position classification, their approaches still require quite a large number of sensors. For this concern, we reduced the number of sensors to only four in our study while maintaining high accuracy in bed position classification.

In this paper, we propose a bed position classification based on a neural network combined with a Bayesian network, with signals from only four sensors. The results of our study can be applied to prevent elderly bedsores and bed falls. We classify the bed positions into five classes, namely, off-bed, sitting, lying center, lying left, and lying right. The off-bed and sitting positions are highly important for detecting the bed exit activity because they normally are the positions just before or after the bed exit according to our statistical analysis. With the bed position, the system will alert the caregiver to assist an elderly patient to prevent falls when the elderly patient moves towards the edge of the bed. The system will also alert

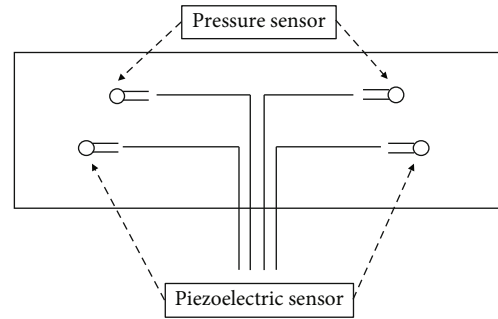


FIGURE 1: Sensor panel.

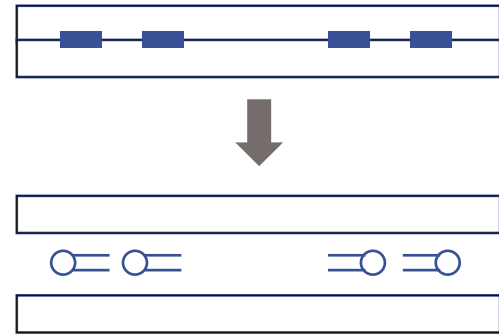


FIGURE 2: Components of a sensor panel.

the caregiver to turn the elderly patient's body when staying in the same position for almost the allowed time period (normally two hours) to prevent bedsores.

2. Materials

2.1. Sensor Panel. The sensor panel is a ready-made set of sensors provided by AIVS Co., Ltd. The size of the panel is 60×18 cm. The panel is equipped with two types of sensors, i.e., two piezoelectric sensors and two pressure sensors. Each pair of sensors is embedded symmetrically on each side of the panel as shown in Figure 1. The sensors are sandwiched between two ABS boards, which has an advantage in stiffness and being firm and difficult to bend. The sandwich structure keeps the sensors firm avoiding the signal distortion as shown in Figure 2.

To detect the weight applied on the bed, we use two low-cost force-resistive sensors (FRS) from Interlink 402. Each is installed on the left and the right side of the panel. The FRS consists of two membranes separated by a thin air gap. Resistance decreases when force is applied, and resistance is infinite when force is zero. The force sensitivity range is ~ 0.2 to 20 N. The temperature operating range is -30 to 70°C . The sensor is low-cost and can be used to detect physical pressure, squeezing, and weight, though it is rarely accurate. However, its sensitivity is sufficient for detecting a weighted object on the bed.

The piezoelectric sensor, Murata Piezoelectric Diaphragms 7BB-15-6L0, can change the energy between the kinetic energy and electric energy. When a vibration force is applied, the voltage is changed. The resonance frequency

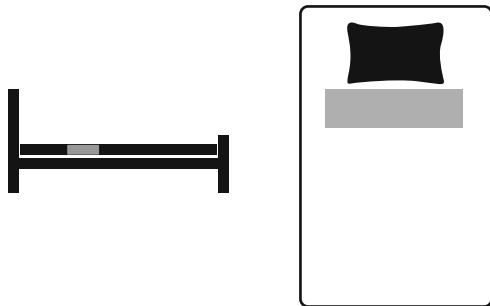


FIGURE 3: Sensor panel under the mattress in the thoracic area.

is 2.8 kHz. In the sensor panel, it is installed to detect the vibration transmitted from the patient activities.

The combination of both pairs of different types of sensors is used to detect the position from each side of the body on the bed. The panel is simply set under the mattress in the thoracic area, as shown in Figure 3. The panel is fixed to the bed board to keep the constant relative position to the patient body. It is designed to work 24 hours in common use, avoiding the wet circumstance since there is not much temperature change in the hospital ward or at home. In our case, the sensor is not designed to be used in a severe condition.

Placing the panel in such a position can distinguish between sitting and lying positions on the bed. Figure 4 shows the correlation between signals of four sensors and positions. For example, Figure 4(a) is the signal of four sensors of the off-bed position. The activation of both sensor signals is low compared to the signal of the sitting position which has low activation of pressure signals while the signals from the piezoelectric sensors are still being detected. Normally, the signals from the piezoelectric sensors in any positions on the bed show high activation, whereas they are very low in the off-bed position. The pair of pressure sensors can be used to distinguish between the positions of lying. For example, in the lying center position, the weight of the body is on both sides of the sensors while in the lying left or lying right positions, only one side of the sensors is activated, as shown in Figures 4(c)–4(e). In lying positions, the activation of pressure sensors is quite high in contrast to sitting positions in which the activation of the pressure sensors is low.

2.2. Data Structure. The control device outputs a package of data in a sample rate of 30 samples in one second. The data package contains 45 bytes. It is divided into 3 parts: 8 bytes for the header, 34 bytes for the data from four sensors, and 3 bytes for the ender. In the 34 bytes for the data from four sensors, the first two bytes contain the sensor ID, and the next 32 bytes contain four 8-byte blocks (one block for each sensor), i.e., the left piezoelectric signal, left pressure signal, right piezoelectric signal, and right pressure signal. The magnitude of the sensors is 256. The range of the value of the piezoelectric signal is -127 to 128, and the pressure signal is from 0 to 256. The sampling rate of each sensor is 30 Hz. Table 1 shows the details of the structure of the signal data package.

2.3. Data Collection. The collected data include the sensor signal data and the corresponding videos. Three elderly patients, whose ages are between 60 and 85, participated in the experiment. To evaluate the effects of the environment, the data from two different rooms are collected with different sets of sensors. The data of two patients are collected from two different rooms. The total collected data are 459 hours long. The position labels are annotated by observing the corresponding video. The position labels are defined in five classes, i.e., off-bed (O), sitting (S), lying center (C), lying left (L), and lying right (R). The definition of each position is described as follows:

- (i) Off-bed (O): nobody is on the bed
- (ii) Sitting (S): a subject is sitting on the bed
- (iii) Lying center (C): a subject is lying in the center of the bed
- (iv) Lying left (L): a subject is lying on the left-hand side of the bed
- (v) Lying right (R): a subject is lying on the right-hand side of the bed

Lying left (L) and lying right (R) positions are defined as positions in which the subject is lying on either the left or the right side of the bed, regardless of the subject's lateral position. An ambiguous position or changing movement is not considered in this experiment.

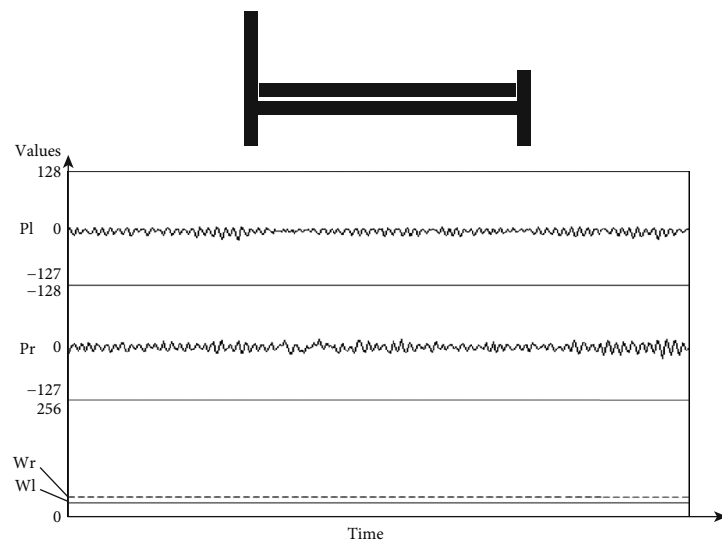
The structure of the dataset is shown in Figure 5. Each set of the accumulated data is composed of 30 samples \times 4 sensors = 120 samples, which is called the *time slot* in one second. The holding period of one position is called the *interval time*. Normally, one position held in one interval time lasts more than one second. Therefore, there are many time slots in one interval time. The time length of each position can then be measured by accumulating the number of time slots. The change of interval time shows the change of position. The sequence of changing positions can then be detected by the sequence of time intervals.

3. Position Detection

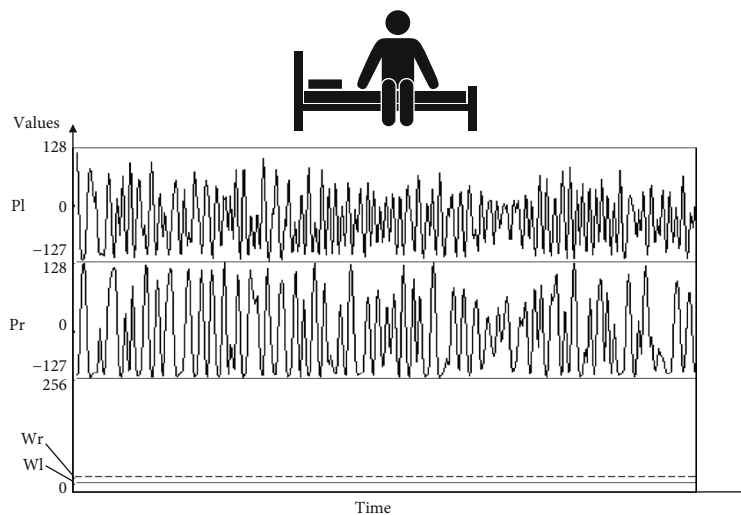
3.1. Position Classification by the Neural Network. To classify a position on the bed, the signal data from the control device output, i.e., the left piezoelectric signal (P_l), right piezoelectric signal (P_r), left pressure signal (W_l), and right pressure signal (W_r), are used as the input for the neural network. These four inputs are passed through the neural network as defined in (1) and depicted in Figure 6.

$$X = \{x_1, x_2, x_3, x_4\} = \{P_l, W_l, P_r, W_r\}. \quad (1)$$

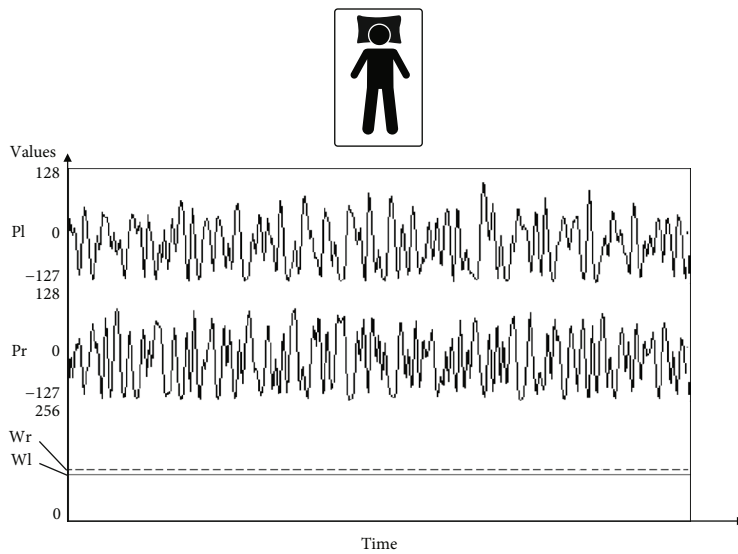
Since the initial weight and the scale of the signal from the piezoelectric sensor and pressure sensor are different, instead of using the raw values from the sensors, we apply the unity-based normalization (or feature scaling) method to eliminate the biases of the weight from different bodies



(a) Off-bed



(b) Sitting



(c) Lying center

FIGURE 4: Continued.

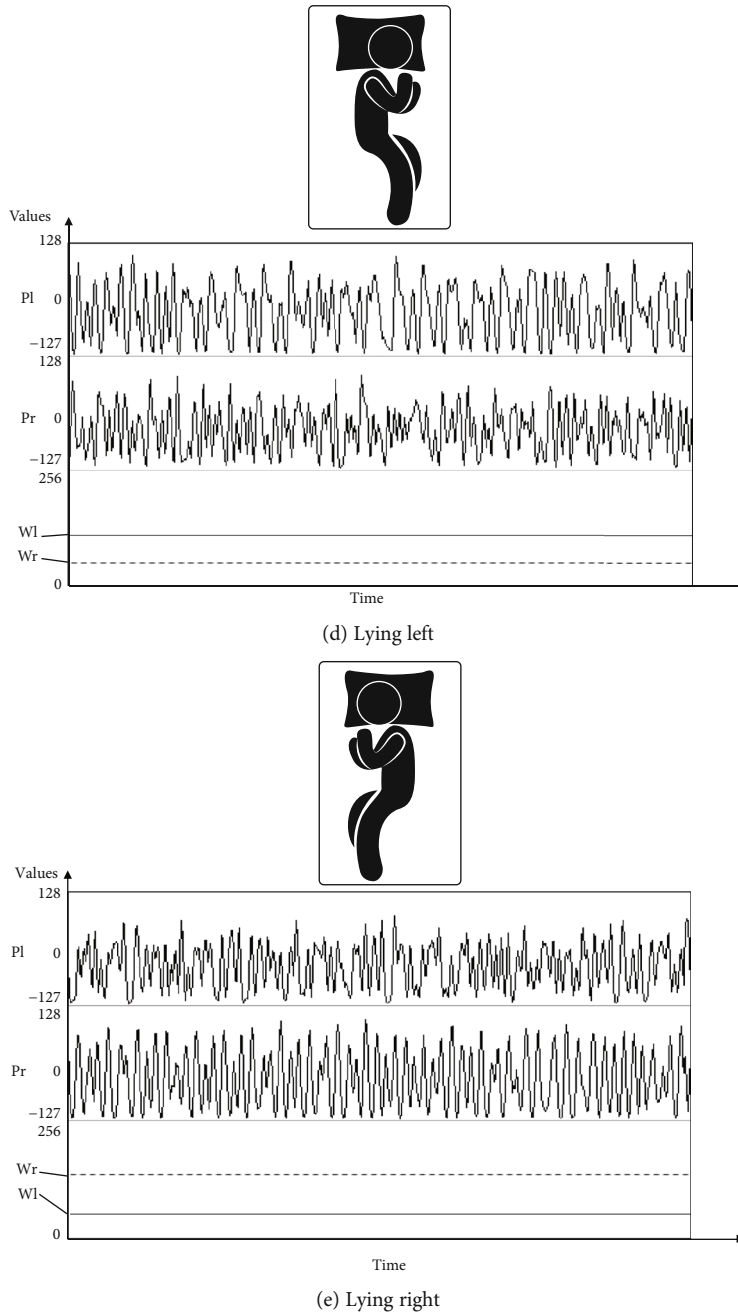


FIGURE 4: Correlation between signals and positions, where the first bold line is the signal of the piezoelectric sensor on the left, the second bold line is the signal of the piezoelectric sensor on the right, the solid line is the signal of pressure on the left, and the dashed line is the signal of pressure on the right.

and the different types of sensors. All sensor data are normalized into the same range of 0 to 1 by [30]

$$Y_i = \frac{x_i - \min}{\max - \min}, \quad (2)$$

where Y_i is the normalized value, x_i is the sensor data in the i^{th} time position of the sequence, min is the minimum value, and max is the maximum value of the collection.

To accumulate the signal data in one second from the property of the sensors where the sampling rate is 30 Hz,

one set of data is composed of 30 samples of 4 types of sensors, which makes 120 data signals as defined in

$$X = \{x_1, x_2, x_3, \dots, x_{120}\} \\ = \{P_{l1}, W_{l1}, P_{r1}, W_{r1}, P_{l2}, W_{l2}, P_{r2}, W_{r2}, \dots, P_{l120}, W_{l120}, P_{r120}, W_{r120}\}. \quad (3)$$

3.2. Estimation of Consecutive Position by the Bayesian Network. In normal practice, not all positions are equally transitioned to form a specific position. For example, it is

TABLE 1: Structure of the signal data package.

Header	Sensor ID	Piezo right	Data from four sensors Weight right	Piezo left	Weight left	Ender
8 bytes	2 bytes	8 bytes	8 bytes	8 bytes	8 bytes	3 bytes

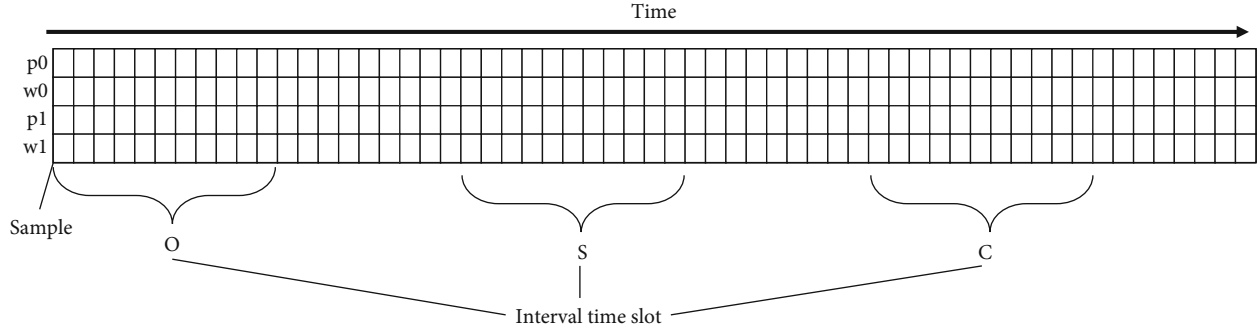


FIGURE 5: Structure of the dataset.

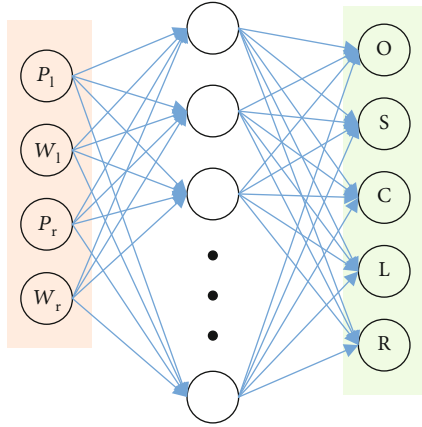


FIGURE 6: Neural network diagram of four input signal types, where O is off-bed, S is sitting, C is lying center, L is lying left, and R is lying right.

more likely that a subject will sit on the bed before lying down to a sleeping position, while it is rarely found that a subject will jump to lying down on the opposite side of the bed. To estimate the next possible transition positions, the Bayesian network [31] is applied. This method can depress the noise of the signal that is caused by other activities in an uncontrolled environment. The probability of a consecutive position can be estimated by the former n positions and the current signal, as shown in (4) and (5) for the trigram model estimation.

$$P(S, P) = P(S)P(P | S) = P(P)P(S | P), \quad (4)$$

$$P(S, P) = P(P_i | P_{i-1}, P_{i-2})P(S | P_i), \quad (5)$$

where P_i , P_{i-1} , and P_{i-2} are, respectively, the positions in the $(i-2)^{\text{th}}$, $(i-1)^{\text{th}}$, and i^{th} time positions of the sequence. S is the current set of signals consisting of four

sensor signals (P_1 , W_1 , P_r , and W_r). The normalized signal is divided into three levels, i.e., low, middle, and high, by converting the continuous values of signal data to nominal values. For piezoelectric signals, 0-0.25, 0.26-0.50, and 0.51-1 are defined as low, middle, and high, respectively. For pressure signals, 0-0.35, 0.36-0.70, and 0.70-1 are defined as low, middle, and high, respectively.

3.3. Combination of the Neural Network and Bayesian Network. We apply the weighted arithmetic mean for the combination of the results from the neural network and Bayesian network, as shown in Figure 7 and (5).

$$\alpha N + \beta B = C, \quad (6)$$

where N is the neural network probability, B is the Bayesian probability, C is classes, and α and β are coefficients where the sum of α and β is 1.

4. Experiment and Result

4.1. Input Feature Evaluation. To evaluate the coverage of the trained model, the clean datasets are prepared by eliminating the possible noise of the signals. The evaluation set is defined in five categories, i.e., subject A, subject B, subject C, the combination of subject A and subject B in the same room, and the combination of data from two different rooms (subjects A, B, and C). The features of input are conducted for 4 inputs, 120 inputs, 4 inputs with normalized signals, and 120 inputs with normalized signals.

The selected datasets are tabulated in Table 2. The dataset of subject A consists of 2,000 samples (5 positions \times 400 samples), the same as subject B. This means that the combination of subject A and subject B in the same room includes 4,000 samples (5 positions \times 800 samples). For subject C, collected from another room, the dataset includes 1,335 samples (5 positions \times 267 samples). Totally, there are 5,335 samples (5 positions \times 1067 samples) as shown in the ‘‘Total’’ row in

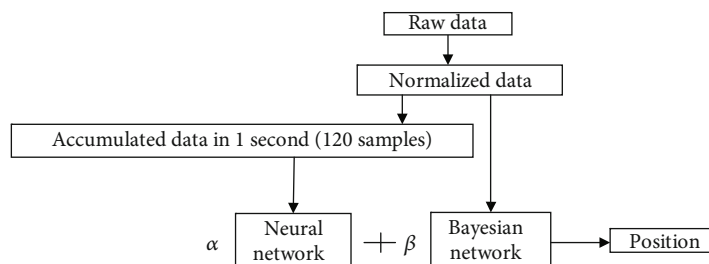


FIGURE 7: Diagram of the position classification approach.

TABLE 2: Small clean dataset.

Subject	Position	Clean dataset			
		Training set		Test set	
		# of samples	# of time intervals	# of samples	# of time intervals
A	Off-bed	280	4	120	4
	Sitting	280	4	120	4
	Lying center	280	4	120	4
	Lying left	280	4	120	4
	Lying right	280	4	120	4
B	Off-bed	280	4	120	4
	Sitting	280	4	120	4
	Lying center	280	4	120	4
	Lying left	280	4	120	4
	Lying right	280	4	120	4
C	Off-bed	187	4	80	4
	Sitting	187	4	80	4
	Lying center	187	4	80	4
	Lying left	187	4	80	4
	Lying right	187	4	80	4
Total	Off-bed	747	12	320	12
	Sitting	747	12	320	12
	Lying center	747	12	320	12
	Lying left	747	12	320	12
	Lying right	747	12	320	12

Table 2. The datasets are selected from four different time intervals for each subject and randomly divided into 70% for training and 30% for testing. In the combination of two rooms, the dataset consists of 12 time intervals, as shown in the “Total” row in Table 2.

Table 3 shows the result of the feature evaluation test with the small clean dataset. The overall performance on the 120 inputs with normalized signals can reach 100% accuracy. In total, the model based on the normalized signal data and the model based on the accumulated signal data of 120 inputs can provide a better result when compared to the 4-input model.

In the off-bed and sitting positions, the signals are quite similar. For example, in the sitting position, the activation of the pressure sensors is low, similar to that in the off-bed position, but not for the signals from the piezoelectric sensors. Therefore, at some points, the signals of both positions

TABLE 3: Accuracy of input features on the small clean dataset.

Dataset	Input			
	Raw signal data		Normalized signal data	
	4 inputs	120 inputs	4 inputs	120 inputs
A (room 1)	99.3	99.8	99.6	99.9
B (room 1)	99.5	100	100	100
C (room 2)	99.9	99.9	100	99.9
A+B (room 1)	97.6	98.2	98.2	98.8
Room 1+room 2	97.2	98.1	98.5	100

look the same, as shown in Figures 8 and 9. In the case of 4 inputs, the accuracy of the off-bed position is 99.2 and that of the sitting position is 93.2, showing an error of 0.8 in

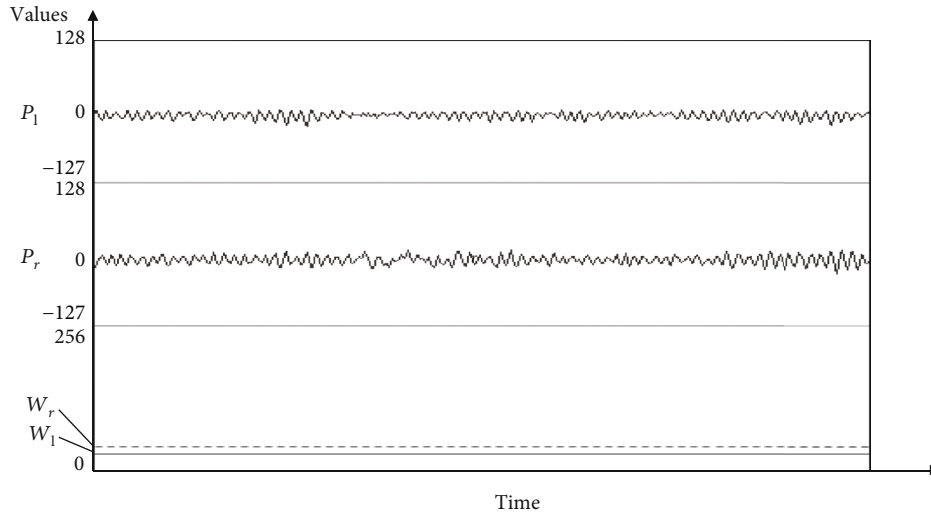


FIGURE 8: Signal of the off-bed position (the first bold line is the signal of the piezoelectric sensor on the left, the second bold line is the signal of the piezoelectric sensor on the right, the solid line is the signal of pressure on the left, and the dashed line is the signal of pressure on the right).

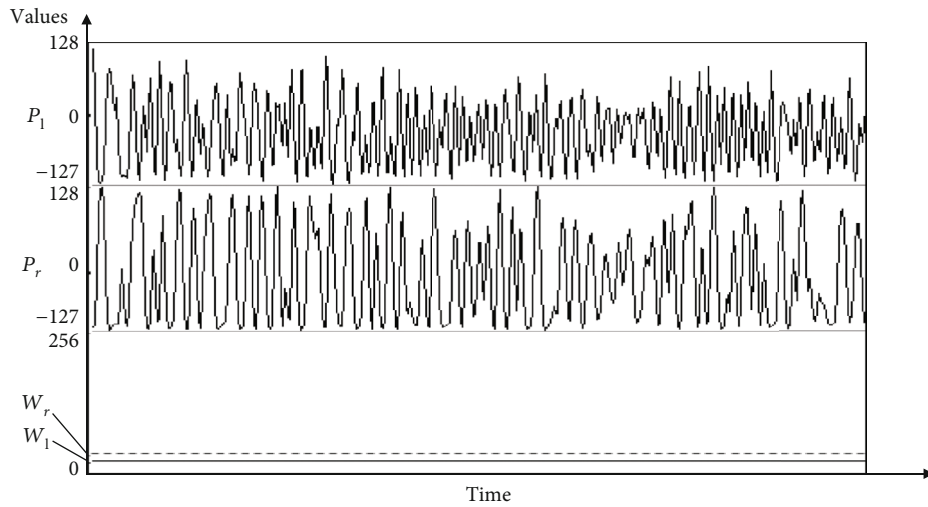


FIGURE 9: Signal of the sitting position (the first bold line is the signal of the piezoelectric sensor on the left, the second bold line is the signal of the piezoelectric sensor on the right, the solid line is the signal of pressure on the left, and the dashed line is the signal of pressure on the right).

classifying off-bed as sitting and an error of 6.8 in classifying sitting as off-bed, as shown in Figure 10.

The accumulation of the signal data in a one-second time slot (120-input set) can solve the confusion between the sitting position and the off-bed position, as shown in Figure 11. This is because by using the 120 inputs, the neural network can capture more context features, to distinguish the off-bed position from the sitting position.

Expanding the size of the dataset on the single subject A from 2,000 to 394,113 samples, we evaluated the features of input in four categories. The selected dataset includes many signal errors and unexpected noise. The dataset is also divided randomly into 70% for training and 30% for testing.

Table 4 shows the number of time intervals, sampled from the position data. The total size of the unclean data-

set of the single subject A consists of 394,113 samples. The sizes of the 5 positions are 44,172, 32,012, 90,486, 4,820, and 222,643 for off-bed (O), sitting (S), lying center (C), lying left (L), and lying right (R), respectively. The total number of time intervals for each position is 42, 160, 111, 26, and 173, respectively.

The result of the feature evaluation test on subject A is shown in Table 5. The best result is 96.64% for the accuracy of the 120 inputs with normalized signals. The accuracy of the larger dataset decreases because of the signal ambiguity. The accuracy of the large and unclean dataset (Table 5) decreases, compared to that of the small and clean dataset as shown in Table 3. The best result of Table 5 is 96.64% while the best result for subject A in Table 3 is 99.9%. This is because the larger dataset includes much-unexpected noise.

	Target class					Output
	Off-bed	Sitting	Lying center	Lying left	Lying right	
Off-bed	99.2	6.8	0	0	0	
Sitting	0.8	93.2	0	0	0	
Lying center	0	0	100	0	0	
Lying left	0	0	0	100	0	
Lying right	0	0	0	0	100	

FIGURE 10: Confusion matrix of the 5-position classification of subject B with 4 inputs.

	Target class					Output
	Off-bed	Sitting	Lying center	Lying left	Lying right	
Off-bed	100	0	0	0	0	
Sitting	0	100	0	0	0	
Lying center	0	0	100	0	0	
Lying left	0	0	0	100	0	
Lying right	0	0	0	0	100	

FIGURE 11: Confusion matrix of the 5-position classification of subject B with 120 inputs.

TABLE 4: Large unclean dataset.

Position	Unclean dataset From one subject			
	Training set		Test set	
	# of samples	# of time intervals	# of samples	# of time intervals
Off-bed	30,650	42	13,522	42
Sitting	22,408	160	9,604	160
Lying center	64,340	111	26,146	111
Lying left	3,674	26	1,146	26
Lying right	15,5850	173	66,793	173
Total	276922	512	117211	512

4.2. *Position Classification by the Combination of the Neural Network and Bayesian Network.* The very large and unclean dataset includes many signal errors and much-unexpected noise. Figures 12 and 13 show some examples of errors. For the signals shown in Figure 12, the signals of the sitting posi-

TABLE 5: Accuracy of the unclean dataset.

Input	Normalized signal data			
Raw signal data	120 inputs		4 inputs	
4 inputs	120 inputs	4 inputs	120 inputs	
95.17	95.45	96.54	96.64	

tion are similar to the signals of the lying right position. This is because the subject gets on/off on the right side of the bed. Before getting out of bed, the subject usually moves to sit on the right side of the bed, applying force on the right pressure sensor. Therefore, sitting before getting out of bed can cause the signal to look similar to lying right.

Similarly, the signals in Figure 14 show the similarity of signal patterns between the lying center position and the lying right position because the subject tends to stay on the right side of the bed.

To solve the problems of signal ambiguity, we introduce the Bayesian network to estimate the likelihood of the consecutive position, to eliminate the unexpected result of the output position from the neural network model. We create the Bayesian network from the large unclean dataset of subject A, as shown in Table 4. All possible connecting positions are calculated from the transition network, as shown in Figure 14. We estimate the Bayesian network by using the position trigram model, according to (5).

The results from both the neural network and the Bayesian network estimations are combined by the weighted arithmetic mean. To evaluate the coefficient (α , β) of the weighted arithmetic mean in (5), the values of α and β are varied for the dataset of subject A, as shown in Table 6. α is the coefficient of neural network probability, and β is the coefficient of Bayesian network probability. The accuracy can reach 97.06% when the proportion of the coefficient for the neural network is 0.3 and that for the Bayesian network is 0.7, as shown in Table 6. As a result of this combination model, the Bayesian network effectively shows the improved performance in position estimation in the case of signal confusing errors.

Looking into the details of improvement, Figure 15 shows a significant change in recognizing the sitting position better by reducing the fault detection of the lying right position, while still maintaining other position classification in similar accuracy. The sitting position detection is improved from 86.10% to 89.07% by reducing the confusion errors of the detection with lying right and out of bed positions from 8.06% to 6.24% and 4.68% to 3.91%, respectively. The improvement of sitting position detection is crucial for care givers in making decision of supporting help.

4.3. *Comparative Evaluation with Other Approaches.* It is quite difficult to evaluate the performance against other approaches because of the differences in datasets, number of bed positions, and number of sensors. The best we can do is to compare the results on the estimation of the common target position. Table 7 is tabulated by accumulating the results of the sleeping position estimation only. Our approach can reach 97.8% accuracy in classifying the three

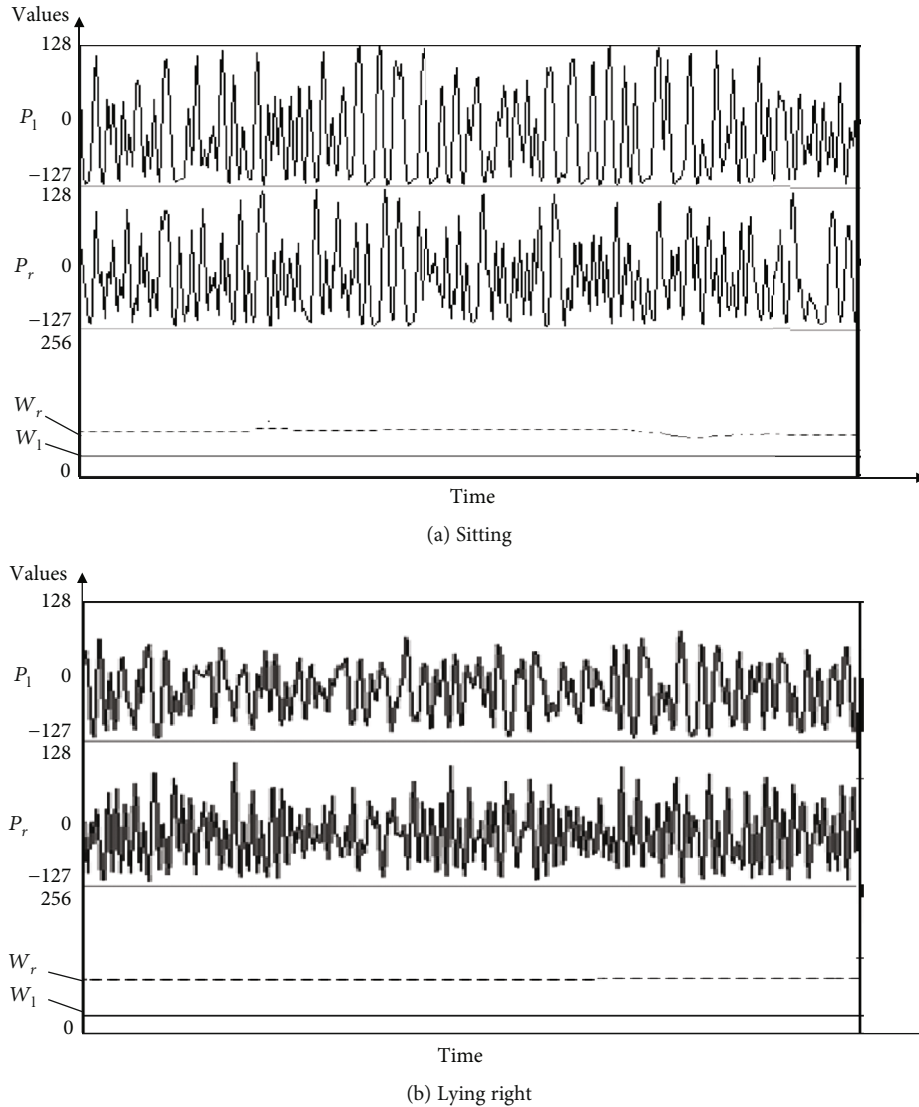


FIGURE 12: Similarity of the signal patterns between the sitting position and lying right position.

sleep positions, i.e., lying center, lying left, and lying right. Our approach, using only four sensors, outperforms the approaches proposed by [13] using 2,048 sensors, [15] using 360 sensors, [18] using 2,048 sensors, [19] using 56 sensors, and [20] using 60 sensors in overall evaluation.

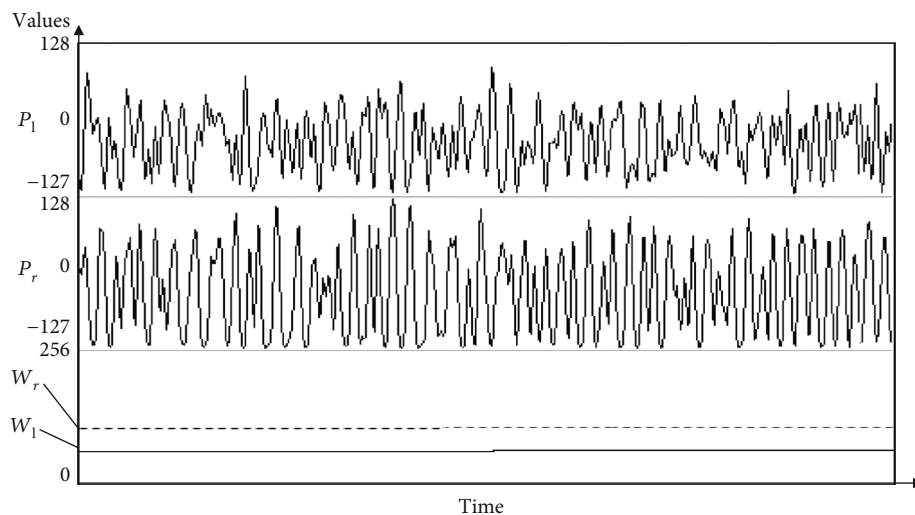
In terms of a position-by-position comparison, there is only one report from Hsia et al. [21], which has the same three bed positions as defined by our model. The position-by-position comparison result is shown in Table 8.

The result of our approach is not the best though it shows that our model is promising with a limited number of sensors, and the model can be created by a small number of testing subjects. In terms of practicality, our approach has advantages in cost performance and maintenance.

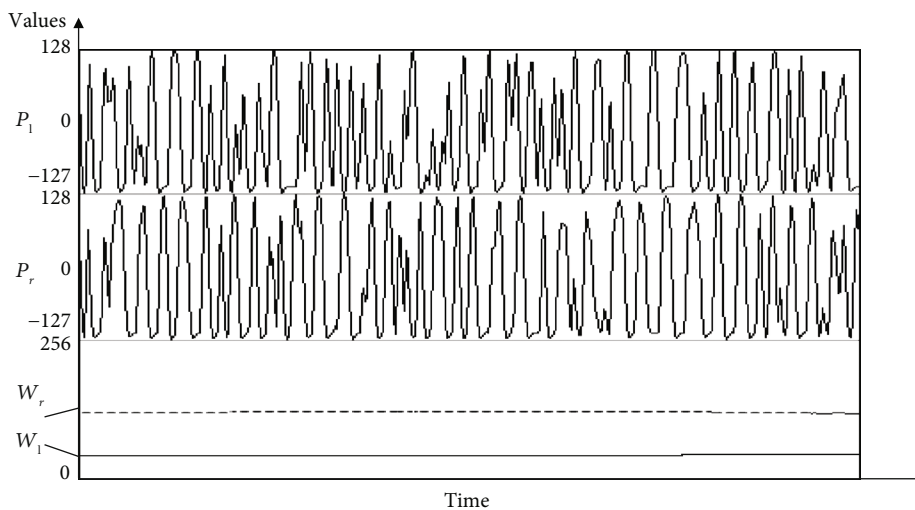
5. Conclusion

A bed alarm for fall prevention needs a highly accurate bed position detection system. The system must be able

to issue an alert as early as possible once it detects a position where there is a high risk of falling. In this study, a neural network is used to classify the signals from the designed sensors into five types of positions. The signal data from the sensors are normalized by using the unity-based normalization (or feature scaling) method to eliminate the biases of body weight and different types of sensors. In addition, the accumulation of the signal data in a one-second time slot (a set of 120 inputs) can also help improve the accuracy of the sitting and off-bed positions. The performance of 120 inputs with normalized signal data yields a better result than the three other types of inputs, i.e., 4 inputs, 4 inputs with normalized signal data, and 120 inputs. Furthermore, when the dataset is extended to a large and unclean dataset, the accuracy of the single neural network model significantly drops. To improve the performance of the neural network approach, we adopt the Bayesian network to restrict the possibility of transition of a position. As a result, the Bayesian network



(a) Lying center



(b) Lying right

FIGURE 13: Similarity of the signal pattern between the lying center position and lying right position.

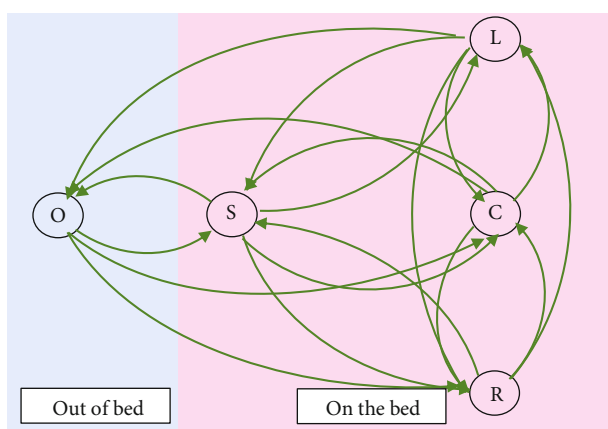


FIGURE 14: State transition of the 5 positions, i.e., off-bed (O), sitting (S), lying center (C), lying left (L), and lying right (R).

TABLE 6: Accuracy of the combination of the neural network and Bayesian network.

α	β	Accuracy rate
1	0	96.64
0.7	0.3	96.74
0.5	0.5	96.85
0.3	0.7	97.06
0	1	91.40

trigram probability effectively improves the accuracy from 96.64% to 97.06%, with a coefficient of 0.3 and 0.7 for the neural network and the Bayesian network probability, respectively. The combination model essentially improves the sitting position detection from 86.10% to 89.07% by reducing the confusion errors of the detection with lying right and out of bed positions from 8.06% to 6.24% and 4.68% to 3.91%, respectively. The evaluation of our

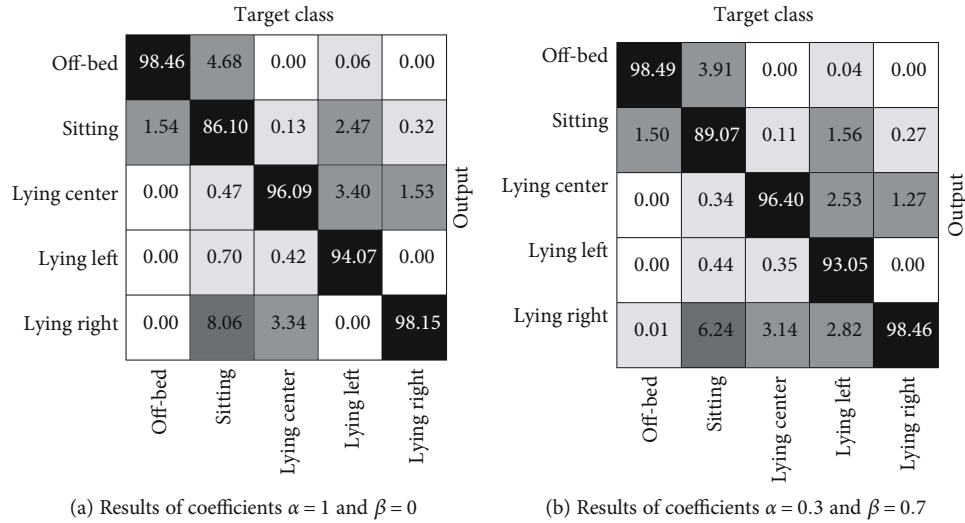


FIGURE 15: Detailed comparison between the results of classification of using only a neural network and a neural network with a Bayesian network.

TABLE 7: Comparison of sleep position classification algorithms.

Ref	# of positions	Accuracy (%)	Algorithm	Type of sensors	# of sensors
[13]	8	97.1	kNN	Pressure sensors	2,048
[14]	3	98.4	GMM+kNN	Pressure sensors	1,728
[15]	5	97.7	PCA+SVM	Pressure sensors	360
[16]	5	98.1	HoG+DNN	Pressure sensors	2,048
[17]	4	99.7	SVM	Pressure sensors	512
[18]	5	97.7	kNN	Force sensing array	2048
[19]	6	83.5	Raw data+SVM	FSR sensors	56
[20]	9	94.1	Joint feature extraction and normalization+SVM+PCA	FSR sensors/video	60
[21]	3	100	Kurtosis+skewness	FSR sensors	16
[22]	5	98.4	SVM (linear)+SVM (RBF)+LDA	CC-electrodes	12
Ours	3	97.8	NN+Bayesian network	Pressure and piezoelectric sensors	4

TABLE 8: Comparison of sleep three-position classification algorithms.

Ref	Accuracy (%)			# of sensors
	Left	Middle	Right	
[21]	100	100	100	16
Ours	93.05	96.40	98.46	4

approach against others is also promising. Even though it cannot outperform some of the other previously proposed methods that need a large number of sensors, our approach needs only four sensors. It can be concluded that our approach can perform at high accuracy for position detection and requires the fewest number of sensors.

Data Availability

The data of this study are available from the corresponding author upon request.

Disclosure

The manuscript is based on the thesis of the author Waranrach Viriyavit.

Conflicts of Interest

The authors declare that they have no conflicts of interest.

Acknowledgments

The sensor panel and IP camera, utilized in data collection, are provided by AIVS Co., Ltd. under the Japan International Cooperation Agency (JICA) grants for SME development support. The video and patient data are recorded under the consent of the patients and acknowledgment of Banphaeo Hospital. We are very thankful to Mr. Shunichi Yoshitake, Chairman of AIVS, for his strong support of the equipment and the director together with the staff of Banphaeo Hospital for the overall support in data collection. The research is financially supported by the Thammasat University Research Fund

under the National Research Council of Thailand (Contract No. 25/2561) for the project of “Digital platform for sustainable digital economy development,” based on the RUN Digital Cluster collaboration scheme.

References

- [1] National Statistical Office, “The 2014 survey of the older persons in Thailand,” 2014.
- [2] U S DEPARTMENT OF HEALTH AND HUMAN SERVICES Centers for Disease Control and Prevention National Center for Health Statistics, “Long-term care providers and services users in the United States, 2015–2016,” November, 2019, https://www.cdc.gov/nchs/data/series/sr_03/sr03_43-508.pdf.
- [3] Health Systems Research Institute, ““Fall down” major cause of accident that affects the injury of elderly,” May 2018 <https://www.hsri.or.th/people/media/infographic/detail/5319>.
- [4] Department of Disease Control May 2018, <http://www.riskcomthai.org/2017/detail.php?id=35499&m=news&gid=1-001-002>.
- [5] L.-Y. Tsai, S.-L. Tsay, R.-K. Hsieh et al., “Fall injuries and related factors of elderly patients at a medical center in Taiwan,” *International Journal of Gerontology*, vol. 8, no. 4, pp. 203–208, 2014.
- [6] R. L. Shinmoto Torres, D. C. Ranasinghe, Q. Shi, and A. P. Sample, “Sensor enabled wearable RFID technology for mitigating the risk of falls near beds,” in *2013 IEEE International Conference on RFID (RFID)*, pp. 191–198, Penang, Malaysia, May 2013.
- [7] A. Wickramasinghe, D. C. Ranasinghe, C. Fumeaux, K. D. Hill, and R. Visvanathan, “Sequence learning with passive RFID sensors for real-time bed-egress recognition in older people,” *IEEE Journal of Biomedical and Health Informatics*, vol. 21, no. 4, pp. 917–929, 2017.
- [8] A. Kononova, L. Li, K. Kamp et al., “The use of wearable activity trackers among older adults: focus group study of tracker perceptions, motivators, and barriers in the maintenance stage of behavior change,” *JMIR Mhealth Uhealth*, vol. 7, no. 4, p. e9832, 2019.
- [9] M. Uddin, W. Khaksar, and J. Torresen, “Ambient sensors for elderly care and independent living: a survey,” *Sensors*, vol. 18, no. 7, p. 2027, 2018.
- [10] H. Yamaguchi, H. Nakajima, K. Taniguchi, S. Kobashi, K. Kondo, and Y. Hata, “Fuzzy detection system of behavior before getting out of bed by air pressure and ultrasonic sensors,” in *2007 IEEE International Conference on Granular Computing (GRC 2007)*, pp. 114–119, Fremont, CA, USA, November 2007.
- [11] Y. Hata, H. Yamaguchi, S. Kobashi, K. Taniguchi, and H. Nakajima, “A human health monitoring system of systems in bed,” in *2008 IEEE International Conference on System of Systems Engineering*, pp. 1–6, Singapore, Singapore, June 2008.
- [12] C. L. Wu, Y. W. Chien, and L. C. Fu, “Monitoring bed activities via vibration-sensing belt on bed,” *2017 IEEE International Conference on Consumer Electronics-Taiwan (ICCE-TW)*, 2017, pp. 85–86, Taipei, Taiwan, June 2017.
- [13] M. B. Pouyan, S. Ostadabbas, M. Farshbaf, R. Yousefi, M. Nourani, and M. D. M. Pompeo, “Continuous eight-posture classification for bed-bound patients,” in *2013 6th International Conference on Biomedical Engineering and Informatics*, pp. 121–126, Hangzhou, China, December 2013.
- [14] S. Ostadabbas, M. Baran Pouyan, M. Nourani, and N. Kehtarnavaz, “In-bed posture classification and limb identification,” in *2014 IEEE Biomedical Circuits and Systems Conference (BioCAS) Proceedings*, pp. 133–136, Lausanne, Switzerland, October 2014.
- [15] R. Yousefi, S. Ostadabbas, M. Faezipour et al., “A smart bed platform for monitoring & ulcer prevention,” in *2011 4th International Conference on Biomedical Engineering and Informatics (BMEI)*, pp. 1362–1366, Shanghai, China, October 2011.
- [16] M. Heydarzadeh, M. Nourani, and S. Ostadabbas, “In-bed posture classification using deep autoencoders,” in *2016 38th Annual International Conference of the IEEE Engineering in Medicine and Biology Society (EMBC)*, pp. 3839–3842, Orlando, FL, USA, August 2016.
- [17] W. Cruz-Santos, A. Beltrán-Herrera, E. Vázquez-Santacruz, and M. Gamboa-Zúñiga, “Posture classification of lying down human bodies based on pressure sensors array,” in *2014 International Joint Conference on Neural Networks (IJCNN)*, pp. 533–537, Beijing, China, July 2014.
- [18] R. Yousefi, S. Ostadabbas, M. Faezipour et al., “Bed posture classification for pressure ulcer prevention,” in *2011 Annual International Conference of the IEEE Engineering in Medicine and Biology Society*, pp. 7175–7178, Boston, MA, USA, September 2011.
- [19] C. C. Hsia, K. J. Liou, A. P. W. Aung, V. Foo, W. Huang, and J. Biswas, “Analysis and comparison of sleeping posture classification methods using pressure sensitive bed system,” in *2009 Annual International Conference of the IEEE Engineering in Medicine and Biology Society*, pp. 6131–6134, Minneapolis, MN, USA, September 2009.
- [20] W. Huang, A. A. P. Wai, S. F. Foo, J. Biswas, C. C. Hsia, and K. Liou, “Multimodal sleeping posture classification,” in *2010 20th International Conference on Pattern Recognition*, pp. 4336–4339, Istanbul, Turkey, August 2010.
- [21] C.-C. Hsia, Y.-W. Hung, Y.-H. Chiu, and C.-H. Kang, “Bayesian classification for bed posture detection based on kurtosis and skewness estimation,” in *HealthCom 2008 - 10th International Conference on e-health Networking, Applications and Services*, pp. 165–168, Singapore, Singapore, July 2008.
- [22] H. J. Lee, S. H. Hwang, S. M. Lee, Y. G. Lim, and K. S. Park, “Estimation of body postures on bed using unconstrained ECG measurements,” *IEEE Journal of Biomedical and Health Informatics*, vol. 17, no. 6, pp. 985–993, 2013.
- [23] M. Cholewa and P. Głomb, “Natural human gestures classification using multisensor data,” in *2015 3rd IAPR Asian Conference on Pattern Recognition (ACPR)*, pp. 499–503, Kuala Lumpur, Malaysia, November 2015.
- [24] S. L. Videbeck, *Nursing Practice for Psychiatric Disorders*, Psychiatric-mental Health Nursing, Lippincott Williams & Wilkins, 2012, 446.
- [25] S. Gaddam, C. Mukhopadhyay, and G. S. Gupta, “Intelligent bed sensor system: design, experimentation and results,” in *2010 IEEE Sensors Applications Symposium (SAS)*, pp. 220–225, Limerick, Ireland, February 2010.
- [26] T. Shino, K. Watanabe, K. Kobayashi, K. Suzuki, and Y. Kurihara, “Noninvasive biosignal measurement of a subject in bed using ceramic sensors,” in *Proceedings of SICE Annual Conference 2010*, pp. 1559–1562, Taipei, Taiwan, August 2010.

- [27] S. Nukaya, T. Shino, Y. Kurihara, K. Watanabe, and H. Tanaka, "Noninvasive bed sensing of human biosignals via piezoceramic devices sandwiched between the floor and bed," *IEEE Sensors Journal*, vol. 12, no. 3, pp. 431–438, 2012.
- [28] M. Adami, M. Pavel, T. L. Hayes, A. G. Adami, and C. Singer, "A method for classification of movements in bed," in *2011 Annual International Conference of the IEEE Engineering in Medicine and Biology Society*, pp. 7881–7884, Boston, MA, USA, September 2011.
- [29] M. Alaziz, Z. Jia, R. Howard, X. Lin, and Y. Zhang, "Motion Tree: a tree-based in-bed body motion classification system using load-cells," in *2017 IEEE/ACM International Conference on Connected Health: Applications, Systems and Engineering Technologies (CHASE)*, pp. 127–136, Philadelphia, PA, USA, July 2017.
- [30] S. Raschka, "About feature scaling and normalization and the effect of standardization for machine learning algorithms," http://sebastianraschka.com/Articles/2014_about_feature_scaling.html#about-min-max-scaling.
- [31] "Bayes' theorem," January 2017, <http://planetmath.org/BayesTheorem>.

Review Article

Noninvasive Glucose Measurement Using Machine Learning and Neural Network Methods and Correlation with Heart Rate Variability

Marjan Gusev ¹, Lidija Poposka,¹ Gjoko Spasevski,¹ Magdalena Kostoska,¹ Bojana Koteska,¹ Monika Simjanoska ¹, Nevena Ackovska,¹ Aleksandar Stojmenski,¹ Jurij Tasic,² and Janez Trontelj³

¹*Ss. Cyril and Methodius University, Skopje, Macedonia*

²*Innovation Technologies, Sevnica, Slovenia*

³*University of Ljubljana, Ljubljana, Slovenia*

Correspondence should be addressed to Marjan Gusev; marjan.gushev@finki.ukim.mk

Received 19 September 2019; Revised 1 December 2019; Accepted 10 December 2019; Published 6 January 2020

Academic Editor: Eduard Llobet

Copyright © 2020 Marjan Gusev et al. This is an open access article distributed under the Creative Commons Attribution License, which permits unrestricted use, distribution, and reproduction in any medium, provided the original work is properly cited.

Diabetes is one of today's greatest global problems, and it is only becoming bigger. Constant measuring of blood glucose level is a prerequisite for monitoring glucose blood level and establishing diabetes treatment procedures. The usual way of glucose level measuring is by an invasive procedure that requires finger pricking with the lancet and might become painful and obeying, especially if this becomes a daily routine. In this study, we analyze noninvasive glucose measurement approaches and present several classification dimensions according to different criteria: size, invasiveness, analyzed media, sensing properties, applied method, activation type, response delay, measurement duration, and access to results. We set the focus on using machine learning and neural network methods and correlation with heart rate variability and electrocardiogram, as a new research and development trend.

1. Introduction

A lot of problems arise when a human cannot control the insulin level and thus process the glucose concentration in the blood. This inability initiates diabetes [1], which is a disease where the blood glucose level is high. In this case, only a precise therapy and careful management can prevent a buildup of sugars in the blood and intolerance to glucose [2], increasing the risk of dangerous vascular complications [3], such as coronary artery disease (leading to heart attack) [4], peripheral vascular disease, kidney failure or stroke, and neural complications (diabetic neuropathy) [5], including peripheral neuropathy and autonomic nervous system failure.

Recent studies show that there are 424.9 million diagnosed diabetic patients in the world and that the number is expected to go up to 628.6 million by 2045 [6]. Glucose mea-

surement and diabetes treatment are very expensive; for example, in the USA, the costs rose from \$245M in 2012 [7] to \$327M in 2017 [8]. To indicate the size of this problem, diabetic patients present 6-7% of the total worldwide population according to the International Diabetes Federation [9].

Furthermore, cardiovascular disease is closely linked to diabetes. In fact, a study in the USA [10] concluded that 25% of diabetes patient costs are a consequence of cardiovascular disease and 15% of costs of physician office visits are related to cardiovascular disease. At the same time, diabetes is responsible for more than a quarter of all cardiovascular disease expenditure.

In addition, there is a high proportion of undiagnosed diabetes mellitus globally, especially in developing countries, and Beagley et al. [11] conclude that 45.8% of diabetes cases are undiagnosed and very often associated with cardiovascular risk.

Several studies analyze the history of development of glucose measurement devices [12–14] and a summary of the four generations of glucose monitoring [13] classified by the used technology.

The produced medical devices have been evaluated from the 1970s with the start of the first-generation glucose meters that used reflectance technology and were made as heavy devices requiring a relatively big amount of blood. Second-generation devices used a drop of blood, and due to the available technology, they were made as smaller devices with affordable prices that allowed personalized use.

Finger pricking as the main routine in these invasive techniques is troublesome for diabetic patients because it can lead to scarring, motivating the development of devices that enable glucose measurement to be done cheaply and in a noninvasive way. The third-generation devices started as minimally invasive devices that include an array of small needles on the skin and enabled continuous glucose monitoring (CGM) [15–17].

Recently, a new generation is rising on the horizon, although it is still the king of an alternative, rather than an actual application of these kinds of medical devices, due to its current early stage of development. Nevertheless, we will refer to it as the *fourth-generation* medical devices which include noninvasive methods, providing an environment for remote and real-time continuous monitoring. The noninvasive methods do not invade the human body and are based on various methods, including spectrometry or analysis of other parameters correlated with the glucose level [18].

In this paper, we aim to present the available methods and ongoing projects for noninvasive glucose measurement, focusing on the use of machine learning (ML) and neural network (NN) methods used in a lot of ongoing research to deal with estimation methods of the glucose level.

The focus is also set to the possibility of using an ECG or other methods that determine the HRV parameters for detection of the ability of a human to regulate the blood glucose level with noninvasive methods. This is especially important since the recent wearable ECG sensors successfully emerged on the market, and ECG and HRV can be measured efficiently by a noninvasive method that allows a possibility for remote continuous real-time monitoring.

2. Classification of Noninvasive Glucose Measurement

Glucose measurement is mostly classified by the level of *invasiveness* of the sensing devices, which are usually classified as invasive (devices that are implanted in the patient's body or that invade the body to access a blood sample), minimally invasive (devices that painlessly invade a very small part of the patient's body, such as skin to collect a minimal sample, like a skin part, sweat, tear, and saliva), and noninvasive devices (devices that do not invade the patient's body) [12–14].

Noninvasive blood glucose monitoring methods are based on measuring glucose concentration from its chemical, thermal, electrical, or optical *sensing properties* [14, 19–22]. Some other sensing properties can also be exploited for measurement since the human body shows different physiologi-

cal responses to changes in glucose, such as electric and acoustic impedance, thermal conductivity, and electromagnetic response.

Usual classification of noninvasive methods is based on the used technology, although there are several authors that classify methods based on the subject they analyze, such as differentiation of *media* they target, including tissues (skin, aqueous eye humor, oral mucosa, tongue, and tympanic membrane) and fluids (sweat, urine, saliva, and tears) [21].

Each measurement system is specified by its *size* that determines if it can be used in a specialized laboratory at the healthcare institution or as a part of a smart home system [23]. In addition, it can be a pocket-size measurement device, such as those personal finger pricking devices or a wearable device, which is worn on the patient's body.

A specific *method* is used to process the sensed information and produce intermediate results, including transdermal and optical methods [20] or including nanotechnology [14]. The way the information obtained intermediate results which are further processed may include a specific processing, such as multivariate analysis, multiregression, or various artificial methods, such as deep machine learning or neural networks, which are described in more detail in this paper.

Glucose measurement can be applicable for continuous and real-time monitoring or can provide only on-demand activation of a single measurement, treated to be just a substitute of the existing invasive methods. A measurement is defined to be a single measurement if it is activated on demand to access a sample and then to process a result, while the continuous measurement systems continuously take samples and calculate results.

In addition, if the results are displayed on to a single user, the corresponding medical device is specified to be used in self-monitoring only, and if the results can be shared over the Internet to authorized users, the corresponding systems are systems that allow shared authorized access to results.

Finally, the end results may be obtained immediately or with a certain delay. If the delay is less than 2 minutes, they become near real time, or if the delay is less than 30 sec, they are treated as real time. For example, a blood analysis in the lab may take more time, and these measurement systems are specified to deliver postponed results. Not to be confused, this delay is dependent on the measurement device and processing capabilities, while the time delay needed for glucose concentration to propagate to the analyzed media is usually called lag.

To present a more comprehensive way and specify the domain of noninvasive glucose measurement techniques, we have introduced a methodology based on criteria, which determine several dimensions of glucose measurement devices, as illustrated in Figure 1. Each classification criterion is displayed by a rounded rectangle, and each category within a given criterion is presented by a sharpened rectangle.

Glucose measurement systems can be classified according to the following criteria:

- (i) Size: describing the measurement device to be a point-of-care system, home system, portable pocket device, or wearable device

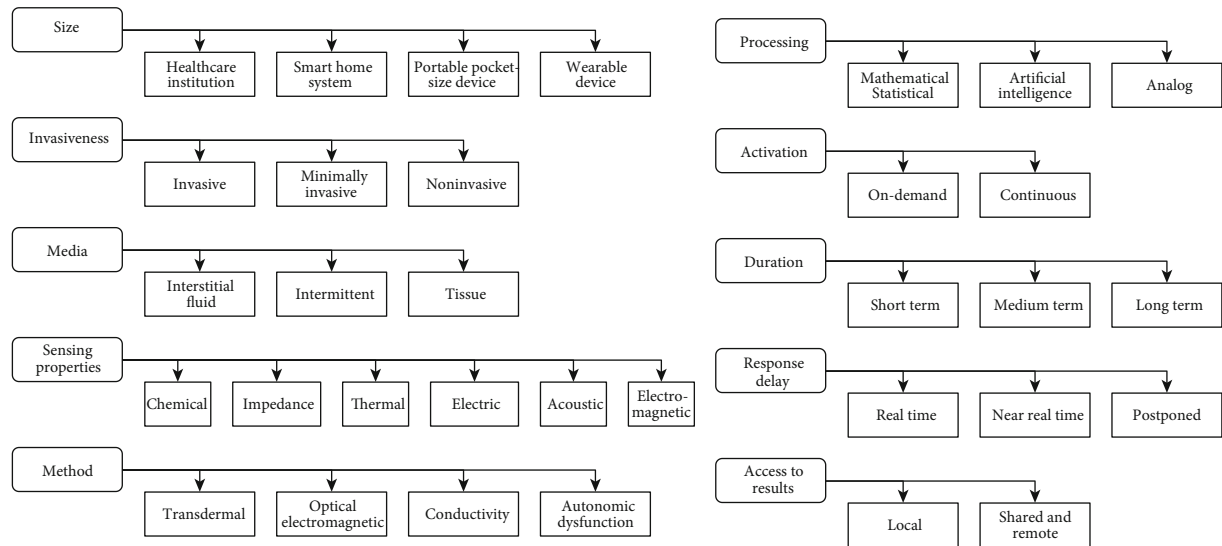


FIGURE 1: Classification of glucose measurements according to different criteria.

- (ii) Invasiveness: determined as an invasive, minimally invasive, and noninvasive technique
- (iii) Media: where the measurement is conducted, including interstitial fluid, intermittent, and tissues
- (iv) Sensing properties: analyzed by the medical device, including chemical, impedance, thermal, electrical, acoustic, or electromagnetic properties
- (v) Method: defined by the used technology to analyze the sensed information, such as transdermal, optical, and thermal conductivity and electromagnetic response, autonomic dysfunction (HRV-based), and nanotechnology
- (vi) Processing: specified by the method used in processing the result, which may include analog (comparison result or indication from the sensed information), mathematical and statistical methods (multivariate analysis with calibration, multiregression, etc.), and artificial intelligence (machine learning, neural network methods, deep learning, etc.)
- (vii) Activation type: determined by the way the measurement is activated: either on-demand activation or continuous measurement
- (viii) Duration type: determined by the measurement time: short term (less than 1 minute), medium term (less than 1 hour), and long term (expressed in days)
- (ix) Response delay: defined by the time required to process the results, including real-time systems (immediately or up to 30 sec), near real-time systems (up to 2 minutes), and postponed systems (more than 1 hour)
- (x) Access to results: specified by the access locality of the results, including self-monitoring systems and systems that use shared authorized remote access

3. Transdermal Noninvasive Glucose Measurements

Transdermal methods use the following technologies:

- (i) The reverse iontophoresis technique [24] accesses the interstitial fluid by a low electric current across the skin between two electrodes [25]. Sodium ions cause convective flow carrying glucose molecules in the opposite direction to that of normal medications (from the skin outward) [26]. Sensing is realized by detecting the glucose oxidase. An FDA-approved medical device is the GlucoWatch [27] targeting a wrist skin, capable of measuring 78 readings per wear (up to six per hour), after 2-hour calibration. It operates by a small current passing between two skin surface electrodes that draw ions and glucose-containing interstitial fluid to the surface and into hydrogel pads incorporating a glucose oxidase biosensor [28, 29]. According to our classification, it is a wearable device, using a noninvasive method to analyze interstitial fluid by sensing the chemical and electrical properties by a transdermal method with analog reading of local near real-time results for medium-term continuous glucose measurement. There are also other commercially unsuccessful medical devices, including GluCal [22, 30]
- (ii) Impedance spectroscopy measures the dielectric properties of a tissue, by passing a small alternating current across a tissue and measuring the impedance frequency spectrum in the range of 100 Hz–100 MHz [31], which is dependent on the glucose interaction with red blood cells [32]. Several issues including water content, temperature variation, sweating, and motion [33] require frequent calibration and equilibration, which generates a lot of implementation problems. Pendra is an FDA- and

CE-approved medical device [34], realized as a wrist watch based on impedance spectroscopy, with sensing conducted by an open resonant circuit, capable of performing up to 4 measurements per minute. However, it lacks a successful commercialization due to calibration problems (the need to change the tape after 24 h and requiring at least 1 h equilibration). GlucoBand is another medical device without successful commercialization, being oriented more to the wellness market instead of the medical one [35]

- (iii) The skin suction blister technique is based on analysis of a blister obtained by a vacuum suction over a small area of the skin [36] as a well-tolerated painless procedure with a low infection risk. Glucose concentration in the analyzed blister is lower than that seen in plasma but correlates well with the concentration in the blood [37], especially to the HbA1c value, which corresponds to a three-month average glucose values. Symphony is a commercially unsuccessful product which is applied to a permeated skin to analyze the electrochemical properties [38] by using a sensitive biosensor which measures the transdermal glucose flux
- (iv) The sonophoresis technique uses low-frequency ultrasound to increase skin permeability and causes expansion and contraction of gaseous inclusions that open pathways for interstitial fluids to transport glucose to the epidermis [39], where it is measured by a conventional electrochemical sensor [40]. This technique is sometimes considered minimally invasive as it creates micropores in the skin to enable the interstitial fluid containing glucose to come outside [22]. SpectRx is a product that is not yet commercialized, which uses laser to create micropores in the outermost skin layer to collect interstitial fluid containing glucose

Bruen et al. [41] discuss several wearable and noninvasive methods based on monitoring the interstitial fluid and wearable devices based on detection of the sweat (eyeglass, flexible wristband, etc.), breath analysis, saliva analysis (tattoo printed on a tooth, etc.), and ocular fluid (smart contact lens). Wearable glucose monitoring using epidermal sensors was reviewed by Kim et al. [42]. Concentration of glucose in interstitial fluid depends on blood glucose levels [43], although there is a significant time difference for transmission of the corresponding blood glucose levels to the interstitial fluids [44].

4. Optical Noninvasive Glucose Measurements

When light meets biological tissues, it can suffer reflection, scattering, and transmission being proportional to the structure and chemical components of the sample [21], as a basis of plenty of optical-based noninvasive glucose measurement methods [45, 46]. These are differentiated according to the analyzed band of electromagnetic radiations and interpreta-

tion of glucose levels from the received spectrum [20] by selectivity and interference to other compounds using multivariate calibration vectors [47] and several detection and multistage separation principles [48].

The following optical noninvasive methods have been analyzed to more or less successfully detect the diabetes level:

- (i) Infrared spectroscopy is based on rotational and vibrational transitions of molecule chemical bonds, and the corresponding fluctuation is measured by the incident radiation [49]
- (ii) Near-infrared (NIR) spectroscopy is based on the investigation of a visible and near-infrared range, including wavelengths 0.59–0.95 μm [50], 1.21–1.85 μm [51], and 2.12–2.38 μm [52] chosen due to weak water absorption and relatively high energy of the measured signal [21]. Although measurements do not depend on skin pigmentation, they depend on molecular structure and absorption spectrum ability, so several wavelengths are used for multivariate analysis with calibration. Although several medical devices (SugarTrac, Dream Beam, Diasensor, MedOptix, etc. [22, 30]) have been developed using the NIR spectroscopy method, they still are commercially unsuccessful
- (iii) Midinfrared (MIR) spectroscopy gives more distinct glucose peaks [21] analyzing the wavelength spectrum 8.38–9.71 μm [53]. Measurements of a specific wavelength before and after interaction with matter are compared, and effects on stretching and bending of molecules are used to determine glucose concentrations. A sensor using depth-selective MIR spectroscopy of skin based on total infrared reflection photothermal deflection has been described in [54] and absorption spectroscopy based on a few wave numbers in [55]
- (iv) Raman spectroscopy [56] evaluates scattering of single wavelength light, which is dependent on rotational or vibrational energy states within a molecule and highly specific absorption bands with respect to original laser light [57]. A multivariate analysis is applied to detected molecule quantity and reduced interference from water compared with MIR or NIR spectroscopy. There are several research projects by LightTouch Medical, C8 Medisensors [58], and Massachusetts Institute of Technology applying the Raman spectroscopy method on skin [22]. Development of a Raman spectrometer suitable for home-use noninvasive glucose monitoring was also reported in [59]
- (v) Photoacoustic spectroscopy measures ultrasonic waves created by tissue absorption of pulsating light created by a laser diode [60], as their interaction generates heat and causes pressure variations in the sample in the form of acoustic signals monitored by a piezoelectric transducer [61]. A theoretical study of resonant photoacoustic

spectroscopy for noninvasive glucose detection was reported in [62]. Aprise is a medical device that was clinically tested [63]. It utilizes the photoacoustic properties of the blood to infer the prevailing glucose levels, when ultrasound waves illuminate the tissue with laser pulses and acoustic signals are analyzed for the depth profile of the light absorbance of the skin above a blood vessel

- (vi) Ocular spectroscopy is applied to tears by using a hydrogel-bound contact lens [64] and using a spectrometer to measure the change in the reflected light received when a light source illuminates the lens. A lot of weakness has been detected in the application of this method, such as delay of glucose concentration, biocompatibility, and difference between the eyes [65]
- (vii) Scattering is the effect when the radiated signal is reflected by the tissue parts, such as cell membranes and collagen fibre in the blood and the interstitial fluid. Since the glucose changes the refractive index of the tissue, measuring the reflected signal provides information to calculate the glucose level [66]. Precision is affected by large interindividual differences and sensor drift, motion, temperature, water, and protein density [21]
- (viii) Occlusion spectroscopy is similar to scattering and optical coherence tomography methods measuring the scattering effects on arterial flow, instead of systolic flow. It uses enhanced light transmission of erythrocyte aggregation to calculate the glucose concentration [67]. The precision is vulnerable to many intravascular variables such as drug treatment, intrinsic erythrocyte aggregation, free fatty acid concentration, and chylomicrons [68]. OrSense is a medical device using near-infrared occlusion spectroscopy, detecting the red optical signal from blood due to changes in the glucose concentrations in blood vessels or finger, which has not yet been commercially successful
- (ix) Electromagnetic sensing uses electromagnetic sensors to measure the conductivity of dielectric parameters changed by the glucose concentration on a specific resonant frequency of 2.664 MHz [69]. Precision of the glucose measurements is strongly affected by environmental temperature and physiological blood dielectric parameter changes. TouchTrak is a high-cost medical device using electromagnetic sensing [22] and is not commercially successful. GluControl GC300 is a medical device, which has no significant proof of its accuracy and is poorly described [30].
- (x) Thermal emission spectroscopy measures the naturally emitted infrared signals generated in the human body due to changes in glucose concentration, similar to clinical tympanic membrane thermometers, based on wavelengths of 9.8 μm and 10.9 μm [70]. This method can be applied on the skin of the forearm, fingertip, or ear to detect glucose concentrations [53]. Infratec develops a portable handheld glucose measurement device built on a thermal emission spectroscopy method, not being yet commercialized [22]
- (xi) Temperature-regulated localized reflectance uses the scattering of a localized reflected light signal with wavelengths of 0.59 μm and 0.935 μm [71]. Measured temperature variations between 22°C and 38°C are related to glucose concentration [50]. Precision of measurements is affected by probe position, physiological parameters, and disease conditions
- (xii) The metabolic heat conformation technique uses thermal and optical sensors to measure thermal generation, blood flow rate, and hemoglobin and oxyhemoglobin concentrations strongly related to glucose concentration [72]. Multivariate statistical, regression, and cluster analyses, including multiwavelength spectroscopy (wavelengths 0.47 μm , 0.53 μm , 0.66 μm , 0.81 μm , 0.88 μm , and 0.95 μm), are used to calculate the glucose value [73]
- (xiii) The far-infrared (thermal infrared) technique uses the dependence of the cutaneous microcirculation on the local glucose concentration, which is observed by inducing controlled, periodic temperature variations in the skin and assessing MIR light scattering [53]. The far-infrared dielectric properties of sugars in the condensed state are dominated by vibrational modes of their intermolecular hydrogen-bonded network [74]. The basic principle of absorption is due to the existence of particular vibrational and rotational transitions of weak bonds and bonds of heavy atoms with wavelengths between 10 μm and 1000 μm
- (xiv) Terahertz time-domain spectroscopy measures the radiation absorption obtained from single-frequency (wavelength 0.9 μm) very short laser pulses (in the order of picoseconds). The method is based on time-domain analysis to get the phase change from reflected and scattered signals which allows the detection of the optical properties dependent on glucose concentration [75]. An ultrafast laser pump with a specific pulse shape can allow a broad frequency sweep and by applying time-domain signal processing of the detected spectroscopic information can extract crucial frequency-dependent information and determine glucose levels [76]
- (xv) Millimeter and microwave sensing allows going deeper into the tissue to reach regions with sufficient blood concentration using lower energy per photon and less scattering for accurate glucose

readings [77]. The sensing is realized by a near-field antenna using reflection methods

- (xvi) Ultrasound technology is based on measurement of the propagation time of ultrasound waves through the extracellular fluid, which is dependent on the glucose concentration due to the strength of intermolecular bonding forces and the density of the fluid [78]. Precision is affected by the ambient temperature. The noninvasive ultrasound or spectroscopy (light) technology measuring the heat capacity and conductivity as a two-parameter approach was used with GlucoTrack [79], which is still a not commercially successful product, although reporting good clinical results [78]
- (xvii) The polarimetry method estimates the optical rotary dispersal of polarized light by a millidegree precision polarization through tissue less than 4 mm thick across the anterior chamber of the eye [80]. Multiple linear regression or similar methods used for multispectral polarimetry minimize glucose prediction errors [81]. There is a time delay for glucose peak concentrations to propagate in the aqueous humour [82]
- (xviii) The fluorescence method relies on measuring the glucose levels in tears, since they reflect concentrations similar to those in blood, and the idea is to build a glucose-sensitive fluorescence system to monitor glucose metabolism by detection of either intrinsic cell fluorescence or fluorescent reporters of cell metabolism [83]. Fluorescence uses the principle of varying light emission from molecules in different states [84, 85]. GluMetrics uses the fluorescence method on an intravascular target, based on a glucose sensing polymer that glows in the case of high glucose concentration, but still not a commercially successful product [22]
- (xix) Optical coherence tomography is based on irradiation of a low-power laser source with coherent light to the skin and an in-depth scanning system to record the backscattered radiation (wavelength between $0.8 \mu\text{m}$ and $1.3 \mu\text{m}$) [86]. Since the dermal layer is dependent on the glucose concentration, measurements include induced changes [87]. Precision is sensitive to motion, tissue heterogeneity, and interfering analytes [88]. GlucoLight is a portable medical product that targets the skin and is still not being commercialized [22]
- (xx) Kromoscopy is based on a near-infrared analog of human color perception [89]. Four detector channels with complementary bandpass functions are used for the evaluation of collected electromagnetic radiation [90]. Complex vector analysis is applied for observed significant differences in channel responses for glucose and urea over different wavelengths of NIR light

Note that metabolic heat conformation and thermal emission can be differentiated from optical methods as a special class of thermal methods [91].

5. ML and NN Methods for Noninvasive Glucose Measurement

In order to extract knowledge from the gathered measured data, many studies use ML and NN methods. There are several studies that successfully include ML and NN techniques in methods of extraction and monitoring of glucose levels. Monte-Moreno [92] proposed a system for a simultaneous noninvasive estimate of the blood glucose level based on machine learning techniques and using a photoplethysmograph (PPG) sensor. The system idea is to find the relationship between the shape of the PPG waveform and the glucose levels. The system was tested on 410 individuals, and it used several machine learning techniques. The best results were obtained by the random forest technique. The distribution of the points on a Clarke error grid placed 87.7% of points in zone A, 10.3% in zone B, and 1.9% in zone D.

Yadav et al. [93] measured the blood glucose noninvasively by using the galvanic skin response and temperature measurements along with PPG. They used the multiple linear regression (MLR) and artificial neural network (ANN) techniques to estimate the blood glucose concentration from the multisensors. A significantly low mean absolute percentage error (MAPE) (9.21%) and high R^2 (0.94) demonstrated the accuracy of this multisensory approach.

Malik et al. [94] detected fasting blood glucose levels (FBGLs) in a mixed population of 175 healthy and diseased individuals in India. Their detecting algorithm uses machine learning techniques such as logistic regression (LR), support vector machine (SVM), and artificial neural network (ANN). The occurrence of elevated FBGL was estimated noninvasively using the status of an individual's salivary electrochemical parameters such as pH, redox potential, conductivity, and concentration of sodium, potassium, and calcium ions. The best performance for classifying high FBGLs was achieved by the SVM using RBF kernel showing approximately 85% accuracy, 84% precision, 85% sensitivity, and 85% F1 score.

A noninvasive nocturnal hypoglycemia monitoring system for type 1 diabetes patients is presented by Ling et al. [95]. The system uses an extreme learning machine-based neural network model. The results show that hypoglycemia in type 1 diabetes mellitus children can be detected noninvasively from the real-time heart rate and corrected QT interval. The testing performances of the proposed algorithm for the detection of hypoglycemia achieved sensitivity of 78.00% and specificity of 60.00%.

Reddy et al. [96] proposed a noninvasive blood glucose measurement method based on microwave transmission and the machine learning technique. The blood glucose concentration is detected by analyzing the reflected microwave signals.

The machine learning technique is used to facilitate real-time processing and to provide an alert for the patients with

hyperglycemia conditions. The system can also suggest a precise dose of insulin to intake.

Carter et al. [97] proposed a noninvasive diagnostic method using concentrations of twenty-two elements in toenails and personal information such as age, gender, and smoking history. The authors used seven different machine learning techniques to perform the robust classification of type 2 diabetes. They compared the performance of forty-six distinct machine learning models on resampled training data and testing data. The best results were achieved with the random forest model (seven out of nine test samples were predicted correctly).

Das et al. [98] measure the galvanic skin response of 11 diabetic patients and 8 normal controls. The novel noninvasive system is based on the principle of skin impedance spectrogram and heart rate variability. To compute the heart rate variability, they acquired ECG signals from 20 normal controls and 20 diabetic patients. In the study, they use features such as Welch's power spectral density estimation. Artificial neural networks were used to classify GSR signals, and the obtained accuracy is 100%. During the analysis of diabetes mellitus, they have proven that there is a change in some parameters related to heart rate variability.

A compact microwave sensor has been proposed [99] for glucose sensing based on the utilization of the artificial neural network and has been simulated with the proposed models and measured with a fingertip as well as glucose/water solutions. It has been concluded that the presence of biological tissues decreases the measurement sensitivity. However, the sensor can measure the glucose level when the solution is directly placed on the sensor.

Low-cost continuous glucose and noninvasive BG detection system is presented [100] based on a combination of the conservation-of-energy method with a sensor for collecting oxygen saturation (SPO_2), blood flow velocity, and heart rate. Also, methods for a basal metabolic rate (BMR) and BV detection are proposed based on human body heat balance and PPG signals. The system includes a module for multisensor information fusion. The intelligence is implemented by using a decision tree and backpropagation neural network. The reported achieved accuracy is 88.53%.

Artificial neural networks (ANNs) combined with particle swarm optimization (PSO) are proposed to model the nonlinear relationship between the blood glucose concentration and near-infrared signal [101]. The weight coefficients of the ANNs represent the difference between individual and daily physiological rule. The Bland-Altman method has been applied to show that the predictions and measurements are in good agreement. The PSO-2ANN model is concluded to be a nonlinear calibration strategy with accuracy and robustness using $1.55 \mu\text{m}$ spectroscopy, able to correct the individual difference and physiological glucose dynamics.

Another low-cost portable noninvasive blood glucose measurement system based on near-infrared light is presented in [102]. Regression analysis is applied to model the relationship between the detector output voltage and the glucose concentration. The accuracy of the device has been tested by comparing the noninvasively estimated and invasively measured blood glucose. The neural network method

is used to estimate the glucose concentration. The results of the prediction of glucose concentration show that the system errors are in the clinically acceptable region.

Todd et al. [103] review existing research in methods of extraction and monitoring of glucose levels, especially focusing on the performance of ML methods, such as fuzzy logic, neural networks, and decision trees. The most promising result with the accuracy of nearly 98% was produced by neural networks and recurrent neural networks.

The presented work in [104] focuses on the design of low-cost, painless, and noninvasive blood glucose measurement system by using near-infrared LED and four photodiodes. The attenuated light is transformed into a voltage signal. The voltage signal is calibrated using the Levenberg-Marquardt-based artificial neural network to obtain the glucose concentration. The accuracy of the proposed system has been tested by comparing it with invasively measured blood glucose. The errors obtained are in a clinical range.

6. HRV-Based Noninvasive Glucose Measurement

An ECG is the electrical signal representation of the heart action potential. The heart rate is being controlled by the autonomous nerve system, the same that regulates the blood pressure and the glucose level. Thus, the last group of methods is used to produce medical devices including wearable ECG sensors and different HRV trackers, mainly represented by smart watches, smartphones, or similar devices, including belts, special shirts, and patches.

The autonomic nervous system constituted the parasympathetic and sympathetic parts which operate independently of each other or interact cooperatively to control heart rate, cardiac output, myocardial contractility, cardiac electrophysiology, and the constriction and dilatation of blood vessels [105]. Thus, HRV is an essential tool to diagnose the cardiac autonomic neuropathy for both clinically asymptomatic and symptomatic patients as a serious complication of diabetes mellitus.

Heart rate variability is a physiological phenomenon consisting of oscillations in consecutive heartbeat intervals controlled by the autonomic nervous system and is caused by the ability of the heart to handle the ever stresses and relaxations placed on the body. Several studies show that there is a correlation between HRV and the glucose level of the subjects.

Recent studies [106–108] show a big correlation between the HRV from one side and glucose level from the other side, since they show that diabetes caused progressive autonomic dysfunction and decreased variability in the heart rate [109, 110].

The overall result is the differentiation of diabetic patients from normal whenever a reduction of HRV parameters is detected. Kudat et al. [107] investigated cardiovascular autonomic neuropathy in diabetics and healthy controls by analysis of heart rate variability and concluded that diabetes patients had lower values for time-domain and frequency-domain parameters than other normal subjects. They have analyzed that diabetes mellitus is a cause of autonomic

dysfunction in the gastrointestinal and urogenital systems besides the cardiovascular system but focused their research on autonomic dysfunction.

Five different tests have been introduced by Ewing et al. [111] of short-term R-R alterations to identify cardiac autonomic neuropathy in patients with diabetes, based on heart rate response to respiration and to standing, during and after a provoked increase in intrathoracic and intra-abdominal pressures (Valsalva maneuver), and blood pressure response to orthostasis and isometric exercise.

An increase in the ability to detect minor changes in cardiac autonomic function with long-term HRV monitoring is reported [112] when compared with standard tests of autonomic function. There was evidence of significant HRV reductions for those diagnosed with diabetes compared with nondiabetic subjects, indicating that the presence or absence of neuropathy may conceal important information. Some studies included data recorded by wearable heart rate sensors. They have also confirmed high accuracy at detecting diabetes (0.8451) by a semisupervised training method, semi-supervised sequence learning, and heuristic pretraining and show that they outperform hand-engineered biomarkers from the medical literature [106].

HRV parameters can be classified as a time series domain, a frequency domain, and other domains [113] such as long-term (24 h), short-term (5 min), and ultra-short-term measurements (less than 5 min) [114–116]. Most of the studies [109, 113] conclude that long-term HRV variability is more sensitive for detecting diabetes autonomic neuropathy from the conventional short-term measures.

7. Discussion

A comprehensive overview of the progress of glucose measurement is elaborated by Villena Gonzales et al. [14]. They specify using various glucose detection techniques based on electric, thermal, and optical methods, and recently, the nanotechnology approaches are essential for minimally invasive and noninvasive glucose measurement technologies.

Several properties of glucose are manifested under different phenomena. García-Guzmán et al. [19] conclude that chemical, electrical, optical, thermal, acoustic, or any combination of these glucose properties can achieve greater accuracy in the determination of glucose concentration in blood and that both optical and electrical properties are the most suitable for noninvasive glucose measurement. In this paper, we also give advantage to the analysis of glucose properties by the analysis of autonomic dysfunction.

Methods using sweat-based glucose monitor wearable biosensors are reported as ongoing projects [117, 118].

A hybrid approach [19], which includes sensing of more than one physiological parameter, is becoming popular, such as electrochemical or combination of measuring the sound speed, conductivity, and heat capacity obtaining thereafter a weighted average or a combination of absorption spectroscopy and complex bioimpedance measurements [119]. In addition, a complex big data analysis of several parameters with corresponding artificial intelligence methods are hot topic research and can produce promising results.

Data analytics in processing various glucose properties for noninvasive and minimally invasive techniques is an emerging technology [120] contributing to the field of diabetes informatics and providing a more data-rich approach to understanding and managing diabetes.

Analyzing the accuracy, the American Diabetes Association [121] recommends the control of all glucometers both at the start of usage and at regular intervals and also the accuracy of blood glucose to be <5% of the measured value or accuracy better than 15 mg/dl (0.8 mmol/l) [20]. Solnica et al. [122] conclude that all glucometers examined have small deviations from laboratory reference values (<10%), although there are reports that, yet, some of the glucometers do not meet the recommendations and standard requirements.

Besides the accuracy, there are other socioeconomic parameters that can be treated as a barrier to the adoption of the noninvasive glucose monitoring [19], including commercialization uptake in the global economy. It is believed that next-generation glucometers or continuous glucose sensor systems may become excellent predictable and selective devices and probably in the future become a fully reliable source of information and acceptable for patient use [20].

Lin et al. [91] specify major challenges for development on noninvasive glucose measurements, extracting issues in obtained specificity and sensitivity, variable physiological time lag, need for the calibration process, and usability. Talking about usability, one needs to describe if the device is a wearable or pocket-size hand-held device. For example, GlucoWise is a U-shaped sensor that fits over the corner of the hand between the thumb and forefinger. Analyte is a hand-held device that is inserted into the ear, whereas GlucoTrack is clipped to the earlobe [123].

A roadmap of continuous glucose measurement initiates next generations of noninvasive techniques [124], and some of the future key challenges [22] include the following:

- (i) Improvement of the sensitivity and positive predictive rate in the detection of glucose levels and corresponding accuracy and precision of glucose measurement medical devices
- (ii) Development of a wearable continuous noninvasive glucose measurement system

Note that besides the lack of precision, robustness, and stability, the cost-effectiveness that is measured as a price per use is the key factor to accept a certain technology and make it commercially successful.

8. Conclusion

In this paper, we have presented an enhanced set of noninvasive techniques for glucose measuring based on HRV and using sophisticated artificial intelligence algorithms. Those methods are important since they enable the patients' comfortable continuous monitoring of the blood glucose levels.

Usually, the noninvasive measurements have been classified as transdermal and optical methods. We specified

autonomic dysfunction as another class, based on an important observation that wearable ECG sensors are capable of measuring HRV. This trend in modern real-time remote noninvasive monitoring by wearable mobile medical devices could be correlated with methodologies for glucose monitoring. Reduction in HRV variability is an indicator of autonomic diabetes dysfunction, and thus, the technology based on wearable ECG sensors may have promising results in the determination of the ability to control the blood glucose level. Although these methodologies may have promising results in terms of patients' comfort, they still lack the needed accuracy. In order to get a better understanding of the gathered measurement data, many of those measurement methods use ML and NN techniques to achieve better accuracy.

Expenses and proving benefit are probably those that need to be made more affordable and demonstrated in further research. However, it takes a lot of time to market the technology from one side and to change the behavior of both the patients and doctors.

Future trends include the use of new sophisticated techniques, such as the use of artificial intelligence algorithms or sensing other psychophysiological parameters, such as the autonomic dysfunction based on heart rate variability, as discussed in this article. Nanotechnologies are also a promising technique, although they are commonly treated as minimally invasive techniques.

Conflicts of Interest

The authors declare that they have no conflicts of interest.

References

- [1] American Diabetes Association, "Diagnosis and classification of diabetes mellitus," *Diabetes Care*, vol. 37, Supplement 1, 2014.
- [2] National Diabetes Data Group, "Classification and diagnosis of diabetes mellitus and other categories of glucose intolerance," *Diabetes*, vol. 28, no. 12, pp. 1039–1057, 1979.
- [3] C. G. Schalkwijk and C. D. Stehouwer, "Vascular complications in diabetes mellitus: the role of endothelial dysfunction," *Clinical Science*, vol. 109, no. 2, pp. 143–159, 2005.
- [4] R. Donnelly, A. M. Emslie-Smith, I. D. Gardner, and A. D. Morris, "ABC of arterial and venous disease: vascular complications of diabetes," *BMJ*, vol. 320, no. 7241, pp. 1062–1066, 2000.
- [5] S. Tesfaye, N. Chaturvedi, S. E. Eaton et al., "Vascular risk factors and diabetic neuropathy," *New England Journal of Medicine*, vol. 352, no. 4, pp. 341–350, 2005.
- [6] International Diabetes Atlas, *IDF Diabetes Atlas, Eighth Edition 2017*, 2018, <https://www.diabete.qc.ca/en/understand-diabetes/resources/getdocumentutile/IDF-DA-8e-EN-finalR3.pdf>.
- [7] American Diabetes Association, "Economic costs of diabetes in the U.S. in 2012," *Diabetes Care*, vol. 36, no. 4, pp. 1033–1046, 2013.
- [8] American Diabetes Association, "Economic costs of diabetes in the U.S. in 2017," *Diabetes Care*, vol. 41, no. 5, pp. 917–928, 2018.
- [9] International Diabetes Federation, "Insulin: concierge medication or human right?," *Diabetes Voice*, vol. 65, no. 1, p. 21, 2018.
- [10] M. A. Ariza, V. G. Vimalananda, and J. L. Rosenzweig, "The economic consequences of diabetes and cardiovascular disease in the United States," *Reviews in Endocrine and Metabolic Disorders*, vol. 11, no. 1, pp. 1–10, 2010.
- [11] J. Beagley, L. Guariguata, C. Weil, and A. A. Motala, "Global estimates of undiagnosed diabetes in adults," *Diabetes Research and Clinical Practice*, vol. 103, no. 2, pp. 150–160, 2014.
- [12] S. F. Clarke and J. R. Foster, "A history of blood glucose meters and their role in self-monitoring of diabetes mellitus," *British Journal of Biomedical Science*, vol. 69, no. 2, pp. 83–93, 2012.
- [13] N. A. B. A. Salam, W. H. b. Mohd Saad, Z. B. Manap, and F. Salehuddin, "The evolution of non-invasive blood glucose monitoring system for personal application," *Journal of Telecommunication, Electronic and Computer Engineering*, vol. 8, no. 1, pp. 59–65, 2016.
- [14] W. Villena Gonzales, A. T. Mobashsher, and A. Abbosh, "The progress of glucose monitoring - a review of invasive to minimally and non-invasive techniques, devices and sensors," *Sensors*, vol. 19, no. 4, p. 800, 2019.
- [15] D. Slattery and P. Choudhary, "Clinical use of continuous glucose monitoring in adults with type 1 diabetes," *Diabetes Technology & Therapeutics*, vol. 19, no. S2, p. S-55, 2017.
- [16] A. L. Carlson, D. M. Mullen, and R. M. Bergenstal, "Clinical use of continuous glucose monitoring in adults with type 2 diabetes," *Diabetes Technology & Therapeutics*, vol. 19, no. S2, p. S-4, 2017.
- [17] T. Danne, R. Nimri, T. Battelino et al., "International consensus on use of continuous glucose monitoring," *Diabetes Care*, vol. 40, no. 12, pp. 1631–1640, 2017.
- [18] A. Ciudin, C. Hernandez, and R. Simo, "Non-invasive methods of glucose measurement: current status and future perspectives," *Current Diabetes Reviews*, vol. 8, no. 1, pp. 48–54, 2012.
- [19] J. García-Guzmán, N. González-Viveros, and H. H. Cerecedo-Núñez, "Comparative analysis of optoelectronic properties of glucose for non-invasive monitoring," in *Emerging challenges for experimental mechanics in energy and environmental applications, Proceedings of the 5th International Symposium on Experimental Mechanics and 9th Symposium on Optics in Industry (ISEM-SOI), 2015. Conference Proceedings of the Society for Experimental Mechanics Series*, A. Martínez-García, C. Furlong, B. Barrientos, and R. Pryputniewicz, Eds., pp. 55–63, Springer, Cham, 2017.
- [20] A. Nawaz, P. Øhlckers, S. Sælid, M. Jacobsen, and M. N. Akram, "Review: non-invasive continuous blood glucose measurement techniques," *Journal of Bioinformatics and Diabetes*, vol. 1, no. 3, pp. 1–27, 2016.
- [21] C. E. F. do Amaral and B. Wolf, "Current development in non-invasive glucose monitoring," *Medical Engineering & Physics*, vol. 30, no. 5, pp. 541–549, 2008.
- [22] S. K. Vashist, "Non-invasive glucose monitoring technology in diabetes management: a review," *Analytica Chimica Acta*, vol. 750, pp. 16–27, 2012.
- [23] E.-H. Yoo and S.-Y. Lee, "Glucose biosensors: an overview of use in clinical practice," *Sensors*, vol. 10, no. 5, pp. 4558–4576, 2010.

- [24] G. Rao, R. Guy, P. Glikfeld et al., "Reverse iontophoresis: noninvasive glucose monitoring in vivo in humans," *Pharmaceutical Research*, vol. 12, no. 12, pp. 1869–1873, 1995.
- [25] R. O. Potts, J. A. Tamada, and M. J. Tierney, "Glucose monitoring by reverse iontophoresis," *Diabetes/Metabolism Research and Reviews*, vol. 18, no. S1, pp. S49–S53, 2002.
- [26] B. Leboulanger, R. H. Guy, and M. B. Delgado-Charro, "Reverse iontophoresis for non-invasive transdermal monitoring," *Physiological Measurement*, vol. 25, no. 3, pp. R35–R50, 2004.
- [27] FDA, "GlucoWatch, summary of safety and effectiveness data," 2002, <https://www.accessdata.fda.gov/cdrhdocs/pdf/P990026S008b.pdf>.
- [28] J. A. Tamada, S. Garg, L. Jovanovic et al., "Noninvasive glucose monitoring: comprehensive clinical results," *JAMA*, vol. 282, no. 19, pp. 1839–1844, 1999.
- [29] M. J. Tierney, J. A. Tamada, R. O. Potts et al., "The GlucoWatch® biographer: a frequent, automatic and noninvasive glucose monitor," *Annals of Medicine*, vol. 32, no. 9, pp. 632–641, 2000.
- [30] A. Tura, A. Maran, and G. Pacini, "Non-invasive glucose monitoring: assessment of technologies and devices according to quantitative criteria," *Diabetes Research and Clinical Practice*, vol. 77, no. 1, pp. 16–40, 2007.
- [31] A. Caduff, E. Hirt, Y. Feldman, Z. Ali, and L. Heinemann, "First human experiments with a novel non-invasive, non-optical continuous glucose monitoring system," *Biosensors and Bioelectronics*, vol. 19, no. 3, pp. 209–217, 2003.
- [32] T. A. Hillier, R. D. Abbott, and E. J. Barrett, "Hyponatremia: evaluating the correction factor for hyperglycemia," *The American Journal of Medicine*, vol. 106, no. 4, pp. 399–403, 1999.
- [33] A. Pfützner, A. Caduff, M. Larbig, T. Schrepfer, and T. Forst, "Impact of posture and fixation technique on impedance spectroscopy used for continuous and noninvasive glucose monitoring," *Diabetes Technology & Therapeutics*, vol. 6, no. 4, pp. 435–441, 2004.
- [34] I. Wentholt, J. Hoekstra, A. Zwart, and J. DeVries, "Pendra goes Dutch: lessons for the CE mark in Europe," *Diabetologia*, vol. 48, no. 6, pp. 1055–1058, 2005.
- [35] A. Fioravanti, G. Fico, A. G. Patón, J.-P. Leuteritz, A. G. Arredondo, and M. T. A. Waldmeyer, "Health-integrated system paradigm: diabetes management," in *Handbook of Biomedical Telemetry*, pp. 623–632, Wiley Online Library, 2014.
- [36] N. Oliver, C. Toumazou, A. Cass, and D. Johnston, "Glucose sensors: a review of current and emerging technology," *Diabetic Medicine*, vol. 26, no. 3, pp. 197–210, 2009.
- [37] B. M. Jensen, P. Bjerring, J. S. Christiansen, and H. ørskov, "Glucose content in human skin: relationship with blood glucose levels," *Scandinavian Journal of Clinical and Laboratory Investigation*, vol. 55, no. 5, pp. 427–432, 1995.
- [38] H. Chuang, M.-Q. Trieu, J. Hurley, E. J. Taylor, M. R. England, and S. A. Nasraway Jr., "Pilot studies of transdermal continuous glucose measurement in outpatient diabetic patients and in patients during and after cardiac surgery," *Journal of Diabetes Science and Technology*, vol. 2, no. 4, pp. 595–602, 2008.
- [39] J. Kost, S. Mitragotri, R. A. Gabbay, M. Pishko, and R. Langer, "Transdermal monitoring of glucose and other analytes using ultrasound," *Nature Medicine*, vol. 6, no. 3, pp. 347–350, 2000.
- [40] Y.-L. Lo and T.-C. Yu, "A polarimetric glucose sensor using a liquid-crystal polarization modulator driven by a sinusoidal signal," *Optics Communications*, vol. 259, no. 1, pp. 40–48, 2006.
- [41] D. Bruen, C. Delaney, L. Florea, and D. Diamond, "Glucose sensing for diabetes monitoring: recent developments," *Sensors*, vol. 17, no. 8, p. 1866, 2017.
- [42] J. Kim, A. S. Campbell, and J. Wang, "Wearable non-invasive epidermal glucose sensors: a review," *Talanta*, vol. 177, pp. 163–170, 2018.
- [43] E. Cengiz and W. V. Tamborlane, "A tale of two compartments: interstitial versus blood glucose monitoring," *Diabetes Technology & Therapeutics*, vol. 11, no. S1, p. S–11, 2009.
- [44] M. S. Boyne, D. M. Silver, J. Kaplan, and C. D. Saudek, "Timing of changes in interstitial and venous blood glucose measured with a continuous subcutaneous glucose sensor," *Diabetes*, vol. 52, no. 11, pp. 2790–2794, 2003.
- [45] G. L. Cote, "Noninvasive and minimally-invasive optical monitoring technologies," *The Journal of Nutrition*, vol. 131, no. 5, pp. 1596S–1604S, 2001.
- [46] V. V. Tuchin, *Handbook of Optical Sensing of Glucose in Biological Fluids and Tissues*, CRC press, Boca Raton, 2008.
- [47] M. A. Arnold, L. Liu, and J. T. Olesberg, "Selectivity assessment of noninvasive glucose measurements based on analysis of multivariate calibration vectors," *Journal of Diabetes Science and Technology*, vol. 1, no. 4, pp. 454–462, 2007.
- [48] M. A. Arnold and G. W. Small, "Noninvasive glucose sensing," *Analytical Chemistry*, vol. 77, no. 17, pp. 5429–5439, 2005.
- [49] F. E. Barton, "Theory and principles of near infrared spectroscopy," in *Proceedings of the Korean Society of Near Infrared Spectroscopy Conference. The Korean Society of Near Infrared Spectroscopy*, pp. 1012–1012, 2001.
- [50] S. Yeh, C. F. Hanna, and O. S. Khalil, "Monitoring blood glucose changes in cutaneous tissue by temperature-modulated localized reflectance measurements," *Clinical Chemistry*, vol. 49, no. 6, pp. 924–934, 2003.
- [51] W. Schrader, P. Meuer, J. Popp, W. Kiefer, J.-U. Menzebach, and B. Schrader, "Non-invasive glucose determination in the human eye," *Journal of Molecular Structure*, vol. 735–736, pp. 299–306, 2005.
- [52] J. T. Olesberg, L. Liu, V. V. Zee, and M. A. Arnold, "In vivo near-infrared spectroscopy of rat skin tissue with varying blood glucose levels," *Analytical Chemistry*, vol. 78, no. 1, pp. 215–223, 2006.
- [53] C. D. Malchoff, K. Shoukri, J. I. Landau, and J. M. Buchert, "A novel noninvasive blood glucose monitor," *Diabetes Care*, vol. 25, no. 12, pp. 2268–2275, 2002.
- [54] O. Hertzberg, A. Bauer, A. Küderle, M. A. Pleitez, and W. Mäntele, "Depth-selective photothermal IR spectroscopy of skin: potential application for non-invasive glucose measurement," *Analyst*, vol. 142, no. 3, pp. 495–502, 2017.
- [55] R. Kasahara, S. Kino, S. Soyama, and Y. Matsuura, "Noninvasive glucose monitoring using mid-infrared absorption spectroscopy based on a few wavenumbers," *Biomedical Optics Express*, vol. 9, no. 1, pp. 289–302, 2018.
- [56] J. R. Ferraro, *Introductory Raman Spectroscopy*, Elsevier, 2003.
- [57] N. C. Dingari, I. Barman, G. P. Singh, J. W. Kang, R. R. Dasari, and M. S. Feld, "Investigation of the specificity of Raman spectroscopy in non-invasive blood glucose measurements,"

- Analytical and Bioanalytical Chemistry*, vol. 400, no. 9, pp. 2871–2880, 2011.
- [58] J. Lipson, J. Bernhardt, U. Block et al., “Requirements for calibration in noninvasive glucose monitoring by Raman spectroscopy,” *Journal of Diabetes Science and Technology*, vol. 3, no. 2, pp. 233–241, 2009.
- [59] S. M. Lundsgaard-Nielsen, A. Pors, S. O. Banke, J. E. Henriksen, D. K. Hepp, and A. Weber, “Critical-depth Raman spectroscopy enables home-use non-invasive glucose monitoring,” *PLoS One*, vol. 13, no. 5, article e0197134, 2018.
- [60] G. Spanner and R. Niessner, “Noninvasive determination of blood constituents using an array of modulated laser diodes and a photoacoustic sensor head,” *Fresenius' Journal of Analytical Chemistry*, vol. 355, no. 3-4, pp. 327–328, 1996.
- [61] Y. Wickramasinghe, Y. Yang, and S. Spencer, “Current problems and potential techniques in in vivo glucose monitoring,” *Journal of Fluorescence*, vol. 14, no. 5, pp. 513–520, 2004.
- [62] Y. Tanaka, T. Tajima, and M. Seyama, “Acoustic modal analysis of resonant photoacoustic spectroscopy with dual-wavelength differential detection for noninvasive glucose monitoring,” *IEEE Sensors Letters*, vol. 1, no. 3, pp. 1–4, 2017.
- [63] R. Weiss, Y. Yegorchikov, A. Shusterman, and I. Raz, “Noninvasive continuous glucose monitoring using photoacoustic technology—results from the first 62 subjects,” *Diabetes Technology & Therapeutics*, vol. 9, no. 1, pp. 68–74, 2007.
- [64] A. Domschke, W. F. March, S. Kabilan, and C. Lowe, “Initial clinical testing of a holographic non-invasive contact lens glucose sensor,” *Diabetes Technology & Therapeutics*, vol. 8, no. 1, pp. 89–93, 2006.
- [65] J. T. Baca, C. R. Taormina, E. Feingold, D. N. Finegold, J. J. Grabowski, and S. A. Asher, “Mass spectral determination of fasting tear glucose concentrations in nondiabetic volunteers,” *Clinical Chemistry*, vol. 53, no. 7, pp. 1370–1372, 2007.
- [66] L. Heinemann, U. Krämer, H. M. Klötzer et al., “Noninvasive glucose measurement by monitoring of scattering coefficient during oral glucose tolerance tests,” *Diabetes Technology & Therapeutics*, vol. 2, no. 2, pp. 211–220, 2000.
- [67] I. Fine, B. Fikhte, and L. D. Shvartsman, “Occlusion spectroscopy as a new paradigm for noninvasive blood measurements,” in *Proceedings Volume 4263, Optical Diagnostics and Sensing of Biological Fluids and Glucose and Cholesterol Monitoring*, pp. 122–130, San Jose, CA, USA, June 2001.
- [68] O. Amir, D. Weinstein, S. Zilberman et al., “Continuous non-invasive glucose monitoring technology based on “occlusion spectroscopy,”” *Journal of Diabetes Science and Technology*, vol. 1, no. 4, pp. 463–469, 2007.
- [69] M. Gourzi, A. Rouane, R. Guelaz et al., “Non-invasive glycaemia blood measurements by electromagnetic sensor: study in static and dynamic blood circulation,” *Journal of Medical Engineering & Technology*, vol. 29, no. 1, pp. 22–26, 2005.
- [70] O. S. Khalil, “Noninvasive photonic-crystal material for sensing glucose in tears,” *Clinical Chemistry*, vol. 50, no. 12, pp. 2236–2237, 2004.
- [71] R. Fusman, R. Rotstein, K. Elishkewich et al., “Image analysis for the detection of increased erythrocyte, leukocyte and platelet adhesiveness/aggregation in the peripheral blood of patients with diabetes mellitus,” *Acta Diabetologica*, vol. 38, no. 3, pp. 129–134, 2001.
- [72] O. K. Cho, Y. O. Kim, H. Mitsumaki, and K. Kuwa, “Noninvasive measurement of glucose by metabolic heat conformation method,” *Clinical Chemistry*, vol. 50, no. 10, pp. 1894–1898, 2004.
- [73] J. B. Ko, O. K. Cho, Y. O. Kim, and K. Yasuda, “Body metabolism provides a foundation for noninvasive blood glucose monitoring,” *Diabetes Care*, vol. 27, no. 5, pp. 1211–1212, 2004.
- [74] M. Walther, B. M. Fischer, and P. U. Jepsen, “Noncovalent intermolecular forces in polycrystalline and amorphous saccharides in the far infrared,” *Chemical Physics*, vol. 288, no. 2-3, pp. 261–268, 2003.
- [75] E. Alarousu, J. T. Hast, M. T. Kinnunen et al., “Noninvasive glucose sensing in scattering media using OCT, PAS, and TOF techniques,” in *Proceedings Volume 5474, Saratov Fall Meeting 2003: Optical Technologies in Biophysics and Medicine V*, pp. 33–41, Saratov, Russian Federation, August 2004.
- [76] W. Withayachumnankul and M. Naftaly, “Fundamentals of measurement in terahertz time-domain spectroscopy,” *Journal of Infrared, Millimeter, and Terahertz Waves*, vol. 35, no. 8, pp. 610–637, 2014.
- [77] M. Nakamura, T. Tajima, K. Ajito, and H. Koizumi, “Selectivity enhanced glucose measurement in multicomponent aqueous solution by broadband dielectric spectroscopy,” in *2016 IEEE MTT-S International Microwave Symposium (IMS)*, pp. 1–3, San Francisco, CA, USA, May 2016.
- [78] I. Harman-Boehm, A. Gal, A. M. Raykhman, J. D. Zahn, E. Naidis, and Y. Mayzel, “Noninvasive glucose monitoring: a novel approach,” *Journal of Diabetes Science and Technology*, vol. 3, no. 2, pp. 253–260, 2009.
- [79] T. Lin, Y. Mayzel, and K. Bahartan, “The accuracy of a non-invasive glucose monitoring device does not depend on clinical characteristics of people with type 2 diabetes mellitus,” *Journal of Drug Assessment*, vol. 7, no. 1, pp. 1–7, 2018.
- [80] B. D. Cameron, J. S. Baba, and G. L. Coté, “Measurement of the glucose transport time delay between the blood and aqueous humor of the eye for the eventual development of a noninvasive glucose sensor,” *Diabetes Technology & Therapeutics*, vol. 3, no. 2, pp. 201–207, 2001.
- [81] H. Takahashi, T. Goto, T. Shoji, M. Tanito, M. Park, and E. Chihara, “Diabetes-associated retinal nerve fiber damage evaluated with scanning laser polarimetry,” *American Journal of Ophthalmology*, vol. 142, no. 1, pp. 88–94, 2006.
- [82] B. D. Cameron, J. S. Baba, and G. L. Cote, “Optical polarimetry applied to the development of a noninvasive in-vivo glucose monitor,” in *Proceedings Volume 3923, Optical Diagnostics of Biological Fluids V*, pp. 66–77, San Jose, CA, USA, May 2000.
- [83] J. C. Pickup, F. Hussain, N. D. Evans, and N. Sachedina, “In vivo glucose monitoring: the clinical reality and the promise,” *Biosensors and Bioelectronics*, vol. 20, no. 10, pp. 1897–1902, 2005.
- [84] G. M. Edelman, B. A. Cunningham, G. N. Reeke, J. W. Becker, M. J. Waxdal, and J. L. Wang, “The covalent and three-dimensional structure of concanavalin A,” *Proceedings of the National Academy of Sciences of the United States of America*, vol. 69, no. 9, pp. 2580–2584, 1972.
- [85] R. J. Russell, M. V. Pishko, C. C. Gefrides, M. J. McShane, and G. L. Cote, “A fluorescence-based glucose biosensor using concanavalin A and dextran encapsulated in a poly (ethylene glycol) hydrogel,” *Analytical Chemistry*, vol. 71, no. 15, pp. 3126–3132, 1999.

- [86] K. V. Larin, M. S. Eledrisi, M. Motamedi, and R. O. Esenaliev, "Noninvasive blood glucose monitoring with optical coherence tomography: a pilot study in human subjects," *Diabetes Care*, vol. 25, no. 12, pp. 2263–2267, 2002.
- [87] Y. Zhang, G. Wu, H. Wei et al., "Continuous noninvasive monitoring of changes in human skin optical properties during oral intake of different sugars with optical coherence tomography," *Biomedical Optics Express*, vol. 5, no. 4, pp. 990–999, 2014.
- [88] V. V. Sapozhnikova, R. V. Kuranov, I. Cicinaite, R. O. Esenaliev, and D. S. Prough, "Effect on blood glucose monitoring of skin pressure exerted by an optical coherence tomography probe," *Journal of Biomedical Optics*, vol. 13, no. 2, article 021112, 2008.
- [89] L. A. Sodickson and M. J. Block, "Kromoscopic analysis: a possible alternative to spectroscopic analysis for noninvasive measurement of analytes in vivo," *Clinical Chemistry*, vol. 40, no. 9, pp. 1838–1844, 1994.
- [90] A. M. Helwig, M. A. Arnold, and G. W. Small, "Evaluation of kromoscopy: resolution of glucose and urea," *Applied Optics*, vol. 39, no. 25, pp. 4715–4720, 2000.
- [91] T. Lin, A. Gal, Y. Mayzel, K. Horman, and K. Bahartan, "Non-invasive glucose monitoring: a review of challenges and recent advances," *Current Trends in Biomedical Engineering & Biosciences*, vol. 6, pp. 1–8, 2017.
- [92] E. Monte-Moreno, "Non-invasive estimate of blood glucose and blood pressure from a photoplethysmograph by means of machine learning techniques," *Artificial Intelligence in Medicine*, vol. 53, no. 2, pp. 127–138, 2011.
- [93] J. Yadav, A. Rani, V. Singh, and B. M. Murari, "Investigations on multisensor-based noninvasive blood glucose measurement system," *Journal of Medical Devices*, vol. 11, no. 3, article 031006, 2017.
- [94] S. Malik, R. Khadgawat, S. Anand, and S. Gupta, "Non-invasive detection of fasting blood glucose level via electrochemical measurement of saliva," *SpringerPlus*, vol. 5, no. 1, p. 701, 2016.
- [95] S. H. Ling, P. P. San, and H. T. Nguyen, "Non-invasive hypoglycemia monitoring system using extreme learning machine for type 1 diabetes," *ISA Transactions*, vol. 64, pp. 440–446, 2016.
- [96] Y. Reddy, K. Chandrasekaran, M. Karim, A. Alphones, M. Siyal, and A. Liu, "Machine learning approach for non-invasive detection of blood glucose concentration using microwave," in *2018 International Conference on Advances in Computing and Communication Engineering (ICACCE)*, pp. 89–91, Paris, France, June 2018.
- [97] J. A. Carter, C. S. Long, B. P. Smith, T. L. Smith, and G. L. Donati, "Combining elemental analysis of toenails and machine learning techniques as a non-invasive diagnostic tool for the robust classification of type-2 diabetes," *Expert Systems with Applications*, vol. 115, pp. 245–255, 2019.
- [98] T. Das, A. Ghosh, S. Guha, and P. Basak, "Early detection of diabetes based on skin impedance spectrogram and heart rate variability non-invasively," in *2017 1st International Conference on Electronics, Materials Engineering and Nano-Technology (IEMENTech)*, pp. 1–5, Kolkata, India, April 2017.
- [99] V. Turgul and I. Kale, "Permittivity extraction of glucose solutions through artificial neural networks and non-invasive microwave glucose sensing," *Sensors and Actuators A: Physical*, vol. 277, pp. 65–72, 2018.
- [100] Y. Zhang, J. Zhu, Y. Liang, H. Chen, S. Yin, and Z. Chen, "Non-invasive blood glucose detection system based on conservation of energy method," *Physiological Measurement*, vol. 38, no. 2, pp. 325–342, 2017.
- [101] J. Dai, Z. Ji, Y. Du, and S. Chen, "In vivo noninvasive blood glucose detection using near-infrared spectrum based on the PSO-2ANN model," *Technology and Health Care*, vol. 26, no. S1, pp. 229–239, 2018.
- [102] J. Yadav, A. Rani, V. Singh, and B. M. Murari, "Design of low cost blood glucose sensing system using diffused reflectance near-infrared light," in *Networking Communication and Data Knowledge Engineering*, vol. 3, G. Perez, K. Mishra, S. Tiwari, and M. Trivedi, Eds., pp. 197–216, Springer, Singapore, 2018.
- [103] C. Todd, P. Salvetti, K. Naylor, and M. Albatat, "Towards non-invasive extraction and determination of blood glucose levels," *Bioengineering*, vol. 4, no. 4, p. 82, 2017.
- [104] J. Yadav, A. Rani, V. Singh, and B. M. Murari, "Levenberg-Marquardt based non-invasive blood glucose measurement system," *IETE Journal of Research*, vol. 64, no. 1, pp. 116–123, 2018.
- [105] A. S. Balcioğlu and H. Müderrisoğlu, "Diabetes and cardiac autonomic neuropathy: clinical manifestations, cardiovascular consequences, diagnosis and treatment," *World Journal of Diabetes*, vol. 6, no. 1, p. 80, 2015.
- [106] B. Ballinger, J. Hsieh, A. Singh et al., "DeepHeart: semi supervised sequence learning for cardiovascular risk prediction," in *AAAAI Publications, Thirty-Second AAAI Conference on Artificial Intelligence*, pp. 2079–2086, New Orleans, LA, USA, 2018.
- [107] H. Kudat, V. Akkaya, A. Sozen et al., "Heart rate variability in diabetes patients," *Journal of International Medical Research*, vol. 34, no. 3, pp. 291–296, 2006.
- [108] F. Bellavere, "Heart rate variability in patients with diabetes and other noncardiological diseases," in *Heart Rate Variability*, pp. 507–516, Futura Publishing, Armonk, NY, USA, 1995.
- [109] R. E. Maser and M. J. Lenhard, "Cardiovascular autonomic neuropathy due to diabetes mellitus: clinical manifestations, consequences, and treatment," *The Journal of Clinical Endocrinology & Metabolism*, vol. 90, no. 10, pp. 5896–5903, 2005.
- [110] C. Meyer, F. Milat, B. P. McGrath, J. Cameron, D. Kotsopoulos, and H. J. Teede, "Vascular dysfunction and autonomic neuropathy in type 2 diabetes," *Diabetic Medicine*, vol. 21, no. 7, pp. 746–751, 2004.
- [111] D. J. Ewing, J. M. Neilson, C. M. Shapiro, J. A. Stewart, and W. Reid, "Twenty four hour heart rate variability: effects of posture, sleep, and time of day in healthy controls and comparison with bedside tests of autonomic function in diabetic patients," *Heart*, vol. 65, no. 5, pp. 239–244, 1991.
- [112] S. C. Malpas and T. J. Maling, "Heart-rate variability and cardiac autonomic function in diabetes," *Diabetes*, vol. 39, no. 10, pp. 1177–1181, 1990.
- [113] A. J. Camm, M. Malik, J. T. Bigger et al., "Heart rate variability: standards of measurement, physiological interpretation and clinical use. Task Force of the European Society of Cardiology and the North American Society of Pacing and Electrophysiology," *Circulation*, vol. 93, no. 5, pp. 1043–1065, 1996.
- [114] F. Shaffer and J. P. Ginsberg, "An overview of heart rate variability metrics and norms," *Frontiers in Public Health*, vol. 5, p. 258, 2017.

- [115] H. J. Baek, C.-H. Cho, J. Cho, and J.-M. Woo, "Reliability of ultrashort-term analysis as a surrogate of standard 5-min analysis of heart rate variability," *Telemedicine and e-Health*, vol. 21, no. 5, pp. 404–414, 2015.
- [116] T. Kuusela, "Methodological aspects of heart rate variability analysis," *Heart Rate Variability (HRV) Signal Analysis: Clinical Applications*, pp. 10–42, Taylor Francis, 2013.
- [117] S. Emaminejad, W. Gao, E. Wu et al., "Autonomous sweat extraction and analysis applied to cystic fibrosis and glucose monitoring using a fully integrated wearable platform," *Proceedings of the National Academy of Sciences of the United States of America*, vol. 114, no. 18, pp. 4625–4630, 2017.
- [118] H. Lee, C. Song, Y. S. Hong et al., "Wearable/disposable sweat-based glucose monitoring device with multistage transdermal drug delivery module," *Science Advances*, vol. 3, no. 3, article e1601314, 2017.
- [119] C. F. Amaral, M. Brischwein, and B. Wolf, "Multiparameter techniques for non-invasive measurement of blood glucose," *Sensors and Actuators B: Chemical*, vol. 140, no. 1, pp. 12–16, 2009.
- [120] M. Eadie and R. J. Steele, "Non-invasive blood glucose monitoring and data analytics," in *Proceeding ICCDA '17 Proceedings of the International Conference on Compute and Data Analysis*, pp. 138–142, Lakeland, FL, USA, May 2017.
- [121] American Diabetes Association, "Consensus statement on self-monitoring of blood glucose," *Diabetes Care*, vol. 10, no. 1, pp. 95–99, 1987.
- [122] B. Solnica, J. W. Naskalski, and J. Sieradzki, "Analytical performance of glucometers used for routine glucose self-monitoring of diabetic patients," *Clinica Chimica Acta*, vol. 331, no. 1-2, pp. 29–35, 2003.
- [123] S. Chaplin, "Non-invasive blood glucose testing: the horizon," *Practical Diabetes*, vol. 33, no. 9, pp. 313–315a, 2016.
- [124] D. C. Klonoff, "Continuous glucose monitoring: roadmap for 21st century diabetes therapy," *Diabetes Care*, vol. 28, no. 5, pp. 1231–1239, 2005.

Research Article

Piezoresistive Breathing Sensing System with 3D Printed Wearable Casing

Erik Vanegas, Raul Igual , and Inmaculada Plaza 

EduQTech, Electrical/Electronics Engineering and Communications Department, Escuela Universitaria Politecnica de Teruel, Universidad de Zaragoza, 44003 Teruel, Spain

Correspondence should be addressed to Raul Igual; rigual@unizar.es

Received 4 August 2019; Accepted 5 November 2019; Published 4 December 2019

Guest Editor: Janez Trontelj

Copyright © 2019 Erik Vanegas et al. This is an open access article distributed under the Creative Commons Attribution License, which permits unrestricted use, distribution, and reproduction in any medium, provided the original work is properly cited.

Respiratory rate is an important parameter for many health, home care, work, or sport applications. In this paper, a new wearable sensing system based on a piezoresistive FlexiForce sensor has been developed. The sensor can be attached to any common chest strap. A compact 3D casing has been designed and printed with a 3D printer. This casing integrates the sensor and all auxiliary elements of the system: microcontroller, battery, Bluetooth module, connections, battery charger, and acquisition circuit. To the best of our knowledge, this is the first study presenting a FlexiForce respiration sensor that includes all system elements in a single compact casing. The source files with the design of the casing have been published as supplementary material to be reused by any interested researcher. The sensing system was tested with twenty-one subjects for different breathing rates. Two different algorithms were developed to obtain the respiratory rate from the voltage signals recorded by the sensor. Statistical tests were performed to determine the optimal computation time window and algorithm. This approach is also novel in this field. Low error values were obtained for a time window of 27 s with an algorithm based on the calculation of time between zero-crossings (4.02%) and with an algorithm based on counting them (3.40%). To promote research transparency and reusability, the dataset with the recorded data and the source code of the algorithms and statistical tests have also been published. Therefore, an open, replicable, low-error, wearable, wireless, and compact sensing system to measure respiratory rate was developed and tested.

1. Introduction

Monitoring of physiological vital signs in humans, such as heart rate, respiratory rate (RR), blood oxygen concentration, body temperature, or blood pressure, is a field of growing interest with many applications. Specifically, respiratory rate is widely used in health applications such as detection of abnormal breathing patterns [1] or pulmonary disorders [2]; diagnosis of obstructive sleep apnea [3], chronic obstructive pulmonary disease [4], or asthma [5]; monitoring of anaesthetized patients [6]; monitoring during magnetic resonance imaging (MRI) [7]; indication for cardiac arrest [8], imbalance or failure in the nervous, cardiovascular, or excretory systems [8]; prevention of sudden infant death syndrome [9]; or admission to intensive care unit, among others. Respiratory rate monitoring has also been applied to occupational health [10]. Respiratory rate provides information on the psychophysiological condition of workers, which

is especially interesting for pilots, drivers, or operators of critical machines. It can be used to detect alarming symptoms of fatigue or fainting. It is also useful in other fields like home care [11] or sports [12].

There are several wearable approaches to properly measure respiratory rate [13]. One possible way is to detect variations in the velocity or volume of the respiratory airflow. For example, Liao et al. [14] presented a capacitive flow sensor. Pressure changes caused by airflow induced capacitance changes in the sensing plates. Other sensors that detect airflow variations to monitor breathing are described in [15, 16].

There are studies that presented sensors based on the recording of the sound associated with the air flowing through the airways of subjects. In this regard, Nam et al. [17] used built-in microphones of smartphones or simple headset microphones placed under the nose. The built-in microphone was manually held in a fixed position by

subjects, assuming no displacement during experiments. The amplitude of the envelope of the respiratory sounds was in the range 0.45-0.9 (amplitude units). For reliable estimates of RR, background noise was kept to a minimum. Respiratory rates could be estimated accurately even if microphones were 30 cm away from the nose.

Another set of studies recorded the temperature of inhaled or exhaled air during breathing. Cao et al. [5] presented a Bluetooth-based hot-film flow sensor. It was based on convective heat transfer. Changes in the fluidic flow condition led to variations in the resistance of the film. The sensor consisted of a micro/nanofilm inserted into a tube. Flow rates covering 0.1-100 L/min were considered in sensor design. Motion was incorporated in the validation tests, and three-axis accelerations were also recorded to assess motion intensity. Similar sensors based on this principle were developed by Huang and Huang [18] and Milici et al. [19].

Several authors registered changes in air humidity to obtain RR. Pang et al. [20] designed a porous graphene network to monitor breathing. It can be used to monitor mouth and nose respiration, including breathing patterns such as normal and deep respiration. The system described is an initial prototype that needs to be improved for commercialization. Other approaches to detect humidity variations were described in the reviews by Farahani et al. [21] and Ascorbe et al. [22].

Chemical sensors have also been used in this field to analyze breathing air components and obtain the RR from the results of analyses. Katagiri et al. [23] presented a sensor to measure carbon dioxide (CO₂) based on optical absorption spectroscopy. Other chemical approaches were discussed in the surveys by Imani et al. [24] and Güntner et al. [25].

Images taken with mobile phone cameras were also used to determine RR. The work of Karlen et al. [26] was based on placing a finger on the lens of a mobile phone's camera and extracting imaging photoplethysmogram from the region of interest to estimate the RR. Motion artifacts were detected and labeled. Then, two algorithms were used to obtain the RR. The system presented a root mean square error of 6 breaths/min, being much higher for respiratory rates greater than 20 breaths/min. Recordings with incorrect counts due to artifacts in the reference device were excluded. The same was done with RR recordings of less than 6 breaths/min or greater than 40 breaths/min. Scully et al. [27] presented a similar approach using intensity changes in the green band of the video signal.

A set of studies measured the changes in electrical bioimpedance that occur during breathing. The work of Metshein [28] presented an electrode shirt to measure electrical bioimpedance using large surface plate electrodes. They were made of aluminium foil and covered with contact gel. Electrical bioimpedance measurements were in the range of 175-300 Ω , approximately. The validation experiments included movements to show the influence of motions of human body on the measured signal. Motions and displacement of the electrodes affected the results. Displacement of the shirt was specially important in long experiments. The best electrode placement configurations were identified, matching the locations of the heart, lungs, and large blood

vessels. Similarly, Ansari et al. [29] determined RR from electrical impedance. In this case, it was measured in the arms using only four electrodes.

There are also studies that use radar for the measurement of RR. Kukkapalli et al. [30] presented a micro radar-based system designed as a wearable neck pendant. The system used the relative motion between the radar and the chest wall to estimate the RR. The radar was operated at 24 GHz; a custom active analog amplifier circuit was designed to improve sensitivity. A module with WiFi data transfer was used for data collection. Ten subjects participated in the validation experiments performed in static position. Radar technology has been widely used for RR detection, but mainly in non-wearable systems [31].

Several sensing systems were also proposed to detect chest movements associated with breathing. Dan et al. [4] described an inertial sensor platform to obtain angular velocity waveforms to calculate RR. Sensors were placed in the suprasternal notch, which is located on the upper border of the sternum. This position caused noises in signals, which had to be filtered. The sensing system was wired, ensuring stability of signal transmission. Inertial sensors were also used in the works of Hernandez et al. [32] and Estrada et al. [33].

Finally, a set of sensors registered deformations in the chest due to breathing. The sensor developed in this work is based on this principle. Several previous works in this category already exist. Table 1 shows a comparison of the sensing system proposed in this paper with several related works found in the state of the art. Some of the most relevant features of respiratory sensing systems are compared. All studies included in Table 1 detect thoracic movements. They have in common the use of a chest strap to attach the sensor to the body, which is the approach adopted in the sensor presented in this study. However, there are large differences in sensing principles, hardware processing units, data processing techniques, or data transfer technologies, among other factors.

Hesse et al. [12] designed a respiration sensor using a force-sensing resistor. Thoracic movements were recorded, and the RR was calculated using a peak detection algorithm. A simple mechanical housing mechanism consisting of two quadratic plates integrated the force-sensing resistor exclusively. The housing mechanism was attached to a chest strap, which included the rest of the elements of the system. Therefore, the mechanical housing mechanism did not contain the microcontroller, memory, battery, or any other auxiliary elements since they were attached to the strap separately. The sensor evaluation was performed with five subjects, obtaining good results for normal and deep breathing. Data were processed locally on the same strap.

A sensor to be worn on the chest was also designed by Mahbub et al. [1]. In this case, the sensing element was a piezoelectric transducer composed of a ferroelectric polymer, polyvinylidene fluoride (PVDF). PVDF had fast response time to vibration due to chest dilation. The sensor was modeled by a first-order equivalent circuit composed of a thermal capacitance shunted by a thermal resistance. The sensor generated charge (peak-to-peak amplitude of 400 pA) in response to vibrations due to breathing. A charge amplifier

TABLE 1: Comparison of several features of the proposed sensor and other state-of-the-art sensors.

Study	Sensor	Processing unit	Data display	Sampling rate (Hz)	Data transfer	Energy storage
Proposal	Piezoresistive FlexiForce A201	Arduino Pro Mini (Atmega 328p)	PC, Android device	50	Bluetooth (HC-05 module)	3.7 V-150 mAh, Li-battery
Hesse et al. [12]	Piezoresistive FlexiForce A201	MSP430FG4618	PC	100	Flash memory/nRF24L01 module	CR2025 coin cell
Mahbub et al. [1]	PVDF transducer	ADC	—	—	IR-UWB	3 V-600 mAh Li-polymer battery
Rotariu et al. [35]	Piezoelectric belt	Arduino Leonardo	Tablet, PC	10	USB serial port	—
Ciobotariu et al. [34]	Piezoelectric belt	Personal digital assistant	PC	10	WiFi, GSM/GPRS, USB serial port	CR2023 3 V, 225 mAh Lithium coin battery
Hoffman et al. [2]	Capacitive	MSP430F1612	PC	6	Bluetooth (Stollmann BlueMod+B20)	590 mAh Li-polymer battery
Grlica et al. [36]	Capacitive	DAQ commercial unit	PC	9.1	USB serial port	2,000 mAh Li-ion battery
Yang et al. [37]	Capacitive	—	Smartphone	—	Bluetooth	Coin battery
Yang et al. [38]	Capacitive	PIC24FJ256	PC	10	Bluetooth	—
Mim et al. [39]	Capacitive	DAQ commercial unit	PC	100	USB serial port	—
Witt et al. [6]	FBG	DAQ unit	DAQ unit	250	Optical fiber RF nanoLOC AVR module for telemonitoring	—
Jonckheere et al. [67]	FBG	DAQ unit	PC	—	USB serial comm.	—
Presti et al. [40]	FBG	DAQ commercial unit (interrogator)	PC	250	USB serial comm.	—
Massaroni et al. [41]	FBG	DAQ commercial unit (interrogator)	PC	250	USB serial comm.	—
Yang et al. [42]	Fiber optic microbend	Optical transceiver	PC	—	Bluetooth	—
Padasdao et al. [9]	DC brushed motor	—	—	—	—	—
Teichmann et al. [43]	Electromagnetic coupling sensing coil	Microcontroller	PC, Android device	100	Bluetooth	LiPo 2.95 Wh battery

produces an output voltage proportional to the integrated charge. This voltage ranges from 0.7 to 1 Vpp. A custom integrated circuit was responsible for processing and sending the data wirelessly. The sensor was validated with only one subject, showing respiration detection. Similarly, the works of Ciobotariu et al. [34] and Rotariu et al. [35] presented piezoelectric thoracic belts to measure respiratory activity. The first work is wireless using GSM/GPRS transmission, while the second prototype communicates with a central computer through a USB cable. None of the studies included a structured evaluation of the sensors.

Hoffman et al. [2] estimated respiration volume using a textile integrated force sensor based on the principle of plate capacitors. The sensors were composed of different layers of textiles. A compressible 3D textile was the core of the sensor. On the top and bottom of the 3D textile, conductive fabrics formed the electrodes of the plate capacitor. Expansion of the thorax during breathing caused a change in fabric thickness, which was measured as a change in the value of capacitance. The tightness of the belt that supported the sensor was set at 10 N. The pressure range to be measured was 0.3 to 0.7 N/cm. Position of the belt and the sensor changed frequently during measurements due to body movement. This led to larger errors. The authors stressed that one possible solution could be frequent recalibration of the system. However, this would affect usability and comfort. Eighteen subjects participated in the validation tests and results showed a high correlation of the measurements with respect to a reference device, although the estimation of the respiratory volume was not accurate enough (37.9% error). Tests included activities with movements. Similarly, Grlica et al. [36] presented a capacitive sensor that detected changes in capacitance in the range from 0.1 to 0.5 pF for normal breathing. The sensor consisted of a fixed triangular electrode and a rectangular moveable electrode. Total electrode displacement was approximately 40 mm for deep breathing. The sensor of Yang et al. [37] included a low-energy Bluetooth wireless communication module to transmit capacitance values to a smartphone. This same transmission technology was used in the work of Yang et al. [38] with the sensor integrated in a shirt. Min et al. [39] also presented a capacitive sensor made of conductive fabric and polyester. The sensor designed was linear with sufficient resolution to measure a wide range of breathing from different subjects. Force was increased from 0 to 3 N, producing a capacitance change of 445-510 pF. The authors stressed that the position during tests may affect performance.

Witt et al. [6] designed a system to measure thoracic motion continuously based on optical fiber sensors. Specifically, the sensor was based on fiber Bragg gratings (FBG), macrobending effect, and optical time-domain reflectometry. The sensor was specifically for patients under MRI. It was tested in simulators and in climate chambers. FBG sensor can be stretched up to 3% elongation with a sensitivity 0.32 nm. Results showed that the sensor retained its stability for different elongations. The same principle (FBG) was also used in the sensor of Presti et al. [40]. In that case, an array of 12 FBG was designed. The placement of the 12 FBG in subject's torso was optimized. Five subjects participated in the

validation of the sensor and measurements were analyzed offline, obtaining a minimum error. FBG were also used by Massaroni et al. [41] to monitor compartmental and global volumetric parameters. Six subjects participated in the experiments, obtaining an error in the tidal volume of 14%. Similarly, Yang et al. [42] developed a fiber optic respiratory sensor based, this time, on the microbend effect. That study verified the RR by counting the number of breaths manually. The sensing belt was stretched 20 mm and 40 mm, which corresponded to elongations of 2.14% and 4.28%.

Padasdao et al. [9] presented a respiratory chest sensor based on human energy harvesting. An off-the-shelf dc brushed motor was used to detect thoracic movements as a function of average harvested power. The expansion of the chest due to respiration turned the armature, which transmitted the movement to the gears and the rotor of the machine. The motor was integrated into a plastic casing and mounted on a piece of felt to stabilize the device against the body. Displacements of 1 cm and 3 cm were considered in the experiments. Average output power harvested by the motor was in the range 6-72 μ W. To eliminate motion artifacts, voltage outputs were filtered with a low-pass finite impulse response (FIR) filter. The sensor was validated with twenty subjects, obtaining that RR was measured with a low error value.

The proposal of Teichmann et al. [43] is also innovative, since they presented a sensor based on magnetic induction to obtain RR. A coil was the core element of the sensor. The sensor detected variations in the distribution of human impedance due to thoracic movements associated with breathing through electromagnetic coupling. The sensing system was completed with a microcontroller and a Bluetooth module. The sensor was placed on a flexible PCB. All other electronic components (except for the power management) were also mounted on there. The impact of coil deformation was also investigated since the sensor was designed to be carried in the shirt pocket. Four subjects participated in the evaluation. The authors stressed that the spatial fusion of different sensors could allow the cancellation of motion artifacts. However, this was not tested in the study.

This paper presents a compact wireless sensing system based on a piezoresistive sensor (A201 FlexiForce sensor, Tekscan [44]) to monitor respiratory rate. As can be seen in Table 1, the proposal of Hesse et al. [12] is the most related work to the sensing system presented in this paper. A systematic search was conducted in the literature, and no other works were found that use a piezoresistive FlexiForce sensor, to the best of our knowledge. This paper contributes with several novelties to the state of the art:

- (i) One key aspect of the piezoresistive FlexiForce sensor is the casing, since it determines the sensor detection capabilities. In the work of Hesse et al. [12], a casing was designed only for the sensor, while the rest of the elements (microcontroller, transmission unit, flash memory, etc.) were considered separately. Therefore, the casing did not include them in a compact way. In this paper, we present a wireless FlexiForce sensor integrated in a single casing to

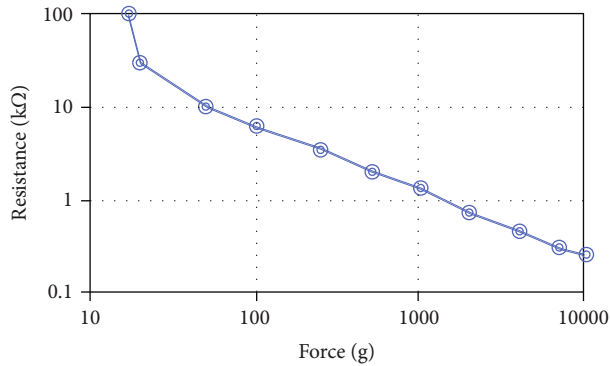


FIGURE 1: Force-resistance curve of FlexiForce A201 sensor provided by the manufacturer [46].

measure RR. All system components (FlexiForce sensor, microcontroller, Bluetooth module, battery, etc.) are integrated in the wearable casing. A 3D casing was designed and printed on a regular 3D printer. The files with the 3D design of the casing have been published as supplementary material (available here) to be reused by any interested researcher

- (ii) The system has been tested with several subjects using a metronome. Two popular algorithms have been used for the calculation of respiratory rate. Additionally, both algorithms have been compared to determine which one measures RR more accurately. Statistical tests have been used for that purpose. The optimal time window of the algorithms has also been determined using statistical tests. This is a novel approach in this field
- (iii) Another novelty of this work is that a public dataset has been created with all the data recorded in the tests. It is publicly available for use by any interested researcher [45]. In addition, the files with all data processing (algorithms and statistical tests) have been published as supplementary material to this paper. We have not found any other study on respiratory monitoring that makes public all study data and resources

2. Prototype Design

2.1. Physical Prototype. A sensor has been developed to measure respiratory rate by detecting variations in chest movement. The sensing system was designed to be placed around the chest with a strap. The system uses a force-sensitive resistor (FSR) based on the piezoresistive effect (FlexiForce A201 sensor, Tekscan). The characteristic curve of this sensor is not linear, but logarithmic, as shown in Figure 1 (curve provided by the manufacturer). The resistance provided by the sensor drops as the exerted force increases. This sensor is suitable for applications in which force variations must be detected. This is the case of RR measurement. The conditioning circuit for this sensor is a simple voltage divider as shown in Figure 2. An analysis of the typical operating region of the

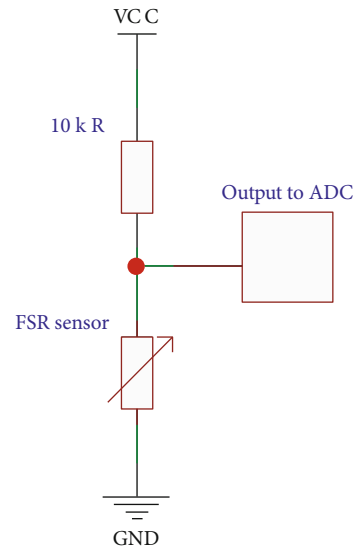


FIGURE 2: Conditioning circuit of the piezoresistive FlexiForce sensor.

FSR has been performed for the application presented in this paper. For this analysis, the data collected according to the experiments described in Experimental Setup have been used. First, the histogram associated with the voltage recorded by the sensor has been represented in Figure 3(a). For this application, it is important that the voltage varies over a wide range. The typical operating region ranges from 0.2 V to 1.7 V. Second, the histogram of resistance variation is represented in Figure 3(b). Third, Figure 3(c) shows the histogram of the forces related to those resistance values. The typical operating region corresponds to force values in the range of 50-500 g. These force values have been calculated after fitting the equation of the resistance-force curve provided by the manufacturer.

$$\text{Force(g)} = \sqrt[0.827]{\frac{399.88}{R(\text{k}\Omega)}} \quad (1)$$

In the typical region of operation (2kΩ – 10kΩ), the force can be considered to vary linearly with the conductance, according to the datasheet provided by the manufacturer [46].

The sensing system takes samples from the piezoresistive sensor through an Arduino Pro Mini that operates at a sampling frequency of 50 Hz, and sends the data using an HC-05 Bluetooth module. Data are received by a processing unit with Bluetooth technology (i.e., computer, Android, or iOS device), as shown in Figure 4. Then, they are downloaded to be processed offline in MATLAB or any other numerical computing software. The range of the Bluetooth module is around 10 m with a data transfer rate of up to 3 Mbps [47, 48]. The reliability of the Bluetooth module as part of the sensing system was also measured. For that, four experiments were performed. They consisted of transmitting a known value to the receiving unit at different distances: 1 m,

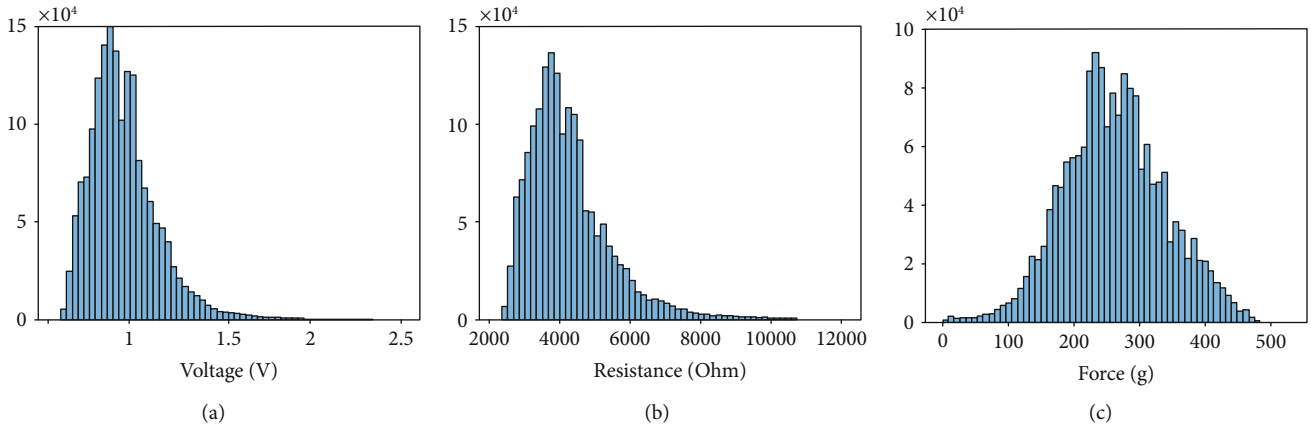


FIGURE 3: Histograms with the distribution of voltage (a), resistance (b), and force (c) for the signals captured in the experiments performed in this study.

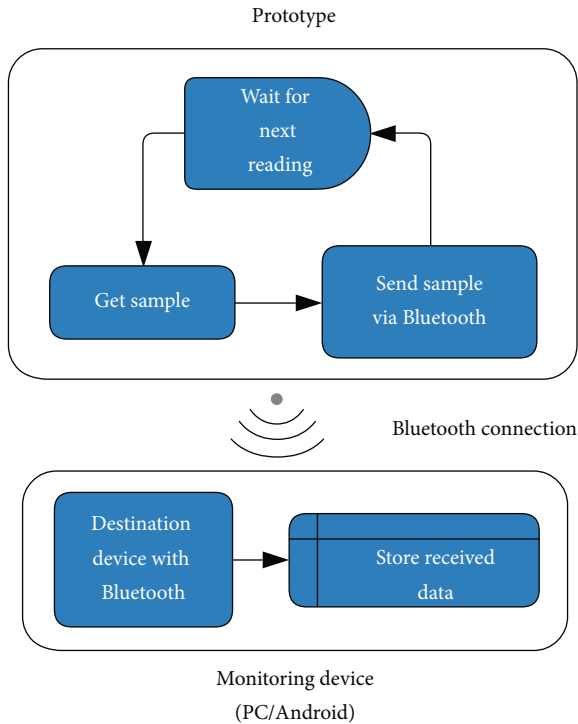


FIGURE 4: Block diagram of data acquisition and communication of the proposed system.

3 m, 5 m, and 10 m. The transmission frequency was 50 Hz. The sensing system was in motion during the experiments and there were obstacles between the transmitter and the receiver. Each experiment was performed for 30 min. As a result, no corrupted value was received. The average percentage of lost packets was 0.03% (standard deviation of 0.01%).

The sensing unit was powered by a 3.7 V, 150 mAh lithium battery, although the casing was also designed to accommodate batteries of 300 mAh, 400 mAh, and 500 mAh capacity. These batteries were selected since they can be

TABLE 2: Current consumption of the main components of the sensing system.

Component	Current consumption
Arduino Pro Mini	9.65 mA
Bluetooth	30.5 mA
FSR sensor	0.2-360 μ A
Total	40.15-40.51 mA



FIGURE 5: Elements of the sensing system mounted: front of the prototype with the Arduino Pro Mini, battery charger, and FSR (a) and back of the prototype with the Bluetooth module and battery (b).

integrated into the casing in a compact way. The current consumption of the different components of the prototype was measured. The average values are shown in Table 2. These values are in line with those provided in the datasheets by the manufacturers [46–49]. The battery life of the prototype was also measured, obtaining average values of 3.83 h, 7.88 h, and 13.01 h for batteries of 150 mAh, 300 mAh, and 500 mAh capacity, respectively. A battery was considered discharged when the voltage was below 3.6 V, following the recommendation of Lee et al. [50]. Regarding their safety, lithium-ion batteries are used massively. Statistically, they are very reliable since failure rates for rechargeable units are on the order of one in 10 million cells [51].

A TP4056 board is used to manage battery recharge. It ensures that both current and voltage remain constant during battery charging. The board consists of a processor and a battery protection circuit. It regulates the charging current

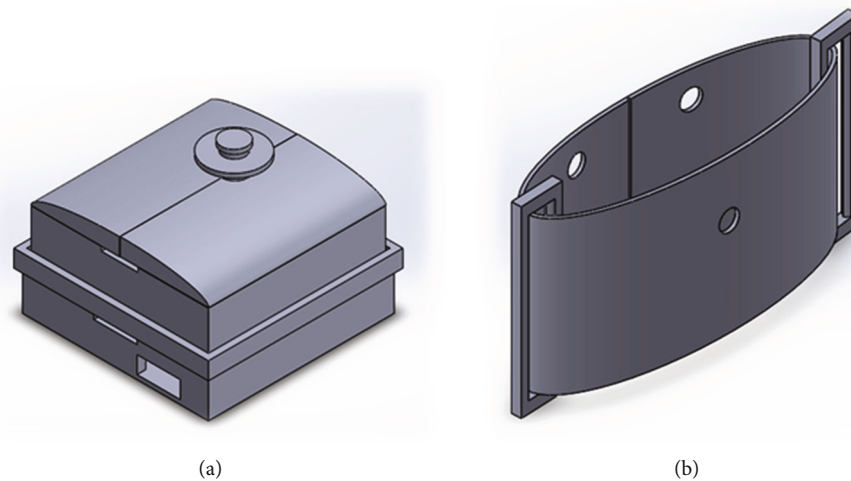


FIGURE 6: 3D design of the casing. PLA-printed part (a) and flexible PLA-printed part (b).

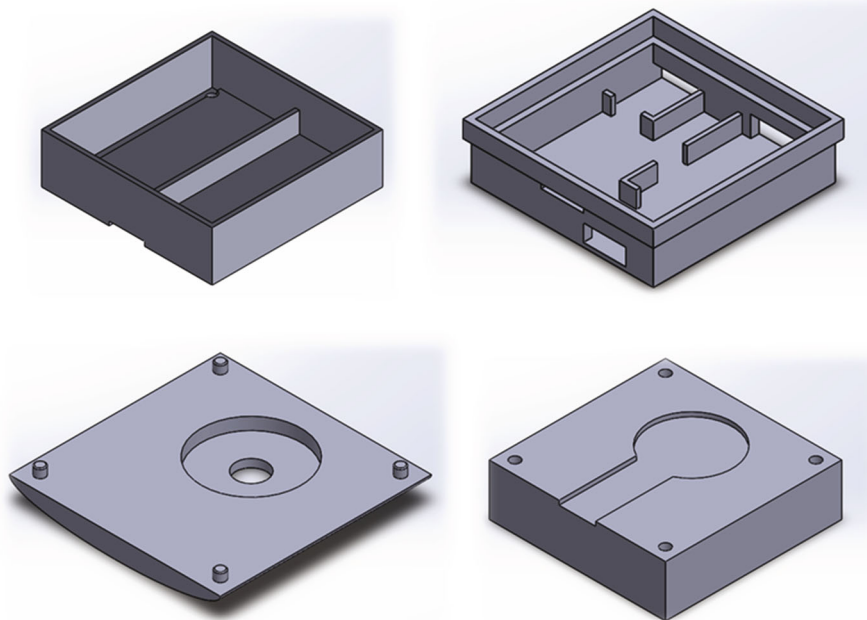


FIGURE 7: Internal design of the prototype (details in the Supplementary Materials).

under conditions of high power operation or high ambient temperature. The board also ends the charging cycle when the current drops 10% of the programmed value. It also has an internal MOSFET battery disconnect switch to avoid negative charging currents [52].

With respect to the operating temperatures supported by the prototype, the values for the different components were extracted from their datasheets: Bluetooth (-20 to 55°C), Arduino Pro Mini (-40 to 85°C), battery charger (-40 to 85°C), and battery (-20 to 60°C). The sensing system is not designed to be submerged in water. However, it is not different from any other object printed with polylactic acid mate-

rial, which means that the casing can withstand weak levels of rainwater. Figure 5 shows a photograph of the mounted components of the sensing system outside the casing.

A casing to contain all the elements of the sensing unit was designed in the Autodesk software. This casing has two main parts:

- (i) An element printed with standard polylactic acid (PLA) containing the piezoresistive sensor, the conditioning circuit, the microprocessor, the Bluetooth module, the battery, and the battery charger (Figure 6(a), Figure 7, and pink case of Figure 8)



FIGURE 8: Prototype designed with all the circuitry embedded inside.

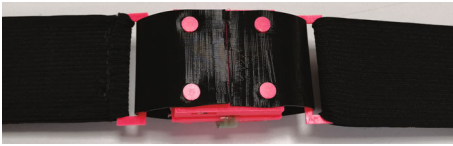


FIGURE 9: Back of the casing showing the fixation of the flexible part to the solid part. The belt is attached to both sides of the flexible part by two rings.

- (ii) An element printed with flexible PLA that allows transmitting chest movements to the sensing element (Figure 6(b) and black cover of Figure 8)

The sensing system is attached to the belt through two rings coupled to the flexible part. Figure 9 shows a photograph of the back of the casing. The sensing unit was designed to be worn on a garment, although direct contact with the skin would also be possible. The total size of this prototype is 73 mm wide \times 45 mm high \times 37 mm deep (Figure 8). The internal volume of the pink case is 30.42 cm³, while the weight of the entire prototype is 103 g (21 g for circuitry, 23 g for the 3D printed casing, and 59 g for the belt and the rings). The 3D design of the casing has been published as supplementary material and is available to be reused or reprinted by any interested researcher.

2.2. Data Processing. To measure the respiratory rate of the signals received on the remote unit via Bluetooth, different processing operations are performed. Firstly, data are filtered with a 0.5 Hz-low-pass digital filter, which “smooths” the signals by removing high-frequency noise. A minimum-order FIR or infinite impulse response (IIR) filter with a stop band attenuation of 60 dB and compensation for the delay was used [53]. This frequency has been selected because breathing rates above 30 BPM are rare in daily life activities of humans [54, 55]. An analysis of the system error was also performed considering cut-off frequencies in the range 0.5-4.5 Hz, obtaining the lowest error values for 0.5 Hz. In addition, to prevent that a trend in the signals (systematic increase or decrease) due to sensor or subject movement during the tests affects system performance, a linear fit was made

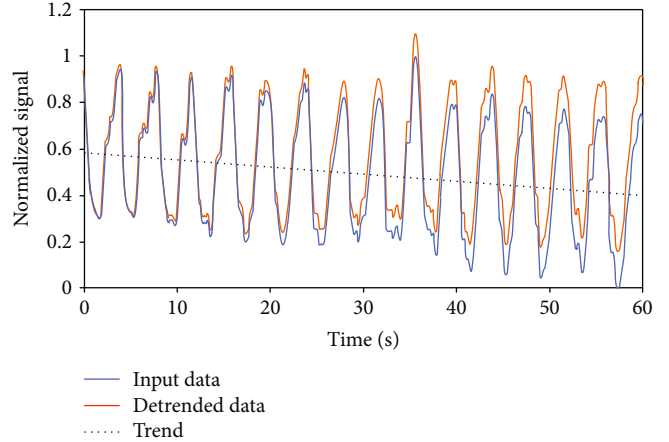


FIGURE 10: Comparison between original signal, its trend line, and the systematic shift correction.

to each signal and was subtracted from the original signal (Figure 10). In this way, systematic shifts were removed. These shifts are not relevant if signals are analyzed in short time windows. However, they affect system accuracy in large windows. Therefore, this preprocessing helps to prevent the algorithm from malfunctioning in large windows due to sensor movements other than breathing.

Then, the maximum and minimum points are obtained in a given analysis time window (w). For that, a subset of data which includes only the values in the time window is segmented. It has the form of a vector (x). This vector is used to calculate the level corresponding to the “zero 280 axis” (ZA), according to the following equation:

$$ZA = \frac{\min(x) + \max(x)}{2}, \quad (2)$$

where x is a vector with the filtered data sequence. The length of x depends on the time window, which is a parameter whose optimal value has to be selected (see Validation Experiments). The time window w slides through the entire signal. To avoid that outliers due to isolated deep breaths may raise the ZA value, peaks with prominence of at least 0.03 V 285 are detected and $\max(x)$ is set to the amplitude of the median of all the detected peaks. The prominence threshold value was selected after performing simulations in the range of 0.013-0.13 V, since it led to the lowest error values.

ZA will be the reference value used to detect zero-crossings in the data. To detect these crossing points, the segmented data set x will be assessed by taking pairs of two consecutive samples (x_k, x_{k+1}). If inequalities 3 are fulfilled, a new zero-crossing will be detected and the time $k(1/f_s)$ will be added to a vector containing the zero-crossings in the time window (z). f_s is the sampling frequency of the sensing system, in this case, 50 Hz.

$$\begin{aligned} x_k &\leq ZA < x_{k+1}, \\ x_k &\geq ZA > x_{k+1}. \end{aligned} \quad (3)$$

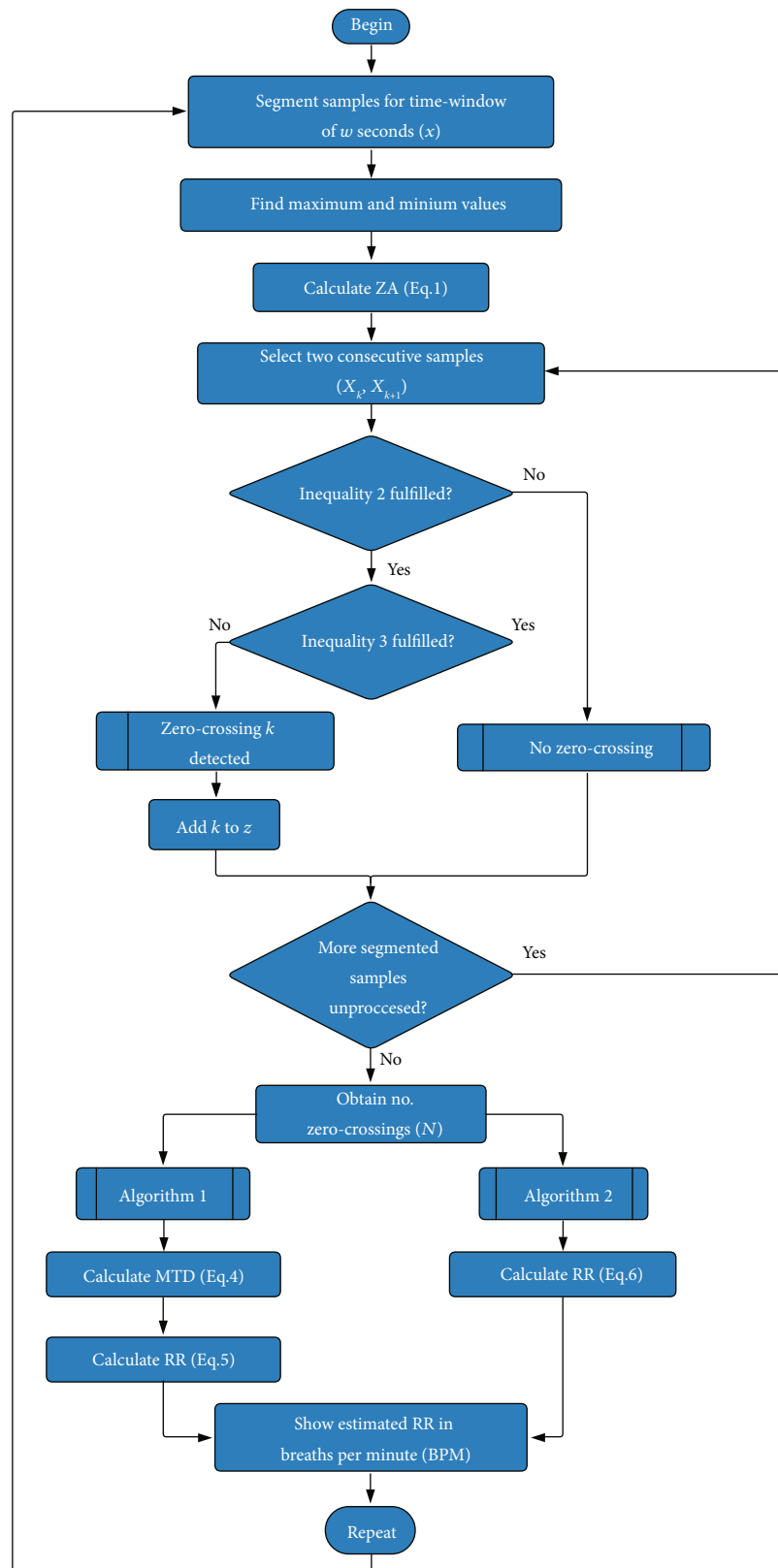


FIGURE 11: Block diagram of the data processing algorithms used to estimate the RR.

To avoid detecting two close zero-crossings due to noise, the zero-crossing at position $j(z_j)$ will be removed from z if z_j does not differ, at least, a set threshold (TH) from the rest of the elements of z , that is, if inequality 4 is satisfied.

$$|z_j - z_i| < \text{TH}, \quad \forall i \in [1, N] | i \neq j, \quad (4)$$

where N is the length of vector z , j is the index of the zero-crossing under analysis, and i is the index for the rest of zero-crossings in z . The value of TH has been empirically set to 500 ms.

Then, two different algorithms are used to measure the RR. Figure 11 shows a block diagram of both algorithms. The operation of the algorithms is as follows:

Algorithm 1. This algorithm is based on the time difference between consecutive zero-crossings [4, 39]. Firstly, the mean time difference (MTD) between consecutive pairs of zero-crossings is obtained as follows:

$$\text{MTD} = \frac{\sum_{i=1}^{N-1} |z_i - z_{i+1}|}{N-1}. \quad (5)$$

Then, with that average value of all times, the respiratory rate RR (in breaths per minute, 305 BPM) is calculated according to the following equation:

$$\text{RR} = \frac{30}{\text{MTD}}. \quad (6)$$

To obtain that equation, it was taken into consideration that two zero-crossings occur in a breathing cycle (2 MTD s, is a breathing period) and that the RR is given in breaths per minute (if one breath occurs in 2 MTD s, in 60 seconds, there should be 60/2 MTD breaths).

Algorithm 2. This algorithm is based on counting the number of crosses by zero [56]. For that, the length of the vector z is obtained, which is directly the number of zero-crossings (N). Then, the RR is obtained according to the following equation.

$$\text{RR} = \frac{30N}{w}, \quad (7)$$

where w is the duration of the time window (in seconds). Equation (7) is obtained by scaling the number of zero-crossings to 60 seconds ($60N/w$), so that the number of zero-crossings in 1 minute is obtained. As each breath is composed of 2 zero-crossings, by dividing this value by 2, the RR is obtained.

The sliding time window (w) used in the algorithms is a parameter that can take any desired value. Once a time window has been selected, the RR is updated every w seconds. The methods of counting peaks or zero-crossings or measuring distances between them have been widely used in previous studies to obtain RR [10, 40, 57–59].



FIGURE 12: Two subjects involved in the validation experiments wearing the prototype around the chest.

3. Materials and Methods

3.1. Experimental Setup. An experimental setup was designed to validate the sensor developed. Experiments involved twenty-one subjects. Fifteen were male and six were female. Ages ranged from 19 to 55 years with an average of 35.95 and a standard deviation of 10.5. Subjects' weights were between 42 and 95 kg (average of 70.76 kg and standard deviation of 14.83 kg). As for heights, they were in the range of 1.52–1.83 m with an average of 1.72 m and a standard deviation of 7.51 cm.

The diameter of the thoracic region was also measured, obtaining values from 68 to 103 cm (average of 87.90 cm and standard deviation of 12.36 cm). The health status of the participants was also noted. Sixteen subjects declared no respiratory problems, while five suffered from breathing allergies and two of them also from asthma. Subjects were asked to wear the breathing sensor placed just below the chest, at the level of the diaphragm, as shown in Figure 12. The sensor was connected via Bluetooth to a computer running a program that was developed specifically for this study. The computer program was written in Processing.

Regarding the validation protocol, each subject was asked to breathe during one minute at the rhythm of a metronome. The metronome was set so that subjects followed a rhythm of 10, 12.5, 15, 17.5, 20, and 22.5 BPM. There are studies in the literature that use this method (metronome as a reference) to validate their sensing systems in a controlled breathing scenario [4, 17, 27, 57, 60, 61]. The reference values of BPM considered are in accordance with the typical respiratory rates in humans [62]. Subjects were asked to repeat the experiment in different positions: sitting without moving, sitting with movement, standing without moving, standing with movement, and walking. A one-minute resting time was given between two consecutive experiments. All participants received written and oral information about the study, and informed consent was obtained from them to publish their data anonymously in a public repository.

Each set of breathing data was recorded in a different text file (two example signals are shown in Figure 13). Thirty files were recorded for each subject (six BPM times five activities).

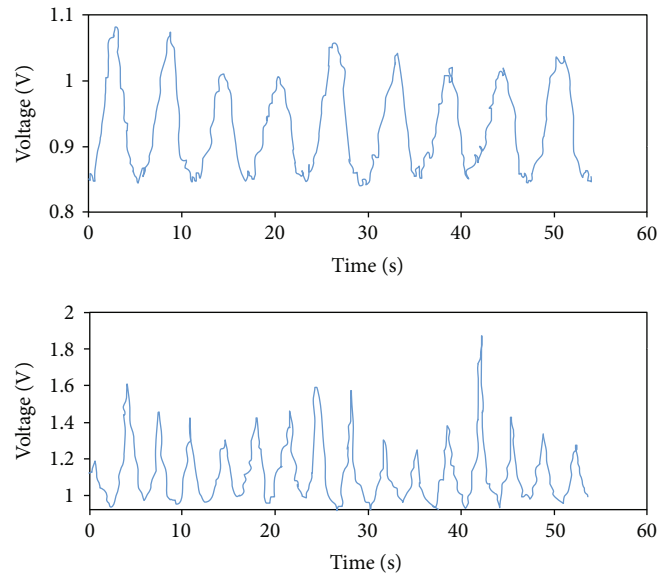


FIGURE 13: Two raw breathing signals captured by the FlexiForce sensor. The upper graph corresponds to an experiment performed at a rate of 10 BPM in a sitting position without movement. The lower signal was captured at 17.5 BPM during the walking activity.

Therefore, a total of 630 files were collected as a result of the experiments. The files were processed offline to obtain the RR according to the algorithms described in Data Processing. MATLAB was used to perform the processing. The MATLAB code is given as supplementary material to this paper.

Figure 13 shows two example of breathing graphs. The upper signal contains nine breathing cycles. A typical breathing signal has an approximate sinusoidal shape with a negative slope for inspiration and a positive slope for expiration. It also has an upper peak corresponding to the situation in which all the air has been exhaled and a lower peak associated with the moment when all the air is inside the lungs. Typical absolute slope values are 0.1-0.2 V/s for low intensity activities, 0.2-0.28 V/s for moderate intensity activities, and 0.28-0.35 V/s for higher intensity activities. These values were estimated theoretically and from the signals recorded in the experiments. Slope values are low since they were measured in the time-voltage graphs and breathing signals are low frequency.

3.2. Validation Experiments. The validation experiments allow in determining the accuracy of the sensor and the optimal processing algorithm and its parameters.

For that, the collected data were processed with the two algorithms described in Data Processing. For each algorithm, a different RR was obtained for each participant and dataset (in total 1260 values, 630 per algorithm). In addition, the algorithms are influenced by the width of the time window used to perform the RR calculation. Therefore, twenty-five different time windows have been considered: from 6 s to 30 s. Windows below 6 s were not considered since the reference BPM value with the lowest frequency had a period of 6 s. At least one period is required to obtain the RR. Windows above 30 s were not considered, since an update time greater than this value may be excessive for many applications

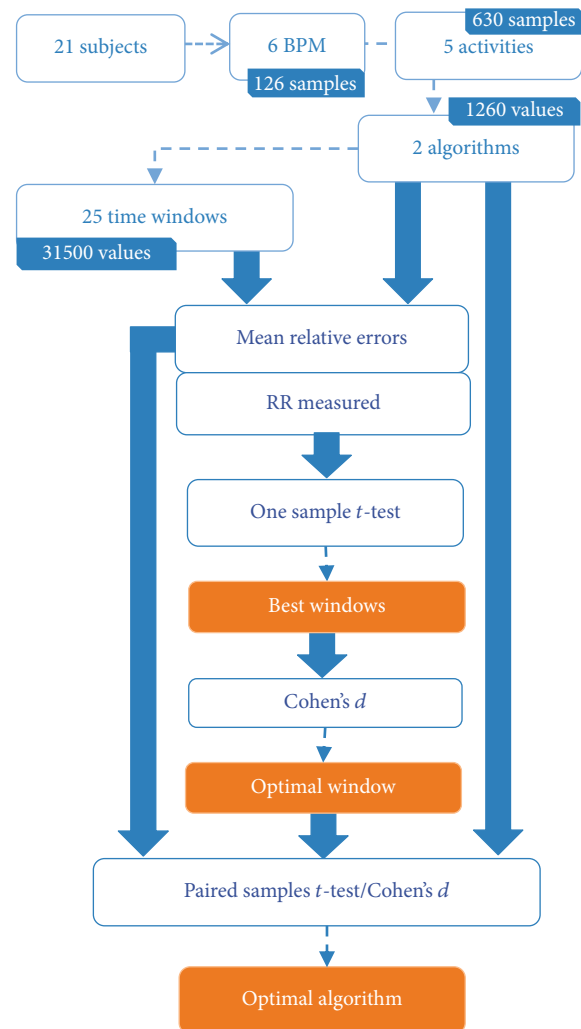


FIGURE 14: Scheme of the validation experiments performed.

TABLE 3: Maximum structural relative errors for Algorithm 1 (extreme cases).

	10 BPM	12.5 BPM	15 BPM	17.5 BPM	20 BPM	22.5 BPM
Error (%)	0.67	0.83	1.00	1.17	1.33	1.50

TABLE 4: Maximum structural relative errors (%) for Algorithm 2 (down and up), considering the time window error and the quantization error for extreme cases. If a single value is provided, it is because the up and down errors are the same.

Window (s)	10 BPM	12.5 BPM	15 BPM	17.5 BPM	20 BPM	22.5 BPM
6	-50, 50	20.0	0.0	-14.3	-25, 25	11.1
7	28.6	2.9	-14.3	22.4	7.1	-4.8
8	12.5	-10.0	-25, 25	7.1	-6.3	-16.7, 16.7
9	0.0	-20.0	11.1	-4.8	-16.7, 16.7	3.7
10	-10.0	20.0	0.0	-14.3	5.0	-6.7
11	-18.2	9.1	-9.1	9.1	-4.5	9.1
12	-25, 25	0.0	-16.7, 16.7	0.0	-12.5, 12.5	0.0
13	15.4	-7.7	7.7	-7.7	3.8	-7.7
14	7.1	-14.3	0.0	10.2	-3.6	4.8
15	0.0	12.0	-6.7	2.9	-10, 10	-2.2
16	-6.3	5.0	-12.5, 12.5	-3.6	3.1	-8.3, 8.3
17	-11.8	-1.2	5.9	-9.2	-2.9	2.0
18	-16.7, 16.7	-6.7	0.0	4.8	-8.3, 8.3	-3.7
19	10.5	-11.6	-5.3	-0.8	2.6	5.3
20	5.0	8.0	-10, 10	-5.7	-2.5	0.0
21	0.0	2.9	4.8	6.1	-7.1, 7.1	-4.8
22	-4.5	-1.8	0.0	1.3	2.3	3.0
23	-8.7	-6.1	-4.3	-3.1	-2.2	-1.4
24	-12.5, 12.5	-10, 10	-8.3, 8.3	-7.1, 7.1	-6.3, 6.3	-5.6, 5.6
25	8.0	5.6	4.0	2.9	2.0	1.3
26	3.8	1.5	0.0	-1.1	-1.9	-2.6
27	0.0	-2.2	-3.7	-4.8	-5.6, 5.6	3.7
28	-3.6	-5.7	-7.1, 7.1	4.1	1.8	0.0
29	-6.9	7.6	3.4	0.5	-1.7	-3.4
30	-10, 10	4.0	0.0	-2.9	-5, 5	2.2

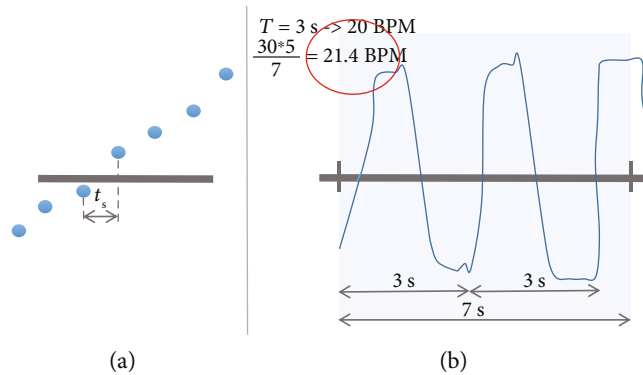


FIGURE 15: Example of possible structural errors associated with Algorithm 1 (a) and Algorithm 2 (a, b).

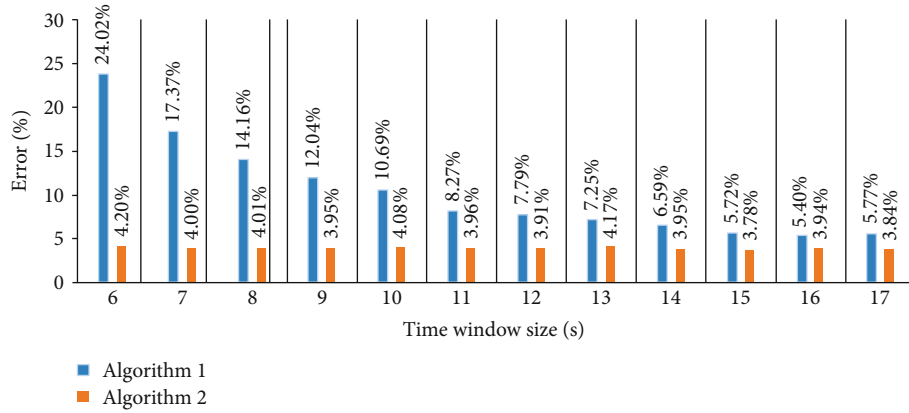


FIGURE 16: Errors (δ) of the proposed sensor for the two processing algorithms for time windows between 6 and 17 s.

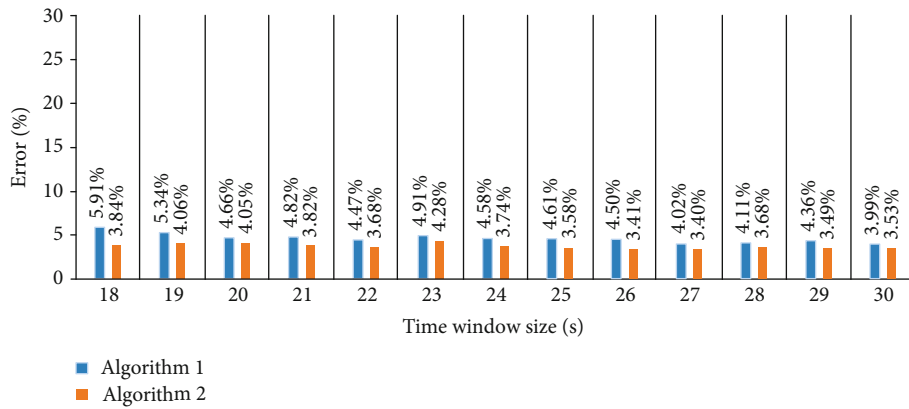


FIGURE 17: Errors (δ) of the proposed sensor for the two processing algorithms for time windows between 18 and 30 s.

[26, 63, 64]. For each time window, the entire analysis was repeated (in total 31,500 RR values; 15,750 per algorithm). The elimination of trends due to movements in the sensor was only applied to large windows (above 21 s for Algorithm 1 and above 19 s for Algorithm 2) since no decrease in error was perceived in shorter windows. Figure 14 shows the structure of the experiments graphically.

To obtain the optimal time window, the one sample t -test was used. This test is suitable to compare the mean of one sample with a known reference value. The null hypothesis (H_0) is as follows:

$$H_0 : m = \mu, \quad (8)$$

where m is the mean of RR and μ is the reference value of BPM set by the metronome, which was considered the gold standard.

Specifically, this test was performed for each time window and repeated for all reference values of BPM tested. In total, 150 tests were conducted.

As a result of this test, the p values greater than the significance level (0.05) were identified. For the time windows and reference values associated with those p values, the null hypothesis could not be rejected. In other words, sample means cannot be assumed to be significantly different from

reference values. Therefore, we can assume that the sensor is measuring RR accurately for those BPM and time windows. The time windows that have the largest number of p values greater than 0.05 could be considered candidates for optimal windows. For those reference values of the candidate windows having p values below 0.05 (the mean is significantly different from the reference value), the Cohen's d test can be performed to quantify the effect size [65]. It can be obtained as the ratio of the difference between two mean values (one of them can be the reference value) divided by their pooled standard deviations. Small effect sizes are desirable. This would indicate that the difference between the means of RR and the reference values is small. A quantification of the effect size magnitude ("rule of thumb") can be made using the thresholds defined in [66]: $d < 0.2$ (negligible effect), $d < 0.5$ (small effect), and $d < 0.8$ 395 (medium effect). Otherwise, the effect can be categorized as large. Therefore, the time window with the smallest effect sizes can be considered optimal.

In parallel, the relative error (δ) was calculated according to the following equation:

$$\delta = 100 \times \left| 1 - \frac{\mu_0}{\mu} \right|, \quad (9)$$

where μ_0 is a measured RR and μ is the reference value of BPM set by the metronome. In total, 1,500 error values were calculated (2 algorithms times 6 reference values times 5 activities times 25 time windows). The means of the errors were made for all activities and reference values, obtaining 50 mean errors (25 per algorithm, 2 per time window).

To determine the optimal algorithm for the optimal time window, the paired sample t -test was performed since it is appropriate to compare the means between two groups of related samples. This test was performed on the means of the relative errors (δ). The null hypothesis (H_0) is as follows:

$$H_0 : m = 0, \quad (10)$$

where m is the mean of differences. If the p value is less than or equal to the significance level (0.05), it can be assumed that the two paired samples (algorithm errors) are significantly different. In that case, the algorithm with the lowest error could be considered the best. Figure 14 presents an overview of the validation experiments. All statistical tests have been performed in the R software. The R code is given as supplementary material to this paper.

In relation to the errors, it is important to highlight that some structural errors are already introduced by the sampling frequency or the time window selected, depending on the algorithm. For Algorithm 1 (based on time measurements), there is a quantization error set by the sampling frequency of up to 1/50 s at each zero-crossing. As one cycle has two zero-crossings, the maximum structural error in one cycle can be expressed in relative terms for each reference BPM value (Table 3). For Algorithm 2 (based on counting zero-crossings), the time window already introduces some error. All time windows that are not divisible by integer multiples of half the breathing period under analysis suffer this error. For this algorithm, the quantization error can also affect in some extreme cases in which the appearance or not of a zero-crossing depends on the sampling frequency (zero-crossings that appear exactly at the beginning or end of a window). Taken into consideration both effects (time window and sampling frequency), their associated maximum relative errors (up and down) are estimated in Table 4. It should be noted that the limits of structural errors calculated in Tables 3 and 4 are maximum values for extreme cases. Figure 15 graphically shows an example of two structural errors.

4. Results

Figures 16 and 17 represent the mean error for the twenty-five time windows under analysis and for the two algorithms used to obtain the RR. The standard deviations of these mean values are shown in Table 5. The values of the RR measured and the source code with the calculation of their mean errors and standard deviations have been attached to this paper as supplementary material.

Table 6 shows the p values of the one-sample t -test for each time window. In view of this table, it is clear that the 27 second window has more p values greater than 0.05: four in this case. This means that RR average values and reference

TABLE 5: Standard deviations (%) of the mean relative errors (δ) for each algorithm and time window.

Window (s)	Algorithm 1	Algorithm 2
6	23.87	5.67
7	17.16	4.76
8	15.32	5.10
9	12.71	4.46
10	11.96	4.49
11	8.78	4.32
12	9.41	4.53
13	8.20	4.63
14	8.00	3.78
15	7.04	3.63
16	6.89	4.06
17	7.09	4.12
18	6.70	4.12
19	5.84	5.13
20	5.04	4.51
21	5.54	4.21
22	5.81	4.61
23	6.35	5.04
24	5.84	4.27
25	5.34	4.06
26	4.99	3.95
27	5.09	4.28
28	5.05	3.96
29	5.42	4.09
30	4.94	3.64

values can be assumed to be equal for this time window and BPM. Therefore, this is the optimal window in the terms defined in this experiment.

Cohen's d was calculated for those BPM of the 27 s window that present statistically significant differences. Table 7 presents the results obtained.

For this window, the error values in the calculation of the RR provided by the two algorithms were compared. Table 8 shows the results. It can be seen that the p value of the t -test for paired samples is above the significance level (0.05). This means that the difference between the two paired means of error values is not significant. Therefore, it is not clear the algorithm that presents the lowest error. Both algorithms seem to behave equally well.

The executable source code associated with all statistical tests has been attached to this paper as supplementary material.

5. Discussion

The accuracy of the sensor designed presents less average error value for Algorithm 2 than for Algorithm 1. However, this difference is not statistically significant. Both algorithms

TABLE 6: p values greater ($>$) or less ($<$) than the significance level (0.05) for the RR calculated for each time window and reference value.

Window (s)	10 BPM	12.5 BPM	15 BPM	17.5 BPM	20 BPM	22.5 BPM
6	<	<	<	<	<	>0.05
7	<	<	<	<	<	>0.05
8	<	<	<	<	>0.05	>0.05
9	<	<	<	<	>0.05	<
10	<	<	<	<	>0.05	<
11	<	<	<	<	>0.05	>0.05
12	<	<	<	<	>0.05	<
13	<	<	<	<	>0.05	<
14	<	<	<	>0.05	>0.05	<
15	<	<	<	>0.05	>0.05	<
16	<	<	<	>0.05	<	<
17	<	<	>0.05	>0.05	<	<
18	<	<	>0.05	>0.05	>0.05	<
19	<	<	<	>0.05	>0.05	<
20	<	<	<	>0.05	>0.05	<
21	<	<	<	>0.05	>0.05	<
22	<	<	<	>0.05	>0.05	<
23	<	<	<	>0.05	>0.05	<
24	<	<	<	>0.05	<	<
25	<	<	<	>0.05	<	<
26	<	<	<	>0.05	>0.05	<
27	<	<	>0.05	>0.05	>0.05	>0.05
28	<	<	<	>0.05	>0.05	>0.05
29	<	<	<	>0.05	>0.05	<
30	<	<	>0.05	>0.05	>0.05	<

TABLE 7: Effect size quantified with Cohen's d test.

	27 s window
10 BPM	1.06
12.5 BPM	0.53

TABLE 8: Comparison of the two algorithms. p values of the t -test for paired samples and Cohen's d for errors calculated with a 27 s window.

	t -test	Cohen's d
p value	0.0884	0.1320

are influenced, at the same time, by the time window considered. The validation results presented have allowed determining the optimal time window.

A time window of 27 s seems optimal to obtain the highest sensing accuracy. This has been verified by different means. Firstly, the mean error values (δ) calculated for each time window have the lowest value for 27 s for Algorithm 2 and the second lowest value for Algorithm 1. Their associated

standard deviations also show low values for the 27 s window (Table 5). This is an indicator that these low error values also have a low level of dispersion. In other words, the individual errors used in the calculation of the average do not differ much from the average errors obtained. Secondly, the calculated p values of the one sample t -test provide statistical evidence that the 27 s time window is optimal. This time window has the highest number of BPM tested that cannot be considered different from the reference values. The Cohen's d results showed a moderate effect size for the 12.5 BPM reference value and large for the 10 BPM. Slow breathing seems to have higher error values for all time windows. This is an expected result since the number of cycles used to obtain the RR is less than in rapid breathing. If the optimal time window was adopted, it could provide a fairly accurate measurement of RR every twenty-seven seconds. This time step is suitable for many applications. If shorter time windows were desired (e.g., 16-20 s also have acceptable error rates), they can be adopted at the expense of lower accuracy.

Some time windows had large errors for Algorithm 1. This is the case of short time windows (6 s to 10 s). This is a logical result since the number of cycles used to make the calculation of time difference is very limited. These time windows are specially affected by the movements of the subject

TABLE 9: Performances provided by other studies in this field. If a percentage is given without any other indication, that value corresponds to a relative error. If a value in breaths/min is given without any other indication, that value corresponds to an absolute error.

Study	Performance
System proposed	3.40%
Chen et al. [60]	98.65% (mean accuracy)
Patwari et al. [61]	0.1-0.4 breaths/min
Liu et al. [8]	1.8-5.7%
Massaroni et al. [57]	2%
Dziuda et al. [10]	12% (maximum)
Nam et al. [17]	<1% (median)
Heldt and Ward [68]	1.2 breaths/min
Dan et al. [4]	0.01-0.02 breaths/min (mean differences)
Taheri and Sant'Anna [31]	0.93-1.77 breaths/min
Min et al. [39]	0.0015 breaths/min (mean differences)
Massaroni et al. [41]	1.59% (RR) 14% (tidal volume)
Presti et al. [40]	0.38%
Hoffman et al. [2]	37.9% (volume)
Hesse et al. [12]	0.32 breaths/min
Lau et al. [7]	2 breaths/min
Kukkapalli et al. [30]	>95% (accuracy)
Padasdao et al. [9]	0.23-0.48 breaths/min (mean differences)

or the sensor. It is important to note that the use of time windows greater than 20 s and less than 30 s has quite similar error values. It is also a fact that error values for those windows were not far from the optimal case, so time windows above or around 20 s might also be acceptable.

Regarding the processing algorithm, Algorithm 2 seems more robust to time window variations than Algorithm 1 since its associated error values are small even for short windows. The statistical tests for the optimal window (27 s) did not identify significant differences. According to the typical interpretations of Cohen's d value, the difference between both algorithms was negligible (0.132).

Results show that the designed sensor can determine the RR with an error of 3.40%. If the error value obtained with the proposed sensor is compared with other error values presented in the literature, it is possible to conclude that this value is in line with other studies in this field (Table 9). However, performances among studies cannot be compared fairly, since each study makes personalized tests. There are strong differences among validation experiments, datasets, and performance metrics. The inclusion of movements in the experiments can also compromise system performance. It is also important to highlight that the novelty of this paper with respect to existing studies is that we have presented a compact piezoresistive sensor with a 3D printed casing integrating all required modules into it, which is an advance in terms of wearability.

6. Conclusion

A respiration sensing system based on a piezoresistive FlexiForce sensor to be worn with a chest strap has been developed. This work is novel since it is the first time that this sensor is integrated in a compact casing including all the necessary elements (microcontroller, Bluetooth module, battery, etc.). The casing design has a direct influence on the sensor's detection capabilities. As part of this work, a compact casing has been designed and printed using a 3D printer. The files with the design have been published as supplementary material to be reused by any interested researcher.

A validation experiment was performed with 21 subjects. Two processing algorithms have been developed to determine the RR. Several statistical tests were conducted to identify both the optimal time window of the algorithms and the best algorithm. A time window of 27 s provides optimal results. This has been verified from the p values of the one sample t -test and the relative errors. This time window allows updating the RR every twenty-seven seconds, which is a suitable time for many applications. No statistically significant differences were identified between both algorithms for this time window. If shorter time windows were required, they could be used with a slightly larger error. This is a feasible scenario since error values remain fairly constant for a wide set of time windows (from 10 s for Algorithm 2 and from 20 s for Algorithm 1). This process of statistical verification is novel in this field.

Regarding the possible use of the information provided by this sensing system, it could be applied to several fields such as ambulatory health monitoring, home treatment of respiratory diseases, detection of alarming symptoms of faintness or fatigue in machine operators or drivers, health condition assessment, prediction and prevention of dangerous health states, monitoring of physical activity, and analysis of human emotions like anger and stress, among others. Customized data processing should be performed depending on the specific application.

Several commercial products that measure physiological parameters exist. However, it is not possible to know their working principle, electronic design, or results of validation experiments, since these data are generally not published. Additionally, most commercial products require data to be analyzed on their proprietary platforms. This contrasts with the sensing system presented in this paper. Data can be received online by any device with Bluetooth communication. They can then be processed offline in any numerical computing software. In addition, we have designed a 3D compact casing and uploaded the source files to a public repository to be rebuilt by any interested researcher. Another important aspect is the price of the system. Adding the cost associated with all elements of the system, it is below \$50. Different commercial chest breathing sensors can be purchased for several hundreds of dollars. However, system design is not available to be reproduced by researchers. In this paper, the breathing dataset with the measurements from the experiments, the files with the error calculations, the source code of the RR computation with the two algorithms, and the source code of the statistical tests have been

published as supplementary material to be reviewed or reused by researchers in this field. This increases transparency in research and promotes reusability. It is the first time that we see this approach in a study in this field, to the best of our knowledge.

This work also has some limitations. Although sensor validation using a metronome is a well-known and accepted method, it would be desirable to validate this sensor against a reference breathing sensor taken as a gold standard. More subjects could have been included in the study, and other 3D casing designs could have been investigated. In addition, programming a smartphone app that receives sensor data via Bluetooth is a necessary step for the real-world implementation of the sensing system.

Nevertheless, this paper has shown that the compact FlexiForce sensor with the 3D casing designed together with the algorithm based on measuring times between zero-crossings or counting zero-crossings allows determining the RR with a low error and an acceptable refresh rate.

Data Availability

The dataset with the breathing data recorded in the validation experiments is deposited in a public repository [45]. The files corresponding to the 3D design of the casing, the calculation of errors and standard deviations, the algorithms to obtain the RR from raw data, and the statistical tests are provided as supplementary materials.

Conflicts of Interest

The authors declare that there is no conflict of interest regarding the publication of this paper.

Acknowledgments

The authors gratefully acknowledge the efforts of the twenty-one volunteers who participated in the validation experiments. This work was supported by the European Social Fund (grant number: Programa Operativo FEDER 2014-2020 Construyendo Europa desde Aragon), the Gobierno de Aragon (grant number T49-17R), the Consejo Nacional de Ciencia y Tecnología (CONACyT, grant number 709365), and the Universidad de Zaragoza and Centro Universitario de la Defensa de Zaragoza (grant number UZCUD2019-TEC-02).

Supplementary Materials

The supplementary materials are categorized in four different folders: (A) STL files with the 3D design of the compact casing. The casing consists of eight different pieces. They can be printed separately. (B) MATLAB files with the algorithms used to calculate respiratory rate from the recorded data (the dataset of breathing signals is also included in that folder). (C) Excel file with the calculation of sensor error values and standard deviations for different algorithms, time windows, and reference values. (D) R files with the statistical tests applied in the paper (one sample *t*-test, Cohen's *d*, and *t*-test for paired samples). (*Supplementary Materials*)

References

- [1] I. Mahbub, H. Wang, S. K. Islam, S. A. Pullano, and A. S. Fiorillo, "A low power wireless breathing monitoring system using piezoelectric transducer," in *2016 IEEE International Symposium on Medical Measurements and Applications (MeMeA)*, pp. 1–5, Benevento, Italy, May 2016.
- [2] T. Hoffmann, B. Eilebrecht, and S. Leonhardt, "Respiratory monitoring system on the basis of capacitive textile force sensors," *IEEE Sensors Journal*, vol. 11, no. 5, pp. 1112–1119, 2011.
- [3] C. Wang, A. Hunter, N. Gravill, and S. Matusiewicz, "Unconstrained video monitoring of breathing behavior and application to diagnosis of sleep apnea," *IEEE Transactions on Biomedical Engineering*, vol. 61, no. 2, pp. 396–404, 2014.
- [4] G. Dan, J. Zhao, Z. Chen, H. Yang, and Z. Zhu, "A novel signal acquisition system for wearable respiratory monitoring," *IEEE Access*, vol. 6, pp. 34365–34371, 2018.
- [5] Z. Cao, R. Zhu, and R. Que, "A wireless portable system with microsensors for monitoring respiratory diseases," *IEEE Transactions on Biomedical Engineering*, vol. 59, no. 11, pp. 3110–3116, 2012.
- [6] J. Witt, F. Narbonneau, M. Schukar et al., "Medical textiles with embedded fiber optic sensors for monitoring of respiratory movement," *IEEE Sensors Journal*, vol. 12, no. 1, pp. 246–254, 2012.
- [7] D. Lau, Z. Chen, J. T. Teo et al., "Intensity-modulated microbend fiber optic sensor for respiratory monitoring and gating during MRI," *IEEE Transactions on Biomedical Engineering*, vol. 60, no. 9, pp. 2655–2662, 2013.
- [8] J. J. Liu, M. C. Huang, W. Xu et al., "Breathsens: a continuous on-bed respiratory monitoring system with torso localization using an unobtrusive pressure sensing array," *IEEE Journal of Biomedical and Health Informatics*, vol. 19, no. 5, pp. 1682–1688, 2015.
- [9] B. Padasdao, E. Shahhaidar, C. Stickle, and O. Boric-Lubecke, "Electromagnetic biosensing of respiratory rate," *IEEE Sensors Journal*, vol. 13, no. 11, pp. 4204–4211, 2013.
- [10] L. Dziuda, F. W. Skibniewski, M. Krej, and J. Lewandowski, "Monitoring respiration and cardiac activity using fiber Bragg grating-based sensor," *IEEE Transactions on Biomedical Engineering*, vol. 59, no. 7, pp. 1934–1942, 2012.
- [11] C. Massaroni, D. S. Lopes, D. Lo Presti, E. Schena, and S. Silvestri, "Contactless monitoring of breathing patterns and respiratory rate at the pit of the neck: a single camera approach," *Journal of Sensors*, vol. 2018, Article ID 4567213, 13 pages, 2018.
- [12] M. Hesse, P. Christ, T. Hörmann, and U. Rückert, "A respiration sensor for a chest-strap based wireless body sensor," in *SENSORS, 2014 IEEE*, pp. 490–493, Valencia, Spain, November 2014.
- [13] C. Massaroni, A. Nicolò, D. Lo Presti, M. Sacchetti, S. Silvestri, and E. Schena, "Contact-based methods for measuring respiratory rate," *Sensors*, vol. 19, no. 4, p. 908, 2019.
- [14] S.-H. Liao, W.-J. Chen, and M. S.-C. Lu, "A CMOS MEMS capacitive flow sensor for respiratory monitoring," *IEEE Sensors Journal*, vol. 13, no. 5, pp. 1401–1402, 2013.
- [15] G. Tardi, C. Massaroni, P. Saccomandi, and E. Schena, "Experimental assessment of a variable orifice flowmeter for respiratory monitoring," *Journal of Sensors*, vol. 2015, Article ID 752540, 7 pages, 2015.

- [16] D. Fan, J. Yang, J. Zhang et al., “Effectively measuring respiratory flow with portable pressure data using back propagation neural network,” *IEEE Journal of Translational Engineering in Health and Medicine*, vol. 6, pp. 1–12, 2018.
- [17] Y. Nam, B. A. Reyes, and K. H. Chon, “Estimation of respiratory rates using the built-in microphone of a smartphone or headset,” vol. 20, no. 6, pp. 1493–1501, 2016.
- [18] Y. Huang and K. Huang, “Monitoring of breathing rate by a piezofilm sensor using pyroelectric effect,” in *2013 1st International Conference on Orange Technologies (ICOT)*, pp. 99–102, Tainan, Taiwan, March 2013.
- [19] S. Milici, J. Lorenzo, A. Lázaro, R. Villarino, and D. Girbau, “Wireless breathing sensor based on wearable modulated frequency selective surface,” *IEEE Sensors Journal*, vol. 17, no. 5, pp. 1285–1292, 2017.
- [20] Y. Pang, J. Jian, T. Tu et al., “Wearable humidity sensor based on porous graphene network for respiration monitoring,” *Biosensors and Bioelectronics*, vol. 116, pp. 123–129, 2018.
- [21] H. Farahani, R. Wagiran, and M. N. Hamidon, “Humidity sensors principle, mechanism, and fabrication technologies: a comprehensive review,” *Sensors*, vol. 14, no. 5, pp. 7881–7939, 2014.
- [22] J. Ascorbe, J. M. Corres, F. J. Arregui, and I. R. Matias, “Recent developments in fiber optics humidity sensors,” *Sensors*, vol. 17, no. 4, p. 893, 2017.
- [23] T. Katagiri, K. Shibayama, T. Iida, and Y. Matsuura, “Infrared hollow optical fiber probe for localized carbon dioxide measurement in respiratory tracts,” *Sensors*, vol. 18, no. 4, p. 995, 2018.
- [24] S. Imani, P. P. Mercier, A. J. Bandodkar, J. Kim, and J. Wang, “Wearable chemical sensors: opportunities and challenges,” in *2016 IEEE International Symposium on Circuits and Systems (ISCAS)*, pp. 1122–1125, Montreal, QC, Canada, May 2016.
- [25] A. T. Güntner, S. Abegg, K. Königstein, P. A. Gerber, A. Schmidt-Trucksäss, and S. E. Pratsinis, “Breath sensors for health monitoring,” *ACS Sensors*, vol. 4, no. 2, pp. 268–280, 2019.
- [26] W. Karlen, A. Garde, D. Myers, C. Scheffer, J. M. Ansermino, and G. A. Dumont, “Estimation of respiratory rate from photoplethysmographic imaging videos compared to pulse oximetry,” *IEEE Journal of Biomedical and Health Informatics*, vol. 19, no. 4, pp. 1331–1338, 2015.
- [27] C. G. Scully, J. Lee, J. Meyer et al., “Physiological parameter monitoring from optical recordings with a mobile phone,” *IEEE Transactions on Biomedical Engineering*, vol. 59, no. 2, pp. 303–306, 2012.
- [28] M. Metshein, “A device for measuring the electrical bioimpedance with variety of electrode placements for monitoring the breathing and heart rate,” in *2015 26th Irish Signals and Systems Conference (ISSC)*, pp. 1–4, Carlow, Ireland, June 2015.
- [29] S. Ansari, A. Belle, K. Najarian, and K. Ward, “Impedance plethysmography on the arms: respiration monitoring,” in *2010 IEEE International Conference on Bioinformatics and Biomedicine Workshops (BIBMW)*, pp. 471–472, Hong Kong, China, December 2010.
- [30] R. Kukkapalli, N. Banerjee, R. Robucci, and Y. Kostov, “Micro-radar wearable respiration monitor,” in *2016 IEEE Sensors*, pp. 1–3, Orlando, FL, USA, October 2016.
- [31] T. Taheri and A. Sant’Anna, “Non-invasive breathing rate detection using a very low power ultra-wide-band radar,” in *2014 IEEE International Conference on Bioinformatics and Biomedicine (BIBM)*, pp. 78–83, Belfast, UK, November 2014.
- [32] J. Hernandez, D. McDuff, and R. W. Picard, “Biowatch: estimation of heart and breathing rates from wrist motions,” in *2015 9th International Conference on Pervasive Computing Technologies for Healthcare (PervasiveHealth)*, pp. 169–176, Istanbul, Turkey, May 2015.
- [33] L. Estrada, A. Torres, L. Sarlabous, and R. Jané, “Respiratory signal derived from the smartphone built-in accelerometer during a respiratory load protocol,” in *2015 37th Annual International Conference of the IEEE Engineering in Medicine and Biology Society (EMBC)*, pp. 6768–6771, Milan, Italy, August 2015.
- [34] R. Ciobotariu, C. Rotariu, F. Adochiei, and H. Costin, “Wireless breathing system for long term telemonitoring of respiratory activity,” in *2011 7th International Symposium on Advanced Topics in Electrical Engineering (ATEE)*, pp. 1–4, Bucharest, Romania, May 2011.
- [35] C. Rotariu, C. Cristea, D. Arotaritei, R. G. Bozomitu, and A. Pasarica, “Continuous respiratory monitoring device for detection of sleep apnea episodes,” in *2016 IEEE 22nd International Symposium for Design and Technology in Electronic Packaging (SIITME)*, pp. 106–109, Oradea, Romania, October 2016.
- [36] J. Grlica, T. Martinović, and H. Džapo, “Capacitive sensor for respiration monitoring,” in *2015 IEEE Sensors Applications Symposium (SAS)*, pp. 1–6, Zadar, Croatia, April 2015.
- [37] C. M. Yang, T. L. Yang, C. C. Wu et al., “Textile-based capacitive sensor for a wireless wearable breath monitoring system,” in *2014 IEEE International Conference on Consumer Electronics (ICCE)*, pp. 232–233, Las Vegas, NV, USA, January 2014.
- [38] C. M. Yang, T. Yang, C. C. Wu, and N. N. Y. Chu, “A breathing game with capacitive textile sensors,” in *2011 IEEE International Games Innovation Conference (IGIC)*, pp. 134–136, Orange, CA, USA, November 2011.
- [39] S. D. Min, Y. Yun, and H. Shin, “Simplified structural textile respiration sensor based on capacitive pressure sensing method,” *IEEE Sensors Journal*, vol. 14, no. 9, pp. 3245–3251, 2014.
- [40] D. L. Presti, C. Massaroni, D. Formica et al., “Smart textile based on 12 fiber Bragg gratings array for vital signs monitoring,” *IEEE Sensors Journal*, vol. 17, no. 18, pp. 6037–6043, 2017.
- [41] C. Massaroni, P. Saccomandi, D. Formica et al., “Design and feasibility assessment of a magnetic resonance-compatible smart textile based on fiber Bragg grating sensors for respiratory monitoring,” *IEEE Sensors Journal*, vol. 16, no. 22, pp. 8103–8110, 2016.
- [42] X. Yang, Z. Chen, C. S. M. Elvin et al., “Textile fiber optic microbend sensor used for heartbeat and respiration monitoring,” *IEEE Sensors Journal*, vol. 15, no. 2, pp. 757–761, 2015.
- [43] D. Teichmann, D. De Matteis, T. Bartelt, M. Walter, and S. Leonhardt, “A bendable and wearable cardiorespiratory monitoring device fusing two noncontact sensor principles,” *IEEE Journal of Biomedical and Health Informatics*, vol. 19, no. 3, pp. 784–793, 2015.
- [44] *FlexiForce a201 sensor*, 2018, <https://www.tekscan.com/productsolutions/force-sensors/a201>.
- [45] E. Vanegas, R. Igual, and I. Plaza, “Breathing data from a piezoresistive breathing sensor,” in *IEEE Dataport*, October 2019.

- [46] Adafruit Learning System, "Force sensitive sensor," 2018, August 2018, <https://cdn-learn.adafruit.com/downloads/pdf/force-sensitive-resistor-fsr.pdf>.
- [47] N. Cotta, T. Devidas, and V. K. N. Ekoskar, "Wireless communication using HC-05 Bluetooth module interfaced with Arduino," *International Journal of Science, Engineering and Technology Research*, vol. 5, no. 4, 2016.
- [48] S. Numeriques, "BTM-5 Bluetooth," *wireless TTL Master/Slave Transceiver Module*, 2011, <http://www.strat-num.fr/IMG/pdf/bluetooth-module-btm5-datasheet.pdf>.
- [49] ATMEL, "8-bit microcontroller with 4/8/16/32k bytes in-system programmable flash," *Arduino's Pro-mini microcontroller*, 2009, <https://www.sparkfun.com/datasheets/Components/SMD/ATMega328.pdf>.
- [50] S. Lee, J. Kim, J. Lee, and B. H. Cho, "State-of-charge and capacity estimation of lithium-ion battery using a new open-circuit voltage versus state-of-charge," *Journal of Power Sources*, vol. 185, no. 2, pp. 1367–1373, 2008.
- [51] M. Jacoby, "Assessing the safety of lithium-ion batteries," *Chemical and Engineering News*, vol. 91, pp. 33–37, 2013.
- [52] NanJing Top Power ASIC Corp, "Tp4056," <https://dlnmh9ip6v2uc.cloudfront.net/datasheets/Prototyping/TP4056.pdf>.
- [53] MathWorks, "Lowpass' function," 2019, <https://es.mathworks.com/help/signal/ref/lowpass.html>.
- [54] L. Schriger, "Approach to the patient with abnormal vital signs," in *Goldman's Cecil Medicine*, pp. 27–30, Elsevier, 2012.
- [55] W. Q. Lindh, M. Pooler, C. D. Tamparo, B. M. Dahl, and J. Morris, *Delmar's Comprehensive Medical Assisting: Administrative and Clinical Competencies*, Delmar Cengage Learning, 4th edition, 2013.
- [56] J. Mann, R. Rabinovich, A. Bates, S. Giavedoni, W. MacNee, and D. K. Arvind, "Simultaneous activity and respiratory monitoring using an accelerometer," in *2011 International Conference on Body Sensor Networks*, pp. 139–143, Dallas, TX, USA, May 2011.
- [57] C. Massaroni, D. Lo Presti, P. Saccomandi, M. A. Caponero, R. D'Amato, and E. Schena, "Fiber Bragg grating probe for relative humidity and respiratory frequency estimation: assessment during mechanical ventilation," *IEEE Sensors Journal*, vol. 18, no. 5, pp. 2125–2130, 2018.
- [58] C. Massaroni, E. Schena, S. Silvestri, F. Taffoni, and M. Merone, "Measurement system based on RGB camera signal for contactless breathing pattern and respiratory rate monitoring," in *2018 IEEE International Symposium on Medical Measurements and Applications (MeMeA)*, pp. 1–6, Rome, Italy, June 2018.
- [59] C. Massaroni, M. Ciochetti, G. Di Tomaso et al., "Design and preliminary assessment of a smart textile for respiratory monitoring based on an array of fiber Bragg gratings," in *2016 38th Annual International Conference of the IEEE Engineering in Medicine and Biology Society (EMBC)*, pp. 6054–6057, Orlando, FL, USA, August 2016.
- [60] C. Chen, Y. Han, Y. Chen et al., "TR-BREATH: time-reversal breathing rate estimation and detection," *IEEE Transactions on Biomedical Engineering*, vol. 65, no. 3, pp. 489–501, 2018.
- [61] N. Patwari, J. Wilson, S. Ananthanarayanan, S. K. Kasera, and D. R. Westenskow, "Monitoring breathing via signal strength in wireless networks," *IEEE Transactions on Mobile Computing*, vol. 13, no. 8, pp. 1774–1786, 2014.
- [62] K. E. Barrett and W. F. Ganong, *Ganongs Review of Medical Physiology*, McGraw-Hill, 2013.
- [63] N. Patwari, L. Brewer, Q. Tate, O. Kaltiokallio, and M. Bocca, "Breathfinding: a wireless network that monitors and locates breathing in a home," *IEEE Journal of Selected Topics in Signal Processing*, vol. 8, no. 1, pp. 30–42, 2014.
- [64] M. H. Li, A. Yadollahi, and B. Taati, "Noncontact vision-based cardiopulmonary monitoring in different sleeping positions," *IEEE Journal of Biomedical and Health Informatics*, vol. 21, no. 5, pp. 1367–1375, 2017.
- [65] J. Cohen, *Statistical Power Analysis for the Behavioral Sciences*, Lawrence Erlbaum Associates, USA, 2nd edition, 1988.
- [66] J. Cohen, "A power primer," *Psychological Bulletin*, vol. 112, no. 1, pp. 155–159, 1992.
- [67] J. De Jonckheere, M. Jeanne, F. Narbonne et al., "Ofseth: a breathing motions monitoring system for patients under MRI," in *2010 Annual International Conference of the IEEE Engineering in Medicine and Biology*, pp. 1016–1019, Buenos Aires, Argentina, August 2010.
- [68] G. P. Heldt and R. J. Ward, "Evaluation of ultrasound-based sensor to monitor respiratory and nonrespiratory movement and timing in infants," *IEEE Transactions on Biomedical Engineering*, vol. 63, no. 3, pp. 619–629, 2016.